TTI: 0-6982

Utilization of UHPC Bridge Superstructures in Texas—Volume 3: UHPC Production Guidelines and Design Recommendations with Design Examples

Technical Report 0-6982-R1-Vol3

Cooperative Research Program

TEXAS A&M TRANSPORTATION INSTITUTE
COLLEGE STATION, TEXAS

sponsored by the
Federal Highway Administration and the
Texas Department of Transportation
https://tti.tamu.edu/documents/0-6982-R1-Vol3.pdf

Technical Report Documentation Page

1. Report No.	2. Government Accession No.	3. Recipient's Catalog No.
FHWA/TX-23/0-6982-R1-Vol3		

4. Title and Subtitle	5. Report Date
UTILIZATION OF UHPC BRIDGE SUPERSTRUCTURES IN TEXAS—VOLUME 3: UHPC PRODUCTION GUIDELINES AND DESIGN RECOMMENDATIONS WITH DESIGN EXAMPLES	Published: October 2023
	6. Performing Organization Code
7. Author(s)	8. Performing Organization Report No.
Mary Beth D. Hueste, Anol Mukhopadhyay, Stefan Hurlebaus, John Mander, Hyeonki Hong, Amreen Fatima, and Tevfik Terzioglu	Report 0-6982-R1-Vol3
9. Performing Organization Name and Address	10. Work Unit No. (TRAIS)
Texas A&M Transportation Institute The Texas A&M University System College Station, Texas 77843-3135	11. Contract or Grant No. Project 0-6982
12. Sponsoring Agency Name and Address	13. Type of Report and Period Covered
Texas Department of Transportation Research and Technology Implementation Office 125 E. 11th Street Austin, Texas 78701-2483	Technical Report: September 2018–October 2022
	14. Sponsoring Agency Code

15. Supplementary Notes

Project sponsored by the Texas Department of Transportation and the Federal Highway Administration.
Project Title: Utilization of UHPC Bridge Superstructures in Texas
URL: https://tti.tamu.edu/documents/0-6982-R1-Vol3.pdf

16. Abstract

The use of ultra-high performance concrete (UHPC) in Texas bridges has the potential to add substantial improvements to bridge construction. Advanced material properties and superior durability of UHPC can result in significant design and construction benefits. Within this context, this project evaluated the application of UHPC for precast, pretensioned bridge girders. The project scope included a detailed review and synthesis of the relevant literature, analytical feasibility study, development of nonproprietary UHPC mixture designs using locally available materials, material-level experiments for selected UHPC mixtures, fabrication of precast, pretensioned UHPC bridge girder specimens at a precast plant in Texas, full-scale experiments to understand UHPC girder behavior, nondestructive evaluation of UHPC girders, fiber distribution and orientation analysis, and development of UHPC production and design guidelines and design examples. Nonproprietary UHPC mixtures were successfully developed to achieve high early strength (14 ksi within 24 hours) for precast applications with desirable outcomes in terms of material properties and durability. Large volume production and girder fabrication were successfully carried out at a precast plant. This Volume 3 research report documents production guidelines, design guidelines, and design examples for precast, pretensioned UHPC girders. The production guidelines describe nonproprietary UHPC mixture design, mixing procedures, transport, placement, finishing, curing, and evaluation methods. The design recommendations document the design procedure for UHPC bridge girders with a composite conventional concrete deck slab. The design guidelines are developed based on the full-scale girder testing results. The design recommendations consider the UHPC draft specifications under consideration by AASHTO and the results of testing UHPC girder specimens. The design guidelines are supplemented with two detailed design example calculations. The Tx34 design example explores the advantage of UHPC to reduce the number of girder lines for a bridge span. The Tx54 design example highlights the potential of UHPC to increase the span length of highway bridge structures in Texas.

17. Key Words	18. Distribution Statement
Ultra-High-Performance Concrete, UHPC, Mixture Design, Mixing Procedure, Precast Plant Production, Girder Fabrication, Design Recommendations, Design Examples	No restrictions. This document is available to the public through NTIS: National Technical Information Service Alexandria, Virginia https://www.ntis.gov

19. Security Classif. (of this report)	20. Security Classif. (of this page)	21. No. of Pages	22. Price
Unclassified	Unclassified	214	

Form DOT F 1700.7 (8-72) Reproduction of completed page authorized

UTILIZATION OF UHPC BRIDGE SUPERSTRUCTURES IN TEXAS—VOLUME 3: UHPC PRODUCTION GUIDELINES AND DESIGN RECOMMENDATIONS WITH DESIGN EXAMPLES

by

Mary Beth D. Hueste, Ph.D., P.E.
Research Engineer
Texas A&M Transportation Institute

Anol Mukhopadhyay, Ph.D.
Research Scientist
Texas A&M Transportation Institute

Stefan Hurlebaus, Ph.D.
Research Scientist
Texas A&M Transportation Institute

John Mander, Ph.D.
Research Engineer
Texas A&M Transportation Institute

Hyeonki Hong
Graduate Assistant Researcher
Texas A&M Transportation Institute

Amreen Fatima
Graduate Assistant Researcher
Texas A&M Transportation Institute

and

Tevfik Terzioglu, Ph.D.
Post-Doctoral Research Associate
Texas A&M Transportation Institute

Report 0-6982-R1-Vol3
Project 0-6982
Project Title: Utilization of UHPC Bridge Superstructures in Texas

Sponsored by the
Texas Department of Transportation
and the
Federal Highway Administration

Published: October 2023

TEXAS A&M TRANSPORTATION INSTITUTE
College Station, Texas 77843-3135

DISCLAIMER

This research was sponsored by the Texas Department of Transportation (TxDOT) and the Federal Highway Administration (FHWA). The contents of this report reflect the views of the authors, who are responsible for the facts and the accuracy of the data presented herein. The contents do not necessarily reflect the official view or policies of FHWA or TxDOT. This report does not constitute a standard, specification, or regulation.

This report is not intended for construction, bidding, or permit purposes. The researcher in charge of the project was Mary Beth D. Hueste. The United States Government and the State of Texas do not endorse products or manufacturers. Trade or manufacturers' names appear herein solely because they are considered essential to the object of this report.

ACKNOWLEDGMENTS

This project was conducted at Texas A&M University and was supported by TxDOT and FHWA through the Texas A&M Transportation Institute as part of Project 0-6982, Utilization of UHPC Bridge Superstructures in Texas.

The authors are grateful to the individuals who were involved with this project and provided invaluable assistance, including Tom Schwerdt (TxDOT, project manager), Robert Owens (TxDOT, project director), and the TxDOT Project Monitoring Committee: Ahmed Al-Basha, Biniam Aregawi, Rachel Cano, Geetha Chandar, Chad Dabbs, Jamie Farris, Igor Kafando, Andy Naranjo, Joe Roche, Prapti Sharma, and Jason Tucker.

Co-authors Hyeonki Hong and Amreen Fatima were the principal Ph.D. students on the project, and this work comprised a major part of their doctoral research.

The authors also wish to acknowledge the students involved in the early stages of the project, particularly master's students Brittni Cooper and Jay Shah.

In addition, the following students contributed to this project by helping with the laboratory work and the precast plant production process: Stephin Joseph Anna, Victor Balangero, William (Jake) Irr, Nuzhat Kabir, Mikhail Lanier, Matthew Leffler, Isabel Mlo, Anirutthan Narayanan, Samir Palepu, Jay Parmar, Pushkar Shivechchhu, Arash Rockey, Nikhil Ganesh Tandel, Xincheng Ethan Wang, Seunghyun Yoon, and Zhen Zhang.

Assistance from the Center for Infrastructure Renewal staff is gratefully acknowledged, including Kai-wei (Victor) Liu, Rick Canatella, Tony Barbosa, Charles Droddy, Kirk Martin, and Dr. Peter Keating (director of the High-Bay Structural & Materials Testing Laboratory).

The TTI staff who supported the project are gratefully acknowledged, especially Madalyn Salcido, who provided overall administrative and business support for the project.

The research team is grateful to Heldenfels Enterprises Inc., San Marcos, Texas, who supported this project by working with the research team to conduct a trial batch of the developed UHPC mixture and fabricated the UHPC girder specimens at its precast plant.

TABLE OF CONTENTS

Page

List of Figures ..... **x**
List of Tables ..... **xi**
List of Acronyms ..... **xii**
1 Introduction **1**
2 UHPC Production Guidelines **3**
2.1 Nonproprietary UHPC Mixture Design 3
2.1.1 An Approach to Develop a Nonproprietary UHPC Mixture 3
2.1.2 Constituent Materials 7
2.1.3 Mixture Design 10
2.1.4 Lab-Scale Trial Batch 10
2.2 UHPC Mixing 12
2.2.1 Mixing Procedure 12
2.2.2 Large-Scale Trial Batch for Quality of UHPC Production 14
2.3 Transport, Placement, Finishing, and Curing 18
2.3.1 Transport 18
2.3.2 Placement 18
2.3.3 Finishing 19
2.3.4 Curing 19
2.4 Evaluation and Quality of UHPC 20
2.4.1 Categories of Testing 20
2.4.2 Recommended Tests 21
2.4.3 Comparison to PCI Recommended Tests 22
2.4.4 Evaluation of UHPC 23
3 UHPC Girder Design Recommendations **25**
3.1 General Design Procedure 25
3.2 Geometric and Material Parameters 26
3.2.1 Material Properties 26
3.2.2 Geometric Properties 29
3.3 Load Demands 30
3.3.1 Dead Loads 30
3.3.2 Live Loads 31
3.3.3 Live Load Distribution Factors 31
3.3.4 Load Combinations 32
3.4 Prestress Losses 32
3.4.1 Prestress Losses at Transfer 33
3.4.2 Long-Term Time Dependent Losses 34
3.5 Transfer Length 40
3.6 Flexure Design for Service Limit State 41
3.6.1 General 41
3.6.2 Notation for Stress Checks 41
3.6.3 Flexural Stress Limits 42

3.6.4 Flexural Stress Checks 44
3.7 Flexure Strength Limit State 48
3.7.1 General 48
3.7.2 Review of UHPC Draft Specifications 48
3.7.3 Composite UHPC Girders with Conventional Concrete Deck 49
3.8 Shear Strength Limit State 51
3.8.1 Nominal Shear Strength 51
3.8.2 Minimum Transverse Shear Reinforcement 53
3.8.3 Transverse Reinforcement for Shear Strength 54
3.9 Interface Shear Design 54
3.9.1 Interface Shear Resistance 54
3.9.2 Reinforcement for Interface Shear Strength 55
3.10 Splitting Resistance 56
3.10.1 General Recommendations 56
3.10.2 Minimum Splitting Resistance Reinforcement 56
3.10.3 Alternate Method 57
3.10.4 Basic Layout of Mild Steel Reinforcement 57
3.11 Camber and Deflection 58
4 Design Example for Tx34 61
4.1 Background and Significance 61
4.2 Detailed Design Example for A UHPC Tx34 girder 61
4.3 Bridge Geometry and Material Properties 61
4.3.1 Geometric Properties 62
4.3.2 Material Properties 63
4.4 Girder Details and Section Properties 66
4.5 Composite Section Details and Sectional Properties 67
4.6 Load Demands 68
4.6.1 Dead Loads 68
4.6.2 Live Loads 69
4.6.3 Unfactored and Factored Moment Demands 71
4.6.4 Unfactored and Factored Shear Demands 75
4.7 Flexural Stress Design at Service Limit State 78
4.7.1 General Procedure 78
4.7.2 Sign Convention 78
4.7.3 Prestress Losses 79
4.7.4 Estimating Required Prestressing Force 89
4.7.5 Flexural Stresses at Transfer 90
4.7.6 Flexural Stresses after Deck Placement 92
4.7.7 Flexural Stresses at Service Limit State 94
4.7.8 Camber Calculation 105
4.7.9 Live Load Deflection Check 107
4.7.10 Flexural Resistance at Strength Limit State 108
4.8 Shear Resistance at Strength Limit State 113
4.8.1 Critical Section for Shear 113
4.8.2 Nominal Shear Resistance 114
4.9 Splitting Resistance 116

4.10 Interface Shear Design 118
4.11 End Block Reinforcement 121
4.12 Design Summary 121
5 Design Example for Tx54 125
5.1 Detailed Design Example for A UHPC Tx54 girder 125
5.2 Bridge Geometry and Material Properties 125
5.2.1 Geometric Properties 125
5.2.2 Material Properties 126
5.3 Girder Details and Section Properties 129
5.4 Composite Section Details and Sectional Properties 130
5.5 Load Demands 131
5.5.1 Dead Loads 131
5.5.2 Live Loads 132
5.5.3 Unfactored and Factored Moment Demands 134
5.5.4 Unfactored and Factored Shear Demands 138
5.6 Flexural Stress Design at Service Limit State 141
5.6.1 General Procedure 141
5.6.2 Sign Convention 141
5.6.3 Prestress Losses 142
5.6.4 Estimating Required Prestressing Force 152
5.6.5 Flexural Stresses at Transfer 153
5.6.6 Flexural Stresses after Deck Placement 155
5.6.7 Flexural Stresses at Service Limit State 157
5.6.8 Camber Calculation 167
5.6.9 Live Load Deflection Check 169
5.6.10 Flexural Resistance at Strength Limit State 170
5.7 Shear Resistance at Strength Limit State 179
5.7.1 Critical Section for Shear 180
5.7.2 Nominal Shear Resistance 180
5.8 Splitting Resistance 182
5.9 Interface Shear Design 184
5.10 End Block Reinforcement 187
5.11 Design Summary 187
References 191
Appendix A. Drawings for Design Examples 197

LIST OF FIGURES

Page

Figure 2.1. A&A Curve for High Packing Density at Matrix-Level. 5
Figure 2.2. Effects of Silica Fume Proportion (Hermann et al. 2016). 6
Figure 2.3. Recommended Mixing Procedure. 13
Figure 2.4. Screen and Vibrator used for Fiber Addition. 16
Figure 2.5. Example of Automated Fiber Feeder (Park et al. 2010). 16
Figure 2.6. Example of Automated Fiber Dosing System at Plant (Berkshire Engineering Supplier 2022). 17
Figure 2.7. Placement using Leading Edge Method (eConstruct 2020). 19
Figure 3.1. Triangular Stress Block for UHPC (adapted from El-Helou and Graybeal (2022)). 48
Figure 3.2. U-shaped Composite Bar Detail used for Interface Shear Resistance. 56
Figure 3.3. Reinforcement Details. 58
Figure 4.1. Bridge Cross-Section Details. 62
Figure 4.2. HS20 Truck Loading (AASHTO 2020; Taly 2014). 70
Figure 4.3. Designated HL-93 Load Model (AASHTO 2018). 71
Figure 4.4. Stress Blocks for the Derived Inequalities. 98
Figure 4.5. Feasible Domain for Flexure Design. 100
Figure 4.6. Strand Layout. 103
Figure 4.7. Stress Checks. 104
Figure 5.1. Bridge Cross-Section Details. 125
Figure 5.2. HS20 Truck Loading (AASHTO 2020; Taly 2014). 133
Figure 5.3. Designated HL-93 Load Model (AASHTO 2018). 134
Figure 5.4. Stress Blocks for the Derived Inequalities. 160
Figure 5.5. Feasible Domain for Flexure Design. 162
Figure 5.6. Strand Layout. 165
Figure 5.7. Stress Checks. 166

LIST OF TABLES

Page

Table 2.1. UHPC Mixture Design. 10
Table 2.2. Recommended Qualification, Acceptance, and Informational Testing. 22
Table 2.3. Recommended Flow Spread Value for Qualification and Acceptance Testing. 24
Table 2.4. Recommended Values for Qualification and Acceptance Testing. 24
Table 3.1. Summary of Dead Load Values. 31
Table 3.2. Comparison of Parameters for Creep Prediction Equations. 39
Table 3.3. Comparison of Parameters for Shrinkage Prediction Equations. 40
Table 4.1. Geometric Properties of Tx34 Bridge. 62
Table 4.2. Properties of UHPC for Tx34 I-Girders. 63
Table 4.3. Comparison of Experimental and Computed MOE. 64
Table 4.4. Properties of Conventional Concrete Deck. 65
Table 4.5. Properties of Wearing Surface and Barrier (T551 Railing). 66
Table 4.6. Mechanical and Geometric Properties of Prestressing Strands. 66
Table 4.7. Girder Details and Sectional Properties. 66
Table 4.8. Computation of Properties of Composite Section. 67
Table 4.9. Properties of Tx34 UHPC Girder with CC Deck Slab. 67
Table 4.10. Load Combinations Considered. 68
Table 4.11. Live Load Details. 71
Table 4.12. Comparison of Prestress Losses. 89
Table 4.13. Comparison of Nominal Moment Capacity. 113
Table 4.14. Summary of Design Details. 122
Table 5.1. Geometric Properties of Tx54 Bridge. 126
Table 5.2. Properties of UHPC for Tx54 I-Girders. 127
Table 5.3. Comparison of Experimental and Computed MOE. 128
Table 5.4. Properties of Conventional Concrete Deck. 128
Table 5.5. Properties of Wearing Surface and Barrier (T551 Railing). 129
Table 5.6. Mechanical and Geometric Properties of Prestressing Strands. 129
Table 5.7. Girder Details and Sectional Properties. 130
Table 5.8. Computation of Properties of Composite Section. 130
Table 5.9. Properties of Tx54 UHPC Girder with CC Deck Slab. 131
Table 5.10. Load Combination Factors. 131
Table 5.11. Live Load Details. 134
Table 5.12. Comparison of Prestress Losses. 152
Table 5.13. Comparison of Nominal Moment Capacity. 179
Table 5.14. Summary of Design Details. 188

LIST OF ACRONYMS

A&A	Andreasen and Andersen model
AASHTO	American Association of State Highway and Transportation Officials
ACCT	Accelerated concrete cylinder test
ACI	American Concrete Institute
ASR	Alkali-silica reaction
ASTM	American Society of Testing and Materials
BSG	Bulk specific gravity
C_2S	Dicalcium silicate
C_3A	Tricalcium aluminate
C_3S	Tricalcium silicate
CC	Conventional concrete
CMOD	Crack mouth opening displacement
CoV	Coefficient of variation
CSA	Canadian Standards Association
CT	Computed tomography
DEF	Delayed ettringite formation
DOT	Department of transportation
DR	Distribution ratio
FHWA	Federal Highway Administration
FRC	Fiber-reinforced concrete
GGBFS	Ground-granulated blast furnace slag
GPR	Ground penetrating radar
HPC	High performance concrete
HPFRCC	High performance fiber-reinforced cement concrete
HRWR	High-range water reducer
HRWR/c	HRWR-to-cement
HRWR/cm	HRWR-to-cementitious material
HSC	High strength concrete
JSCE	Japan Society of Civil Engineers
LRFD	Load and Resistance Factor Design
LSCT	Linear strain conversion transducer
LVDT	Linear variable displacement transducer
MOE	Modulus of elasticity
NIST	National Institute of Standards and Technology
NSC	Normal strength concrete
PCI	Precast/Prestressed Concrete Institute
PSR	Pore solution resistivity
RCPT	Rapid chloride ion penetration test
RDM	Relative dynamic modulus of elasticity
RH	Relative humidity
RPC	Reactive powder concrete
RSRH	Rapid set rapid hardening
SCC	Self-consolidating concrete
SCM	Supplemental cementitious materials

SFRC	Steel fiber-reinforced concrete
SIFCON	Slurry infiltrated fiber concrete
SiO_2	Silicon dioxide
TxDOT	Texas Department of Transportation
UHPC	Ultra-high performance concrete
UHP-FRC	Ultra-high performance fiber-reinforced concrete
UPV	Ultrasonic pulse velocity
w/*b*	Water-to-binder
w/*c*	Water-to-cement
w/*cm*	Water-to-cementitious material

1 INTRODUCTION

This Volume 3 report provides practical information for the implementation of ultra-high performance concrete (UHPC) for precast, pretensioned bridge girders in Texas. Recommended guidelines are provided for production of ultra-high performance concrete (UHPC) at the precast plant. Recommendations are also provided for the design of precast, prestressed UHPC bridge girders with design examples. The following is a brief description of each chapter in this Volume 3 report.

- Chapter 1 provides an introduction and outline for the Volume 3 report.

- Chapter 2 provides recommended guidelines for UHPC production including the following: mixture design, constituent materials, mixing procedure, large-scale trial batching, transport, placement, finishing, curing, and evaluation of UHPC.

- Chapter 3 elaborates the various steps that are recommended for the design of UHPC girders with a conventional concrete (CC) deck slab. The guidelines highlight the design philosophy implemented in this research project for the design of UHPC bridge girders. This section covers the initial design parameters, stress limits, structural loads, prestressing losses, flexure design, and shear design. In addition, the methodology used for interface shear design, splitting resistance, camber, deflection, and transfer length are discussed.

- Chapter 4 provides a design example for a Tx34 girder with a CC deck slab having five girder lines and a span length of 85 ft. This example illustrates the advantage of UHPC to achieve long spans despite eliminating one girder line, and highlights the economy of bridge girder designs using UHPC.

- Chapter 5 provides a design example for a Tx54 girder with a CC deck slab having six girder lines and a span length of 144 ft. This example highlights how the span length limits can be increased when using UHPC for a given girder shape.

2 UHPC PRODUCTION GUIDELINES

This chapter presents guidance for production of ultra-high performance concrete (UHPC) for precast, prestressed bridge girders with specific consideration of precast plants in Texas. Section 2.1 presents constituent materials of the UHPC mixture and the mixture design. Section 2.2 describes a practical mixing sequence suitable for making UHPC at a precast plant. Section 2.3 discusses transport and placement of fresh UHPC, finishing, and curing. Section 2.4 presents a recommended list of standard tests for qualification and acceptance of UHPC produced at a precast plant.

2.1 NONPROPRIETARY UHPC MIXTURE DESIGN

This section provides an approach to develop a nonproprietary UHPC mixture. In addition, the selected constituent materials for the developed nonproprietary UHPC mixture and the proportions of the constituent materials are described. Note that the UHPC mixture was developed for precast pretensioned bridge girders to be fabricated at Texas precast plants based on the following goals and targets:

1. Common materials used in the Texas precast industry,
2. Sufficient flow retention for workability,
3. Multiple batches and placements using a single Tuckerbuilt transport truck,
4. 12–14 ksi compressive strength at release within 20–24 hours without heat treatment,
5. 18–20 ksi compressive strength at service,
6. 0.85 ksi tensile strength at release (0.70–0.75 ksi was observed during testing),
7. 1.0 ksi tensile strength at service (0.75–1.0 ksi was observed during testing),
8. No segregation of steel fibers, and
9. Superior durability.

More details are provided in the Volume 1 report.

2.1.1 An Approach to Develop a Nonproprietary UHPC Mixture

This section briefly summarizes an approach to develop a nonproprietary UHPC mixture for precast plant applications. The Volume 1 report (Section 4.2) describes this information in detail.

2.1.1.1 Particle Packing Density for Constituent Materials

Particle packing density is one of the key parameters to achieve desired fresh and hardened properties and durability of UHPC (de Larrard and Sedran 1994; Li and Kwan 2014; Richard and Cheyrezy 1995; Russell et al. 2013; Wille and Boisvert-Cotulio 2015; Zdeb 2013). Optimization of particle size distribution for spacing packing was introduced by Richard and Cheyrezy (1995). High particle packing density corresponds to low porosity of the UHPC mixture. As a result, mechanical properties and durability can be improved. The following provides a brief summary of the effect of particle packing density on the performance of UHPC.

- An increase in the particle packing density improves rheological behavior, mechanical performance, and durability of UHPC.
- High particle packing density reduces the volume of water-filled voids. As a result, less water is trapped in voids and the remaining water coats cementitious particles. More water covering the surface of the particles reduces the viscosity of the paste and, therefore, the rheological behavior of the paste is improved. This means that the flowability of the paste can be improved while maintaining the *w*/*c* ratio or that the flowability can be maintained while reducing the *w*/*c* ratio.
- In addition, because a low *w*/*c* ratio contributes to limiting the amount of unreacted water in the mix, the formation of capillary pores is decreased. Thus, low porosity of the paste can be obtained by the achievement of high particle packing density. This low porosity improves the durability performance of UHPC.

Therefore, consideration of particle packing density for material selection is necessary. For high packing density, two levels of particle packing are important. The first is paste-level, and the other is matrix-level. For high packing density of paste, the selection of supplementary cementitious materials (SCMs) is key. The preferred particle size of SCMs is between silica fume and cement. At the paste-level, silica fume is the finest material and cement is the coarsest material. The SCM is selected to fill the spaces between silica fume particles and cement particles. For the matrix-level, the modified Andreasen and Andersen model (A&A) is used, as described in detail in Volume 1 report Section 4.2.3.1. Figure 2.1 shows the A&A curve with gradations of three sands.

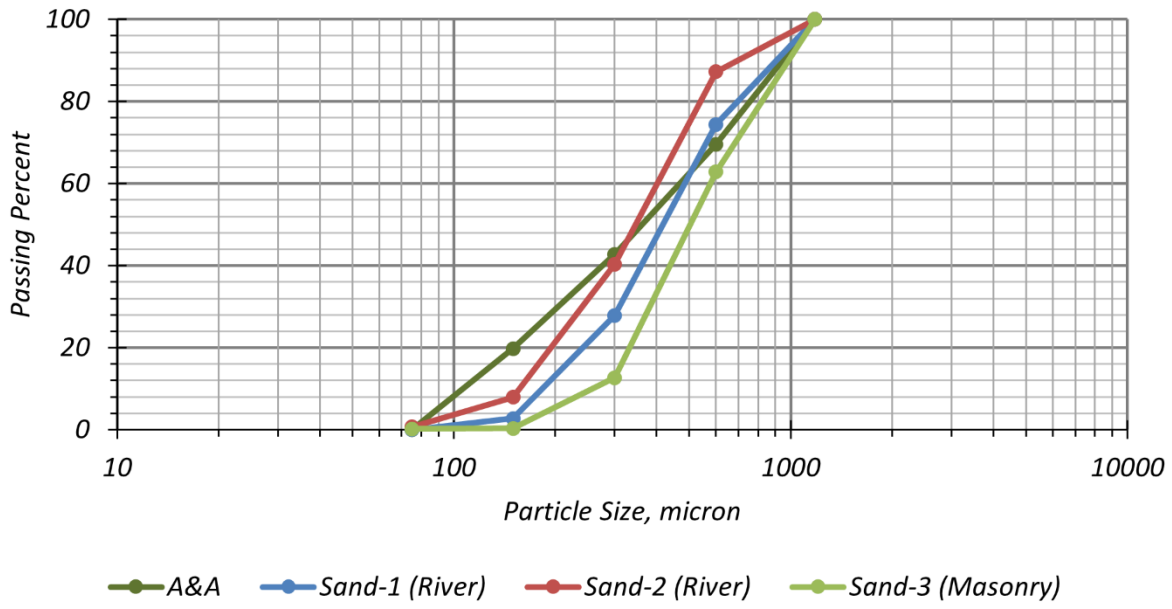

Figure 2.1. A&A Curve for High Packing Density at Matrix-Level.

2.1.1.2 Workability

An increase in solids concentration for high packing density increases viscosity and yield strength due to the flocculation of the cementitious materials (Yahia et al. 2016). Thus, a paste with high solid concentration and a low *w*/*c* like UHPC has a high viscosity and a high yield stress of cement suspensions due to a high attractive force, which reduces the workability substantially. This workability issue can be resolved by HRWR. A polycarboxylate-based HRWR disperses particles by both electrostatic and steric repulsion using its long side chain length (Gelardi and Flatt 2016). Side chains of HRWR hinder flocculation of particles by the steric repulsion. As a result, particles physically separated by HRWR provide sufficient workability and extended slump life (Gelardi and Flatt 2016; Tue et al. 2008).

However, an over-dose of HRWR causes retardation of hydration. As a result, early strength gain cannot be achieved. Therefore, a large amount of HRWR content with high packing density is not a solution for UHPC mixtures that require high early strength. The optimum packing density can be evaluated indirectly by both a flow table test and a compressive strength test at 1 day.

In addition to *w*/*c* and HRWR, mineral admixtures such as fly ash and silica fume may influence the rheology of UHPC positively or negatively depending on particle size distribution, fineness, and morphology (Yahia et al. 2016). Replacing a portion of cement with fly ash improves rheology because it reduces both yield stress and viscosity (Tattersall and Banfill 1983). A small volume of silica fume (between 5–15 percent by cement weight) can improve the rheology of the mix by filling voids between cement particles. Consequently, the water previously trapped between cement particles is released to contribute to the workability of the mix. However, a large proportion of silica fume (larger than approximately 15 percent) diminishes the spread of UHPC due to an increase in water demand. Furthermore, a loosening effect occurs when the volume of silica fume exceeds the volume of gaps between cement particles (Figure 2.2). Small silica fume particles push larger cement particles away from each other, thus creating more voids for water to fill, which leads to reduction in workability (Hermann et al. 2016).

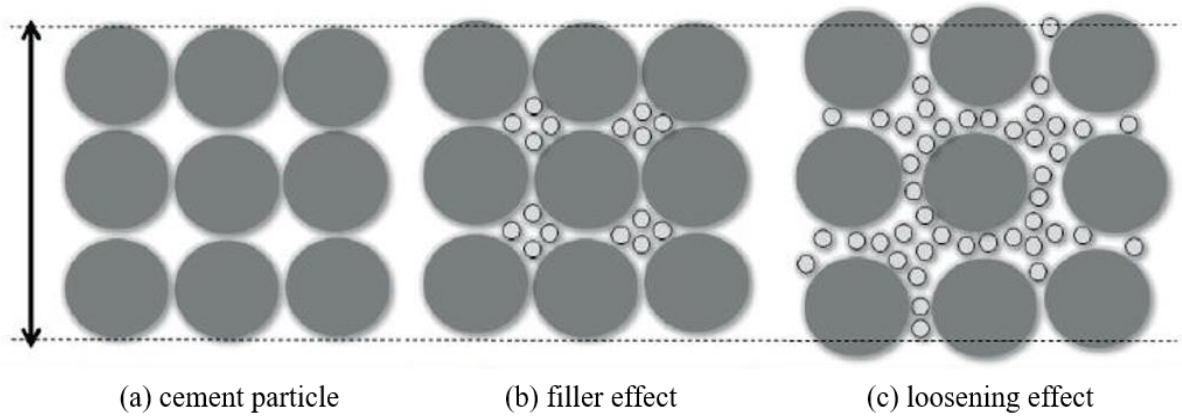

Figure 2.2. Effects of Silica Fume Proportion (Hermann et al. 2016).

2.1.1.3 Strength Development

A low *w*/*c* is key for early strength development of UHPC. The surface of the cement particles begins to form hydrates (e.g., calcium-silicate-hydrate gel) immediately after contacting water. Calcium-silicate-hydrate gel acts as a glue. The hydrated surface grows gradually and is connected with the surface of adjacent cement particles and other particles such as silica fume, fly ash, and fillers (Richardson 2004). The connected hydrates and particles of cementitious materials form a solid network (Barcelo et al. 2001). When the distance between cement particles is short, the hydrates are connected to the adjacent particles with the small amount of hydration at the surface of the cement. Previous research studies (Bentz and Aitcin 2008; Granju and

Grandet 1989; Richardson 2004) have shown that *w*/*c* is a governing factor for the average distance between cement particles, and a low *w*/*c* leads to close distance between cement particles. Therefore, a low *w*/*c* accelerates strength development due to the proximity of cement particles.

However, to keep a desired workability, a low *w*/*c* demands the large amount of HRWR, which causes retardation of hydration, and thus it negatively affects early strength gain. Therefore, finding an optimum balance between *w*/*c*, HRWR content, and packing density that satisfies both the desired workability (i.e., 9.5–10.5 in. flow spread) and early strength (i.e., 12–14 ksi within 16-20 hours) is the key for a successful development of nonproprietary UHPC mixtures for precast, pretensioned bridge girder applications.

2.1.2 Constituent Materials

This section presents the favorable characteristics of constituent materials for selection. The selection of materials, especially for cement and HRWR, is important because early strength gain and workability significantly depend on the characteristics of the cement and HRWR. The two most important factors are the compatibility of cement and HRWR and efficiency of HRWR. If cement and HRWR are not compatible, the desired workability and material properties cannot be achieved. In addition, in case of a low water reduction efficiency of HRWR, a large amount of HRWR is needed. As a result, retardation of hydration may occur and strength gain will be slow. Therefore, the selection of HRWR that is compatible with the selected cement is critical. For the selection of materials (e.g., silica fume, SCM, and sand), particle size distribution is the important criterion that is discussed in following subsections. After selecting constituent materials, trial batches are required to optimize the mixture design. More information is provided in Volume 1 Section 4.3.

2.1.2.1 Cement

Commonly used Type III cement in Texas precast plants was used for the UHPC mixture. To maintain adequate workability and early strength gain, cement water demand higher than normal is not desirable. Therefore, the cement characteristics below are recommended.

- Tricalcium aluminate (C_3A) lower than 11 percent (preferred)
- Blaine Fineness lower than 550 m^2/kg
- Tricalcium silicate (C_3S) greater than 60 percent (preferred)

Note that early strength gain can be achieved by maintaining an optimum *w/cm* through the selection of optimum dosage of HRWR depending on cement characteristics.

2.1.2.2 Silica Fume

Silica fume is the most commonly used and finest cementitious material (average particle size varies from 0.2–1.0 micron) in the UHPC system. It was found to be effective for achieving high packing density through filling the gaps between cement particles and supplementary cementitious materials. The favorable particle size range of silica fume for the developed UHPC mixture is 0.1–10 micron.

2.1.2.3 Supplementary Cementitious Material

A suitable SCM (e.g., fly ash) with particle size range higher than silica fume acts as a filler material in the UHPC system and facilitates achievement of an optimum high packing density. Selecting an SCM (e.g., fly ash) with spherical particle morphology can provide an added benefit of improving flowability / workability through a ball-bearing effect. As fly ash (especially Class F ash) is the most commonly used SCM in Texas, a Class F fly ash was used for developing the nonproprietary UHPC in this project. Fly ash can be replaced by other locally available suitable SCM materials (e.g., ground granulated blast-furnace slag or quartz sand) with comparable particle size distribution.

2.1.2.4 Sand

The use of a natural sand that meets the ASTM C33 (2018) grading requirements for fine aggregates or a masonry sand that satisfies the requirements of ASTM C144 (2018) is recommended for UHPC. In this research project, the impact of the large size particles was studied by removing fine aggregate and masonry sands coarser than #16 from the gradation of ASTM C33 (2018) for fine aggregate and ASTM C144 (2018) for masonry sand. Thus, a comparison of void volumes in the fine aggregate and masonry sand was made between the

maximum particle size of #4 and #16 for fine aggregates composed of natural sand and masonry sand. The results showed that use of a maximum particle size of #4 (natural sand without any particle size adjustment) for both natural sand and masonry sand had less void volume. In addition, the flow spread, the compressive strength, and the resistivity of the UHPC mixture using the #4 sand were comparable with that of the UHPC mixture with #16 sand. Therefore, the use of sands as graded by ASTM C33 (2018) or ASTM C144 (2018) is recommended. Volume 1 report Section 5.3.2 provides more details. Adjustment of the water content and splitting the cement addition in the mix, based on the moisture content of stockpiled sand, is the approach used to maintain the target *w*/*cm*, as described below in Section 2.2.1.

2.1.2.5 High Range Water Reducer

The selection of high range water reducer (HRWR) is important with respect to achieving adequate workability and strength gain. The use of a HRWR with low dispersion efficiency demands a higher quantity of HRWR to get adequate workability but it may lead to retardation of setting time. A polycarboxylate based HRWR has an advanced dispersion efficiency due to its long side chain length (steric repulsion) (Gelardi and Flatt 2016). In addition, a HRWR with a slow adsorption speed increases mixing time, which sometimes may be responsible for creating cold joint between batches when multiple batches are placed sequentially. A highly charged HRWR has a faster adsorption speed (Nkinamubanzi et al. 2016). Thus, the selection of HRWR having a high dispersion efficiency and a fast adsorption speed is recommended. The effectiveness of a HRWR can be compromised if incompatibility exists between HRWR and cementitious materials (cement, silica fume, and a selected SCM). Therefore, it is recommended to select the type and dosage of HRWR through lab-scale trial batch experimentation. It is noted that the dosage of HRWR for UHPC may be higher than the recommended dosage from the manufacturer.

2.1.2.6 Steel fibers

Short straight brass coated steel fibers (0.008 in. diameter and 0.5 in. long) were used for the developed nonproprietary UHPC mixture. The use of other types of fibers (e.g., mineral fibers or synthetic fibers) and hybrid fibers has been reported in the literature. However, studying the performance of UHPC using other fiber types was not in the scope of this project.

2.1.3 Mixture Design

The developed UHPC mixture design is shown in Table 2.1. The mixture design is based on using sand with an oven-dried condition. Therefore, the adjustment of water content and sand content in the mixture design is needed depending on the moisture content of the field sand used at the plant. The UHPC system is sensitive to the combined effects of cement and HRWR. A change in the HRWR and/or a cement type or manufacturer can sometimes lead to an undesirable performance of the UHPC such as an extended mixing time, low flowability, long setting time, or low early strength. Therefore, optimizing the mixture proportions is recommended when constituent material changes. This optimization should be done through trial batches to achieve the desired performance of the UHPC mixture with respect to flowability, setting time, and early strength gain. The process of optimization with new materials is described in Section 2.1.4.

Table 2.1. UHPC Mixture Design.

Constituent Material	Material Weight, lb/yd^3	Description
Cement	1522	Type III cement
Silica fume	114	Densified silica fume
Fly ash	158	Class F
Sand	1706[1]	Max. #4 fine aggregates
Water	326[2]	-
HRWR	36.6	High dispersion efficiency
Steel fiber	200	0.008 in. diameter with 0.5 in. long

Notes:
1. Water and sand weight should be adjusted according to the moisture content of the sand.
2. Water content based on oven-dried sand condition.

2.1.4 Lab-Scale Trial Batch

For the optimization of the mixture proportioning with available materials, the UHPC mixture design shown in Table 2.1 can be considered as a base mixture design. In this project, the analytical feasibility study suggested that the compressive strength at service was not a governing factor for the design of pretensioned bridge girders as long as it was greater than 18 ksi. This was true for the selected geometric and design parameters. The compressive strength

at release was set to be minimum of 65 percent of the compressive strength at service to prevent large creep effects due to releasing strands in relatively premature concrete. More details provide in Volume 2 report Section 3. Note that compressive strengths at service and release and time at release can be determined based upon project specifications. The following steps are the suggested optimization process of the UHPC mixture design.

1. Select constituent materials.
2. Batch the materials as per Table 2.1
3. Mix UHPC following the procedure shown in Section 2.2.1.
4. Conduct a flow table test in accordance with ASTM C1437 (2015)
5. Evaluate the flow spread according to the following criteria.
    a. If the flow spread value is less than 10 in., increase HRWR content while keeping the proportions of the other constituent materials constant. Repeat steps 3 and 4.
    b. If the flow spread value is greater than 10.5 in., reduce the water content while keeping the proportions of the other constituent materials constant. Repeat steps 3 and 4.
    c. If the flow spread value is within 10–10.5 in., the target flowability has been achieved.
6. Prepare a minimum of nine (9) 3x6 in. cylinders for compression testing at 1, 7, and 28 days (3 cylinders per test day).
7. Demold the cylinders at 24 hours $\pm$ 30 minutes. If a compressive strength at release at less than or greater than 24 hours is considered, the cylinders should be demolded at the appropriate time corresponding to the specific target age of release. [Note that in this project, the test times were adjusted for each girder casting as appropriate. For example, compressive strengths were tested at 16 hours and then later at 20 hours or 21 hours, as necessary, to assure the desired compressive strength was obtained prior to release of the prestressing strands.]
8. Conduct end grinding for all the cylinders in accordance with the ASTM C1856 (2017).
9. Determine compressive strength at 1 day. Note that this can correspond to a specific age, such as 16 hours or 24 hours, depending on the planned release time according to the project specifications. If the average 1-day strength is lower than 12 ksi (or the project specific target release strength), reduce the HRWR content with increase in water content

while keeping the proportions of the other constituent materials constant. Repeat Steps 3-9 and ensure that the 1-day strength is greater than 12 ksi.

10. Determine compressive strength at 7 days and 28 days if the compressive strength at 1 day is greater than 12 ksi (or the project specific target release strength).

The optimization process will provide the optimum content of water and HRWR that satisfy both the target flow spread value and the target compressive strength at 1 day (at desired release time) and 28 days. As noted earlier, a HRWR with a low dispersion efficiency may demand a higher dosage. This may cause hydration retardation and strength reduction, which may result in the mixture not meeting the 1-day strength requirement. Therefore, some commercially available HRWR products may not be effective to satisfy both the flow spread value and the compressive strength requirements. As a result, the selection of a HRWR suitable for UHPC is key for a successful UHPC mixture design.

2.2 UHPC MIXING

There are many mixing procedures for proprietary and nonproprietary UHPC mixtures in the literature. However, many of them are for lab-scale UHPC or for proprietary UHPC mixtures that use dried sands. This section presents the mixing procedure with consideration of precast plant environments such as stock-pile condition sand and a large batch volume.

2.2.1 Mixing Procedure

The mixing procedure below is recommended for precast plant applications when using stock-pile sand where the moisture condition must be considered and a batch volume of up to 60 percent of the mixer capacity. The procedure also considers manual fiber addition, as was done in the research project. Automating the fiber addition can reduce the total time needed to mixing each batch. Figure 2.3 shows the recommended mixing procedure and the mixing steps are described as follows.

1. Completely remove the residual water after washing out the mixer drum prior to the first batch.
2. Dry mix the following constituent materials for 3 minutes: the main cement portion (approximately 75 percent of the total weight) plus the silica fume and fly ash.

3. Add water and mix for 2 minutes.
4. Slowly add the HRWR and mix for 6.5 minutes to achieve turnover, which is considered to occur when the paste reaches a good consistency.
5. After turnover of the paste, add sand and mix for 1 minute.
6. Add the tail cement (approximately 25 percent of total weight) and mix for 1 minute.
7. Add steel fibers and mix for 7 minutes.
8. Take a sample for a flow table test and continue mixing for 3 minutes.
9. Discharge the UHPC (26.5 minutes total based on the expected timing).
10. Repeat Step 2–9 for multiple batches as required.

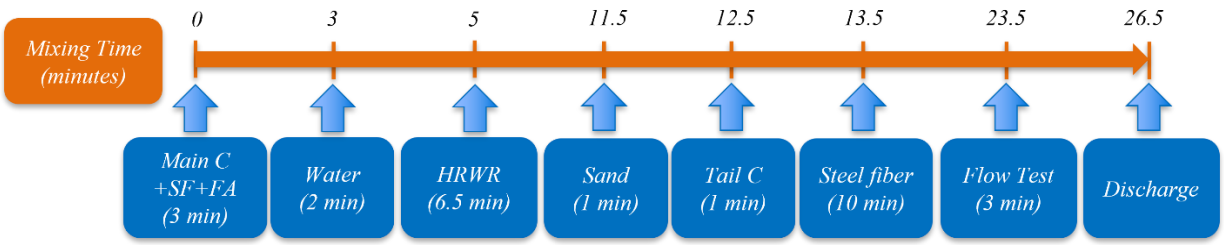

Figure 2.3. Recommended Mixing Procedure.

The flowability of the mixed UHPC is evaluated by a flow table test in accordance with ASTM C1437 (2015). For the flow test, a small amount of fresh UHPC should be sampled and tested immediately. If the flow spread value is within 10–10.5 in., the UHPC can be discharged. The elapsed time for each mixing step may vary depending on the mixer efficiency, the constituent materials, and the use of an automated system for material addition. Therefore, the time can be adjusted according to the specific plant facilities.

There are two main phases within the suggested mixing procedure: (1) the main cement addition, and (2) the tail cement addition. The recommended approach to splitting the cement addition during mixing was adopted to ensure a targeted *w*/*cm* of 0.18 before adding the wet sand. Without splitting the cement addition, the paste has a lower *w*/*cm* than 0.18 prior to adding the wet sand because a portion of the total water content is included in the wet sand. As a result, this condition causes an extension of the mixing time required for turnover of the paste, which is targeted to be achieved within 6.5 minutes after the HRWR addition. Therefore, the cement is split into the main cement portion and tail cement portion to maintain a *w*/*cm* of 0.18 both before and after adding the wet sand. The quantity of the main cement to be added in the first phase is

the amount of cement needed to achieve a *w/cm* of 0.18 using the adjusted water volume based on the moisture content of the sand. The remaining cement quantity is the portion used for the tail cement addition.

Unlike the tail cement, the use of tail HRWR is not intended to split the HRWR. This is additional HRWR that is added to extend the workable time if a longer time for placement is needed. The use of 10 percent additional HRWR can be considered for the extension of the workable time. However, the addition of the tail HRWR should be determined carefully because it may cause a delay in the setting time.

For multiple batches and placements of UHPC, the total mixing time per batch is an important factor because the risk of elephant skin formation on the UHPC surface increases when the time between batches increases. Therefore, minimizing the mixing time is recommended. The key factor contributing to longer mixing times for UHPC is the time for fiber addition. Section 2.2.2.3 describes options to reduce the fiber addition time. In addition, silica fume also was added manually in this research project. Automation of silica fume addition is another potential area to reduce the mixing time and should be considered for safety of workers in order to avoid exposure to the fine silica fume particles.

2.2.2 Large-Scale Trial Batch for Quality of UHPC Production

A trial batch for a representative UHPC volume under precast plant mixing conditions is recommended prior to implementing production of UHPC for use in precast girders or other applications. This trial batch can provide valuable information and experience for UHPC mixing. This section describes the lessons learned from the trial batch conducted in this project prior to mixing UHPC for precast girder fabrication.

2.2.2.1 Removal of Remaining Water in a Mixer Drum

Prior to starting the mixing process for the first batch of UHPC, the mixer drum should be washed out and any remaining water inside the drum should be removed completely. Normally, water and sand are used for cleaning out any remaining concrete in the mixer from the previous batching operations. A small amount of sand and water from the cleaning process might remain in the mixer, and this will impact the flowability. The more water that remains, the higher

flowability and this can lead to segregation of steel fibers. Thus, the remaining water should be removed prior to mixing the first batch of UHPC.

2.2.2.2 Water Addition

The UHPC system is water sensitive. A small increase in water content over the target value can cause an increase in flowability, leading to steel fiber segregation, and can also result in a reduction in strength. Therefore, maintaining the water content close to the designed water content is highly recommended for a successful UHPC batch. The remaining water (if any) inside the mixing drum and/or a higher sand moisture content than the measured value, due to variability in the stockpile, are the potential sources of additional water. This can sometimes be the cause of increasing water content in the first batch of the UHPC if 100 percent water is added at the beginning of the mixing process. As a result, the addition of 90 percent of the total water content is recommended to be added at the water addition step for the first batch. If this provides turnover of the paste within the targeted time (e.g., 6.5 minutes after adding HRWR), there is no need to add the remaining 10 percent water. If the turnover time is longer than the targeted time, which is an indication of insufficient water, adding the remaining 10 percent water is recommended.

2.2.2.3 Fiber Addition

Manual addition of steel fibers is the main time-consuming step in UHPC mixing a 2-3 cyd batch size (i.e., 50–60 percent of the mixer capacity at the precast plant used for this project). Because steel fibers are not a common material for most precast plants, the precast plant may not have an automated system for addition of steel fibers. In addition, pouring steel fibers directly from the bags into the mixer causes clumps of steel fibers to form (eConstruct 2020). The addition of steel fibers in the mixer through a metal screen, which can be fabricated using a wire mesh, that is placed on the mouth of the mixer was found to be effective to ensure proper fiber dispersion during trial batching (see Figure 2.4). To speed up fiber addition, careful application of vibration on the screen using a conventional concrete vibrator was found to be effective. The fiber addition using this screen-vibrator combination took less than 10 minutes for a 3 cyd batch. However, sufficient manpower is needed to facilitate an efficient process. Therefore, automated fiber addition is recommended when producing significant quantities of UHPC.

Figure 2.4. Screen and Vibrator used for Fiber Addition.

There are practices for fiber addition using a fiber feeder (Figure 2.5 and Figure 2.6). Addition of steel fibers into a hopper of a fiber feeder equipped with a vibrator and a screen reduces fiber addition time, and therefore the total mixing time, which can help reduce the possible formation of elephant skin between batches.

(a) Fiber addition into a feeder

(b) Added fibers into a mixer via a feeder

Figure 2.5. Example of Automated Fiber Feeder (Park et al. 2010).

Figure 2.6. Example of Automated Fiber Dosing System at Plant (Berkshire Engineering Supplier 2022).

2.2.2.4 Temperature Control

Many researchers recommended lowering the temperature of fresh UHPC by replacing a portion of the water with ice (El-Tawil et al. 2018; NPCA 2013; Ozyildirim 2011). Based on the findings from this project on UHPC girder fabrication without using chilled water under high ambient temperature conditions (95° F, summer in Texas), adequate workability was achievable at high discharge temperatures (e.g., near 100° F). In addition, the high temperature of fresh UHPC was found to be beneficial for high early strength gain due to acceleration of the cement hydration reaction. Therefore, the use of ice is not recommended for precast, prestressed girder applications as long as the transport and placement of fresh UHPC can be done within 10 minutes.

2.3 TRANSPORT, PLACEMENT, FINISHING, AND CURING

2.3.1 Transport

There are two potential approaches for transport and placement of UHPC with multiple batches: (1) multiple placements using a transport truck at the plant (a Tuckerbuilt was used at the precast plant for this project), and (2) a larger volume single placement where multiple batches are combined using mixer trucks. The use of a mixer truck removes the concern of cold joint formation between the multiple placements. UHPC is prone to quick surface drying, which lead to the formation of a tougher surface layer commonly referred to as elephant skin. If the surface dries sufficiently, this can promote the formation of a barrier between two subsequent batches and potentially formation of a cold joint. However, application of appropriate control measures (e.g., covering the girder using a burlap immediacy after placement with subsequent water sprinkling on continuous basis) was found to be effective to minimize or avoid cold joint formation when placement occurs in multiple batches. In addition, placement can be done in such a way to disturb this outer layer at the surface and break it up so that consecutive batches combine more effectively within the form, as discussed below.

2.3.2 Placement

The UHPC placement procedure affects fiber orientation. Many researchers recommended placing UHPC from one end and let it flow to the other end (AFGC 2013; Wille et al. 2014b; Yoo and Yoon 2016). However, it is not practical for a large volume placement at a precast plant because placement should be done within a relatively short time to avoid forming elephant skin. Moreover, UHPC, unlike conventional concrete, may not maintain adequate flowability to ensure a good flow from one end to the other end over time. Therefore, the leading-edge method, where the fresh UHPC is placed behind the leading edge, is recommended for UHPC placement as shown in Figure 2.7. For multiple placements using a transporter truck, pouring fresh UHPC using the leading-edge placement method allows direct UHPC placement on a previously placed UHPC surface, which facilitates breaking up elephant skin if formed. No internal or external vibration is recommended to avoid segregation of steel fibers.

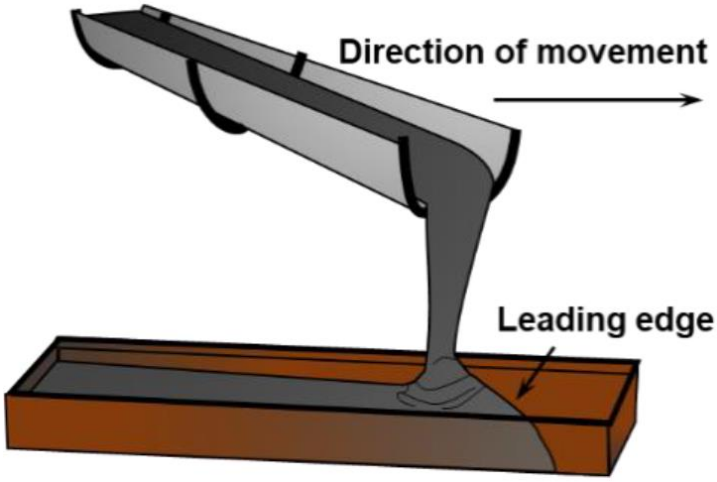

Figure 2.7. Placement using Leading Edge Method (eConstruct 2020).

2.3.3 Finishing

Roughening the top girder surface was attempted to enhance the interface shear strength for composite action with the cast-in-place concrete deck. However, this was found to not be effective. The tendency for the UHPC surface to dry quickly led to a very thin top hard surface with UHPC still in its plastic form immediately below this thin hard layer. An attempt was made to use sharp nails to manually create transverse grooving on the top surface of the first UHPC girder (Tx34-1). However, this procedure was not effective to create adequate grooving because the hardened top surface tended to chip off prior to placing the deck. As a result, this manual method of grooving was not attempted for the remaining two girders (i.e., Tx34-2 and Tx-54). Based on the interface shear performance of the three composite specimens fabricated, it was observed that the shear resistance provided by the U-composite bars was sufficient to provide interface shear resistance without any additional preparation of the top surface of the UHPC. However, if fluting or sand-blasting techniques can be implemented in a precast plant facility, this could aid in enhancing the interface shear resistance and potentially reduce the required amount of interface shear reinforcement.

2.3.4 Curing

After placement, the top girder surface should be covered immediately with a material such as burlap to prevent forming elephant skin due to quick drying. It was found that UHPC girders could be successfully cast without heat treatment while still releasing strands within one day, for

the environmental conditions experienced in this project. However, it is noted that heat treatment can be beneficial for accelerated early strength gain, reduction of shrinkage, improved microstructure, or fabrication of UHPC girders during low ambient temperatures (i.e., lower than 40 °F). The National Precast Concrete Association (NPCA) recommends an environmental temperature between 40 °F and 105 °F for curing (NPCA 2013).

For the UHPC girders cast in this project, heat treatment was not required to reach the desired target compressive strength at release within 21 hours due to the high heat of hydration and outside temperature conditions, which provided an effect similar to heat curing. Note that Tx54 UHPC girder achieved 14.8 ksi at 16 hours using Surecure samples following ambient temperature of 80 °F during the day time and 40 °F during the night time due to the high internal heat of hydration. However, the cast samples had low compressive strengths (3.4 ksi at 18 hours) due to the low temperature during the night time. Therefore, heat treatment can be considered as an option for cooler temperatures.

2.4 EVALUATION AND QUALITY OF UHPC

2.4.1 Categories of Testing

The Precast/Prestressed Concrete Institute (PCI) suggests three categories of testing for UHPC evaluation: qualification testing, acceptance testing, and informational testing (eConstruct 2020), as described below.

- Qualification Testing: The tests under this category are conducted prior to full-scale production to identify if the batching method and mixing process are appropriate. Thus, the qualification testing should be conducted for specimens collected from a large-scale trial batch under the same production environment for a structural element fabrication.
- Acceptance Testing: The tests under this category are conducted for evaluation of fresh and hardened properties using the specimens prepared while fabricating the UHPC girder. The properties measured by the listed tests should meet project specifications.
- Informational Testing: The tests under this category are not required by the project specification but are recommended for informational purposes.

2.4.2 Recommended Tests

Table 2.2 presents the recommended tests for each of these three categories based on the findings from this project, indicated with an "x". Standardized test methods for working time and fiber distribution and orientation are unavailable. The following describe the test methods for working time and fiber distribution and orientation.

Working time: Immediately after completing mixing, place the fresh UHPC in a container (The container used in this project is a 4x8 in. cylindrical mold. A standard for defining the container size was not available). Seal the container completely to prevent dehydration. Conduct a flow table test at discharge and record the flow spread value. Repeat a flow table test every 20 minutes or a preferred time spacing using the UHPC in the container. A recent PCI-sponsored study suggests that for precast applications the working time is considered to be the elapsed time that maintains a flow spread value greater than 7 in. (eConstruct 2020).

Fiber distribution and orientation: Cast a specimen (block) while casting a girder. In this project, 2.0 ft × 1.6 ft × 6.0 ft UHPC block was cast. After hardening, take cores from the specimen along the length and/or the height to see fiber distribution in the direction of interest. If possible, scan the sample by X-ray computed tomography for three-dimensional analysis of fiber distribution and orientation. Cutting a cracked section of a tested prism from a direct tension test or inferred tension bending test is also an option to evaluate distribution of steel fibers. The difference from PCI's recommendations for UHPC evaluation is that Table 2.2 considers direct tension as qualification testing and inferred tension bending test, bulk and surface resistivities, and abrasion resistance as informational testing whereas PCI's recommendations consider inferred tension bending test as qualification testing and do not consider the others.

Table 2.2. Recommended Qualification, Acceptance, and Informational Testing.

Property		Test Method	Qual.	Accept.	Infor.
Fresh Properties	Flow spread	ASTM C1437 (2015)[1]	x	x	NR
	Temperature	ASTM C1064 (2017)	x	x	NR
	Time of set	ASTM C191 (2018)[1]	NR	NR	x
	Density	ASTM C138 (2015)	NR	x	NR
	Working time	-	NR	NR	x
Hardened Properties	Compressive strength	ASTM C39 (2020)[1]	x	x	NR
	Direct tension	AASHTO T 397 Draft (2022)	x	x	NR
	Modulus of elasticity and Poisson's ratio	ASTM C469 (2014)[1]	NR	NR	x
	Inferred tension bending test	ASTM C1609 (2019)[1]	NR	NR	x
	Shrinkage	ASTM C157 (2017)	NR	NR	x
	Creep	ASTM C512 (2015)[1]	NR	NR	x
Durability	Bulk resistivity	ASTM C1760 (2021)	NR	NR	x
	Surface resistivity	AASHTO T 358 (2017)	NR	NR	x
	Rapid chloride ion penetration resistance	ASTM C1202 (2017)[1]	NR	NR	x
	Freeze-thaw resistance	ASTM C666 (2015)[1]	NR	NR	x
	Scaling resistance	ASTM C672 (2012)	NR	NR	x
	Abrasion resistance	ASTM C944 (2012)[1]	NR	NR	x
	Resistance to alkali silica reaction	Mukhopadhyay et al. (2018)	NR	NR	x
Fiber distribution and orientation		-	x	NR	NR

Notes:
1. Use the modified test methods for UHPC according to ASTM C1856 (2017).
2. The following abbreviations are used: Qual. = Qualification testing, Accept. = Acceptance testing, Infor. = Informational testing, NR = Not recommended (considered optional)

2.4.3 Comparison to PCI Recommended Tests

The PCI recommendations for UHPC evaluation (eConstruct 2020) differ somewhat from those provided above. PCI recommends the inferred tension bending test as qualification testing rather

than the direct tension test. In addition, the bulk and surface resistivity tests and abrasion resistance tests are recommended by this project as informational testing, whereas the PCI recommendations do not include these tests.

2.4.4 Evaluation of UHPC

Table 2.3 and Table 2.4 provide the recommended values for evaluation of UHPC by qualification and acceptance testing. The noted values are based on the developed UHPC mixtures for this study and the results obtained while batching the selected UHPC mixtures for three precast, prestressed girder specimens at a precast plant. Some general recommendations are also provided based on this and other studies. For the direct tension test, it should be noted that the recommended 7-day and 28-day strengths are based on the experimental data of the developed UHPC mixture with 1.5 percent fiber volume. It was observed that the 7-day direct tension strength was approximately 0.85 times the 28-day strength for the majority of the specimens fabricated at the precast plant. The design requirements may warrant higher tensile strength values and it must be ensured that the required tensile strength by design is being achieved by the material-level tests conducted.

Table 2.3. Recommended Flow Spread Value for Qualification and Acceptance Testing.

Flow Spread Range, in.	Color Code	Description	Comments
flow < 9.5	Red	Unacceptable	• Poor workability • Higher risk of elephant skin formation
$9.5 \leq$ flow < 10.0	Orange	Acceptable	• Relatively low workability • Some risk of elephant skin formation
$10.0 \leq$ flow ≤ 10.5	Green	Desirable	• Good workability • None or negligible risk of elephant skin • Negligible fiber segregation*
$10.5 <$ flow ≤ 11.0	Yellow	Acceptable	• Some risk of fiber segregation • Better acceptability compared to mixture with flow < 10.0 in.
flow > 11.0	Red	Unacceptable	• High risk of fiber segregation

*Note: This was observed in this project. However, this can vary depending on the viscosity of a UHPC mixture.

Table 2.4. Recommended Values for Qualification and Acceptance Testing.

Property	Recommended Value
Temperature at discharge	80 – 100 °F is recommended. A high discharge temperature near 100 °F demands placement within a relatively short period (less than 10 minutes).
Density	150 – 155 lb/ft^3 is recommended for 1.5 percent fiber volume.
Compressive strength	$f'_{c\ at\ release} \geq 65\%$ of $f'_{c\ at\ sevice}$ [$f'_{c\ at\ release} \geq 12$ ksi when $f'_{c\ at\ service} = 18$ ksi]
Direct uniaxial tension test	0.70 – 0.75 ksi at release, 0.85 – 1.0 ksi at service

3 UHPC GIRDER DESIGN RECOMMENDATIONS

This chapter presents the details of the design recommendations that are generated based on the analytical assessment and the experimental observations of the three UHPC girder specimens tested. The details of the analysis and experiments conducted for this research project are provided in the Volume 1 and 2 reports. This chapter presents the general design procedure followed by guidance on section properties, stress limits, load demands, and prestress loss calculations. In addition, recommended design procedures for UHPC girders with a conventional concrete (CC) composite deck slab are provided for both flexure, web shear, interface shear, splitting resistance reinforcement, camber and deflection, and transfer length. The implementation of these guidelines is documented and elaborated in the form of two detailed design examples in Chapters 4 and 5. It should be noted that at the time of this report, AASHTO was considering proposed draft specifications for design of UHPC members (FHWA 2022) during the final stages of this research. The finalized specifications were approved in May 2023 as this study was being completed. The draft specifications are noted here for reference and discussed with respect to the results and focus of this research. Note that any adopted AASHTO specifications for UHPC girder design should be reviewed and implemented as appropriate.

3.1 GENERAL DESIGN PROCEDURE

The focus of this research project was non the design of precast, pretensioned UHPC bridge girders with a CC composite deck. The general design procedure used for this girder type are listed below.

1. Establish the geometric and material design parameters.
    - Determine the girder properties using the geometric properties of the girder section and material properties of the selected UHPC mixture.
    - Determine the CC deck properties considering the deck geometry and material properties of the selected CC mixture.
    - Determine the composite deck and girder section properties.
2. Determine the design dead load and live load demands on the bridge girder as per the requirements of the *AASHTO LRFD Bridge Design Specifications* AASHTO (2020).

Based on the respective service and strength limit states applicable for the bridge superstructure, the load factors are determined according to AASHTO (2020).

3. Compute the prestress losses, including short-term and long-term effects, for the selected number of strands.
4. Finalize the number of strands, and the initial and final prestressing forces, by checking the stresses at release and at service conditions.
5. Determine the nominal flexural resistance and check the flexural strength limit state.
6. Determine the nominal shear strength and check the shear strength limit state at all critical sections.
7. Compute the camber due to prestressing and deflections due to loading over time.
8. Check the live load deflection versus the limit as per AASHTO (2020).

3.2 GEOMETRIC AND MATERIAL PARAMETERS

3.2.1 Material Properties

3.2.1.1 UHPC

The UHPC material properties are recommended to be obtained from material level-testing of the UHPC mixture according to the guidance provided in Chapter 2. Referencing the experimental record of the data for the UHPC mixture being used is highly recommended because the flexure strength and shear strength of UHPC girders are sensitive to the material properties. In the absence of experimental data, the initial design may assume the values provided in Table 2.4 for the developed nonproprietary UHPC mixture. Qualification and acceptance testing should then be conducted, as discussed in Chapter 2, to ensure the mixture is suitable for the intended application and to confirm that the required properties are achieved when fabricating the girders. Based on the literature and from research conducted in this study, the following recommendations may be adopted.

1. *Compressive Strength of UHPC at Release*: Typically, release of prestress occurs at 16-20 hours after casting. As noted in the Volume 1 report, to limit creep effects, the compressive strength of UHPC at release f'_{ci} is recommended to be taken as:

$$f'_{ci} = 0.65 f'_c \tag{3.1}$$

where:

f'_c =Compressive strength of UHPC at service (typically taken as 28 days), ksi

Therefore, for a f'_c of 18 ksi, the specified f'_{ci} can be taken as 12 ksi.

2. *Tensile Strength of UHPC at Release*: Based on the experimental data of UHPC specimens fabricated from the precast plant mixture, documented in the Volume 2 report, the tensile strength at release f'_{ti} can be taken as follows,

$$f'_{ti} \leq 0.85 f'_t \tag{3.2}$$

where:

f'_t=Tensile strength of UHPC at service, ksi

Therefore, for a minimum f'_t of 0.85 ksi, the maximum specified f'_{ti} should be 0.72 ksi. Note that the service tensile strength f'_t is typically determined at an age of 28 days.

3. *Modulus of Elasticity of UHPC*: Based on the experimental data of UHPC specimens fabricated from the precast plant mixture, documented in the Volume 1 report, the modulus of elasticity E_c can be estimated as follows,

$$E_c = 1430\sqrt{f'_c} \tag{3.3}$$

where:

f'_c= Compressive strength of UHPC at service (28 days), ksi

The E_c values determined during testing ranged from approximately 6300 to 6700 ksi at 3 days and approximately 6300 – 7400 ksi at 28 days. In the absence of experimental data for the modulus of elasticity, the above equation may be used in combination with the early age or 28-day compressive strength, as applicable.

For reference, the AASHTO draft specifications for UHPC (FHWA 2022) provides the following equation for estimating the MOE:

$$E_{UHPC} = 2500K_1 {f'_c}^{0.33} \tag{3.4}$$

where:

f'_c = Specified compressive strength of UHPC at the given age, ksi

K_1 = Correction factor of MOE to be considered as 1.0 unless determined experimentally

3.2.1.2 Conventional Concrete

A compressive strength of 4 ksi for a TxDOT standard Class S conventional concrete deck slab is adopted for the design examples in this volume. The unit weight and modulus of elasticity of conventional concrete may calculated using AASHTO (2020), Section 3.5.1 and Section 5.4.2.4, respectively, as follows:

$$E_c = 120{,}000\ K_1 {w_c}^2 {f'_c}^{0.33} \tag{3.5}$$

where:

K_1 = Correction factor for aggregate source to be taken as 1.0 unless determined by physical test

w_c = Unit weight of concrete (kcf), 0.145 kcf

f'_c = Compressive strength of CC at service, ksi

3.2.1.3 Prestressing Strand

Standard prestressing strand properties are adopted and should be confirmed with the mill report. The design examples and tested UHPC girder specimens use 0.6 in. diameter Grade 270, low relaxation steel strands with a specified ultimate tensile strength of 270 ksi.

3.2.1.4 Mild Steel Reinforcement

The standard TxDOT mild steel reinforcement properties for the deck slab and end block girder reinforcement are used as per the TxDOT Prestressed Concrete I-Girder Details (TxDOT 2017). The CC deck slab consists of Grade 60 mild steel reinforcement as per the TxDOT Bridge Design Manual (TxDOT 2023). As per TxDOT recommendations, the CC deck slab may be

either fully cast-in-place (CIP) or CIP with prestressed concrete panels (PCPs) that serve as stay-in-place (SIP) concrete formwork. UHPC girders are recommended to have reduced transverse reinforcement due to the enhanced shear capacity of the UHPC imparted by the steel fibers. Grade 60 mild steel U-shaped bars are also provided for interface shear resistance. Additional details for the recommended mild streel reinforcement are provided in the specific design examples in this report volume.

3.2.2 Geometric Properties

3.2.2.1 Composite Girder Section

The specified cross-section properties of the standard TxDOT girders are adopted for the noncomposite UHPC girder sections (TxDOT 2017). For the composite girder section, the geometric properties of the CC deck slab and CC haunch are transformed based on the modular ratio of the UHPC and CC materials, where $n = E_{c(UHPC)}/E_{c(CC)}$. The width of the deck slab and haunch are transformed using the modular ratio n, while maintaining the actual thickness. The thickness of the deck slab is considered as the standard 8.5 in. used by TxDOT Bridge Design Manual (TxDOT 2023). A haunch thickness of 2 in. is adopted for the design examples.

3.2.2.2 Bridge Geometry

The total bridge span length is considered as the back-wall to back-wall distance and the girder length is considered as the length spanning between the ends of the girder, which is the difference between the total span length and the gaps between the back-wall and the girder ends. For analysis purposes, the center-to-center bearing span length is adopted and the distance between the center of the bearing pad to the end of the girder, i.e., the bearing offset, is considered as the standard 9 in. dimension used by TxDOT (TxDOT 2015).

The overhang beyond the centerline of the exterior girders on either side is assumed to be 3 ft. The spacing of the girder depends on the number of girders selected. The enhanced strength of UHPC provides additional flexibility to reduce the number of girder lines for standard span lengths. The superior strength also allows for an increase in the span length for a given shape; or the use of a shallower girder section for a given span length, while maintaining the same number

of girder lines. This advantage is due to the superior tensile and compressive stress limits for UHPC.

3.3 LOAD DEMANDS

The bridge girder is evaluated for all forces due to all load demands applied to the superstructure, including dead load, superimposed dead load, and live load. Minimum load requirements, load factors, and load combinations are adopted in this guide as per the recommendations in Table 3.4.1-1 of AASHTO (2020). A brief summary is provided below.

3.3.1 Dead Loads

Dead loads due to the self-weight of the girder, deck, and haunch are considered to act on the non-composite member. The wearing surface and the barrier loads are considered to act on the composite bridge girder. The unit weights for the deck, haunch, and wearing surface are adopted from Table 3.5.1-1 of AASHTO (2020). The average weight of railing is taken from TxDOT standard traffic rail detail for the respective type. The unit weight of the developed UHPC mixture developed is reported as 150.6–152.4 kcf in the Volume 1 report, Section 6.3.2. This unit weight is rounded to 0.155 kcf and an additional 0.005 kcf is included to account for the weight of prestressing strands and mild steel reinforcement, similar to CC, giving a total of 0.160 kcf. This value is then used to estimate the UHPC girder weight in the design examples.

3.3.1.1 Wearing Surface

A standard asphalt wearing surface unit weight of 0.140 kcf was adopted for dead load computation based on AASHTO (2020), Section 3.5.1. A standard two in. thick bituminous wearing surface is considered in the design example calculations.

3.3.1.2 Barriers

A barrier rail is considered along each of the bridge considered. The unit weight of the selected barrier rail is included in the superimposed dead load computation. For example, TxDOT (2014) describes the T551 traffic rail. The weight of both barriers are distributed evenly to each girder of the bridge, such that the weight of one railing is not distributed to more than three girders

following the recommendations provided in the TxDOT *Bridge Design Manual* (TxDOT 2023), Section 4.

3.3.1.3 Summary

Table 3.1 summarizes the values used for computing dead loads.

Table 3.1. Summary of Dead Load Values.

Parameter	**Value**
Unit weight of CC deck and haunch	0.150 kcf
Unit weight of UHPC	0.160 kcf
Unit weight of wearing surface, γ_{ws}	0.140 kcf
Linear weight of railing, T551, w_r	0.382 klf

3.3.2 Live Loads

The standard HL-93 loading is considered for the live load analysis. The loading is considered as a combination of the design truck/tandem and design lane load. The multiple presence factors provided in Table 3.6.1.1.2-1 of AASHTO (2020) are considered based on the number of loaded design lanes selected.

3.3.3 Live Load Distribution Factors

Live load distribution factors may be computed using AASHTO (2020) equations in Section 4.6.2.2. Table 4.6.2.2.2b-1 and 4.6.2.2.2d-1 are used for moment and Table 4.6.2.2.3a-1 and Table 4.6.2.2.3b-1 are used for shear.

For prestressed concrete I-girder with concrete deck and with two or more design lanes loaded, the live load distribution factor for moment g_m is computed as follows:

$$g_m = 0.075 + \left(\frac{S}{9.5}\right)^{0.6} \left(\frac{S}{L}\right)^{0.2} \left(\frac{K_g}{12.0Lt_s{}^3}\right)^{0.1} \tag{3.6}$$

where:

S = Girder spacing, ft

L = Span length, ft

K_g	=	Longitudinal stiffness parameter, in.^{4}
t_s	=	Depth of concrete slab, in.

3.3.4 Load Combinations

Appropriate load factors are adopted in the design examples based on the applicable combination of factored effects specified in the AASHTO LRFD Specifications (AASHTO (2020), Section 3.4.1. For the design examples provided in this report, the Strength I and Service III limit states are evaluated, similar to the feasibility study documented in the Volume 2 report.

3.4 PRESTRESS LOSSES

Prestress losses in pretensioned members arise due to a combination of elastic shortening during the prestressing operation and long-term losses due to shrinkage, creep, and relaxation of prestressing strands. The total losses due to prestress for prestressed girders are typically calculated using the formulas provided in the AASHTO LRFD Specifications (AASHTO 2020), Section 5.9.3. Note that AASHTO draft specifications for UHPC (FHWA 2022) allows the use of AASHTO LRFD Specifications Section 5.9.3 with the following amendments.

- The limit of compressive strength (15 ksi) shall not apply.
- The approximate estimate of time-dependent losses (Section 5.9.3.3) shall not apply.
- The equations for creep and shrinkage parameters shall be replaced by those given in the AASHTO draft specifications for UHPC.

The procedure to estimate prestress losses in this guide follows the current AASHTO LRFD formulas in Section 5.9.3 and amendments from AASHTO draft specifications for UHPC (FHWA 2022) with the following modifications.

- The prestress loss at transfer due to autogenous shrinkage that occurs during the time between final set and transfer is also considered.
- The developed equations for creep and shrinkage predictions from this study are presented as an alternative to the equations from AASHTO draft specifications for UHPC (FHWA 2022) when implementing high early strength UHPC mixtures similar to those tested in this project.

3.4.1 Prestress Losses at Transfer

The prestress loss at transfer in CC pretensioned members is determined by computing the elastic shortening using the expression in the AASHTO LRFD Specifications (AASHTO 2020) Article 5.9.3.2.3a-1. For CC, elastic shortening of concrete is the only factor considered for prestress loss at transfer. For UHPC, however, prestress loss due to autogenous shrinkage occurs during the time between final set and prestress transfer especially for UHPC mixtures designed for high early strength and should also be considered. A value of 200 με is recommended for the autogenous shrinkage that occurs between final set and transfer based on the results of this research (see Volume 2 Report Section 7.2.3.1). Note that AASHTO draft specifications for UHPC (FHWA 2022) does not include the autogenous shrinkage that occurs during the time between final set and transfer, whereas the PCI study considers 600 με autogenous shrinkage at transfer (eConstruct 2020). The prestress loss at transfer due to elastic shortening and autogenous shrinkage is calculated using the following equations,

$$\Delta f_{pST} = \Delta f_{pES} + \Delta f_{pshi} \tag{3.7}$$

$$\Delta f_{pES} = \frac{E_p}{E_{ct}} f_{cgp} \tag{3.8}$$

$$\Delta f_{pshi} = \varepsilon_{shi} E_p K_i \tag{3.9}$$

where:

Δf_{pST} = Prestress loss at transfer, ksi

Δf_{pES} = Prestress loss due to elastic shortening at transfer, ksi, according to AASHTO LRFD Equation 5.9.3.2.3a-1 (AASHTO 2020)

E_{ct} = Modulus of elasticity of concrete at transfer or time of load application, ksi

Δf_{pshi} = Prestress loss due to autogenous shrinkage occurring during the time between final set and transfer, ksi, according to Equation 5.4.1-2 (eConstruct 2020)

f_{cgp} = Concrete stress at the center of gravity of prestressing tendons due to the prestressing force immediately after transfer, ksi

E_p = Modulus of elasticity of prestressing strand, 28,500 ksi

ε_{shi} = Autogenous shrinkage strain occurring between the time between final set and transfer, 200×10^{-6} in./in. (from this study)

K_i = Transformed section coefficient that accounts for initial (elastic) interaction between concrete and bonded steel, assumed to be 0.83 according to Section F.1.6.1 of eConstruct (2020)

3.4.2 Long-Term Time Dependent Losses

3.4.2.1 Long-Term Prestress Losses

The total prestress loss Δf_{pT} has two components: the first component is the short-term prestress loss occurring at transfer, described above, and the second component is the long-term prestress losses occurring due to creep and shrinkage of the UHPC girder and relaxation of prestressing strands as shown in the equations below.

$$\Delta f_{pT} = \Delta f_{pST} + \Delta f_{pLT} \tag{3.10}$$

$$\Delta f_{pLT} = (\Delta f_{pSR} + \Delta f_{pCR} + \Delta f_{pR1})_{id} + (\Delta f_{pSD} + \Delta f_{pCD} + \Delta f_{pR2} - \Delta f_{SS})_{df} \tag{3.11}$$

where:

Δf_{pT} = Total prestress loss, ksi

Δf_{pLT} = Long-term prestress loss, ksi, according to AASHTO LRFD Equation 5.9.3.4.1-1 (AASHTO 2020)

Δf_{pSR} = Prestress loss due to shrinkage of girder occurring between transfer and deck placement, ksi, according to AASHTO LRFD Equation 5.9.3.4.2a-1 (AASHTO 2020)

Δf_{pCR} = Prestress loss due to creep of girder occurring between transfer and deck placement, ksi, according to AASHTO LRFD Equation 5.9.3.4.2b-1 (AASHTO 2020)

Δf_{pR1} = Prestress loss due to relaxation of prestressing strands occurring between transfer and deck placement, 1.2 ksi for low-relaxation strands according to AASHTO LRFD Bridge Design Specifications Section 5.9.3.4.2c (AASHTO 2020)

Δf_{pSD} = Prestress loss due to shrinkage of girder occurring between time of deck placement and final time, ksi, according to AASHTO LRFD Equation 5.9.3.4.3a-1 (AASHTO 2020)

Δf_{pCD} = Prestress loss due to creep of girder occurring between time of deck placement and final time, ksi, according to AASHTO LRFD Equation 5.9.3.4.3b-1 (AASHTO 2020)

Δf_{pR2} = Prestress loss due to relaxation of prestressing strands in composite section between deck placement and final, $\Delta f_{pR2} = \Delta f_{pR1} = 1.2$ ksi for low-relaxation strands according to AASHTO LRFD Bridge Design Specifications Section 5.9.3.4.3c (AASHTO 2020)

Δf_{pSS} = Prestress gain due to shrinkage of deck in composite section, ksi, according to AASHTO LRFD Equation 5.9.3.4.3d-1 (AASHTO 2020)

3.4.2.1.1 Prestress Losses between Transfer and Deck Placement

Prestress losses due to creep and shrinkage time between transfer and deck placement can be calculated using the following equations,

$$\Delta f_{pSR} = \varepsilon_{bid} E_p K_{id} \tag{3.12}$$

$$\Delta f_{pCR} = \frac{E_p}{E_{ci}} f_{cgp} \psi_{b\,(t_d, t_i)} K_{id} \tag{3.13}$$

$$K_{id} = \frac{1}{1 + \frac{E_p}{E_{ci}} \frac{A_{ps}}{A_g} \left(1 + \frac{A_g e_{pg}^2}{I_g}\right) \left[1 + 0.7 \psi_{b\,(t_f, t_i)}\right]} \tag{3.14}$$

where:

ε_{bid} = Shrinkage strain of UHPC girder time between transfer and deck placement, in./in.

K_{id} = Transformed section coefficient that accounts for time-dependent interaction between concrete and bonded steel between transfer and deck placement, according to AASHTO LRFD Equation 5.9.3.4.2a-2 (AASHTO 2020)

$\psi_{b(t_d,t_i)}$ = Creep coefficient of UHPC girder at time of deck placement due to loading at transfer

e_{pg} = Eccentricity of prestressing force with respect to centroid of girder, in.

t_d = Age at deck placement, day

$\psi_{b(t_f,t_i)}$ = Creep coefficient of UHPC girder at final due to loading at transfer

t_f = Final age, day

t_i = Age of concrete at time of transfer, day

3.4.2.1.2 Prestress Losses between Deck Placement and Final Time

Prestress losses due to creep and shrinkage time between deck placement and final can be calculated as follows:

$$\Delta f_{pSD} = \varepsilon_{bdf} E_p K_{df} \tag{3.15}$$

$$\Delta f_{pCD} = \frac{E_p}{E_{ci}} f_{cp} \left[\psi_{(t_f,t_i)} - \psi_{(t_d,t_i)}\right] K_{df} + \frac{E_p}{E_c} \Delta f_{cd} \psi_{b(t_f,t_d)} K_{df} \tag{3.16}$$

$$K_{df} = \frac{1}{1 + \frac{E_p}{E_{ci}} \frac{A_{ps}}{A_c} \left(1 + \frac{A_c e_{pc}^2}{I_c}\right) \left[1 + 0.7\psi_{b(t_f,t_i)}\right]} \tag{3.17}$$

where:

ε_{bdf} = Shrinkage strain of UHPC girder time between deck placement and final, in./in.

K_{df} = Transformed section coefficient that accounts for time-dependent interaction between concrete and bonded steel between deck placement and final time, according to AASHTO LRFD Equation 5.9.3.4.3a-2 (AASHTO 2020)

e_{pc} = Eccentricity of prestressing force with respect to centroid of composite section, in.

A_c = Gross composite section area, in^2

I_c = Moment of inertia of transformed composite section area, in^4

Δf_{cd} = Change in concrete stress at centroid of prestressing strands due to long-term losses between transfer and deck placement, ksi

$\psi_{b_{(t_f,t_d)}}$ = Creep coefficient of UHPC girder at final due to loading at deck placement

Prestress gain due to shrinkage of deck in composite section can be calculated using the following equations.

$$\Delta f_{pSS} = \frac{E_p}{E_c}(\Delta f_{cdf})(K_{df})\left[1 + 0.7\psi_b(t_f, t_d)\right] \tag{3.18}$$

$$\Delta f_{cdf} = \frac{\varepsilon_{ddf} A_d E_{c\ deck}}{\left[1 + 0.7\psi_d(t_f, t_d)\right]}\left(\frac{1}{A_c} - \frac{e_{pc} e_d}{I_c}\right) \tag{3.19}$$

where:

Δf_{cdf} = Change in concrete stress due to shrinkage of deck concrete at centroid of prestressing strands, ksi, according to AASHTO LRFD Equation 5.9.3.4.3d-2 (AASHTO 2020)

$\psi_b(t_f, t_d)$ = Girder creep coefficient at final time due to loading at deck placement

ε_{ddf} = Shrinkage strain of deck concrete between placement and final time, in./in.

A_d = Area of deck concrete, in^2

$E_{c\ deck}$ = Modulus of elasticity of deck concrete, ksi

$\psi_d(t_f, t_d)$ = Creep coefficient of deck concrete at final time due to loading immediately after deck placement

e_{pc} = Eccentricity of prestressing force with respect to centroid of composite section, in.

e_d = Eccentricity of deck with respect to the gross composite section, in.

3.4.2.2 Creep Prediction Models

Table 3.2 shows the expressions and parameters for creep prediction to provide a comparison of the AASHTO LRFD Specifications (AASHTO 2020), the AASHTO draft specifications for UHPC (FHWA 2022), and the findings from this study. The ultimate creep coefficient of the current AASHTO LRFD Specifications, $\psi_{ult} = 1.9$, is quite high for UHPC applications. The

AASHTO draft specifications for UHPC uses 1.2 for the ultimate creep coefficient. This value is based on the creep test results of eight proprietary UHPCs (Mohebbi and Graybeal 2022). However, the considered proprietary UHPC mixtures were not developed for high early strength gain. The ultimate creep coefficient (1.2) determined for those mixtures is higher than the value (0.8) from this study.

For determining the prestress losses for the developed UHPC mixture, the use of the proposed creep prediction equation and parameters provides accurate estimates (see Volume 1 Report Section 6.5.1). Note that the humidity correction factor K_{hc} and loading age correction factor K_L need additional study because of the lack of test data for different humidity conditions and due to the limited testing for different loading ages. However, because of the extremely low water content in the developed UHPC mixture, the mixture should not be highly affected by humidity. Thus, a value of 1.0 for the humidity correction factor is considered reasonable. In addition, due to the high early strength gain characteristics of the developed UHPC mixture, effects from early age loading may be less significant.

Table 3.2. Comparison of Parameters for Creep Prediction Equations.

Factor	AASHTO LRFD	FHWA (2022)	This Study
Creep coefficient equation, $\psi_{(t,ti)}$	$\psi_{ult}K_{hc}K_fK_sK_{td}t_i^{-0.118}$	$\psi_{ult}k_sk_{hc}k_fk_Lk_{td}k_3$	$\psi_{ult}K_{hc}K_fK_sK_{td}$
Ultimate creep coefficient, ψ_{ult}	1.9	1.2	0.8
Humidity correction factor, K_{hc}	$1.56 - 0.008H$	$1.12 - 0.0024H$	1.0
Strength correction factor, K_f	$\frac{5}{(1+f'_{ci})}$	$\frac{18}{(1.5f'_{ci}-3)}$	$\frac{19}{(7+f'_{ci})}$
Size correction factor, K_s	$1.45 - 0.13\left(\frac{V}{S}\right) \geq 1.0$	1.0	$1.0 + 0.2\left[0.45 - 0.13\left(\frac{V}{S}\right)\right] \geq 1.0$
Time development factor, K_{td}	$\frac{t}{12(\frac{100-4f'_{ci}}{f'_{ci}+20})+t}$	$\frac{t}{(\frac{300}{f'_{ci}+30}+0.8t^{0.98})}$	$\frac{t^{0.6}}{(8+t^{0.6})}$
Loading age correction factor, K_L	$t_i^{-0.118}$	1.0 for $t_i < 7$, $(t_i-6)^{-0.15} \geq 0.5$ for $t_i \geq 7$	1.0

Notes:
H = Humidity, %
V = Volume, in^3
S = Surface area, in^2
t = Time, days
t_i = Age of concrete at time of loading application, days
f'_{ci} = Compressive strength at release, ksi
k_3 = UHPC material correction factors for creep, assumed to be 1.0 without a physical test. Using the creep test, according to ASTM 512 (2015), k_3 is taken as the ratio of the measured ultimate creep coefficient to the predicted value.

3.4.2.3 Shrinkage Prediction Models

Table 3.3 shows expressions and parameters for shrinkage prediction to provide a comparison of the AASHTO LRFD Specifications (AASHTO 2020), the AASHTO draft specifications for UHPC (FHWA 2022), and the findings from this study. The current AASHTO LRFD Specifications AASHTO (2020) uses 480 microstrain for the ultimate shrinkage strain. This

value is not applicable for UHPC because UHPC has a higher shrinkage strain due to increased autogenous shrinkage. The AASHTO draft specifications for UHPC (FHWA 2022) and this study recommend an ultimate shrinkage strain 600×10^{-6} and 700×10^{-6}, respectively. These values are quite close. For the developed UHPC mixture in this study, the use of $700 \times 10^{-6}$with additional suggested parameters predicts shrinkage strain accurately (see Volume 1 Report, Section 6.5.2).

Table 3.3. Comparison of Parameters for Shrinkage Prediction Equations.

Factor	AASHTO LRFD	FHWA (2022)	This Study
Shrinkage strain, ε_{sh}	$480 \times 10^{-6} K_{hs} K_f K_s K_{td}$	$600 \times 10^{-6} k_s k_{hs} k_f k_{td} k_4$	$700 \times 10^{-6} K_{hs} K_f K_s K_{td}$
Humidity correction factor, K_{hs}	$2 - 0.014H$	$1.5 - 0.01H$	$1 + 0.2(1 - 0.014H)$
Strength correction factor, K_f	$\frac{5}{(1 + f'_{ci})}$	$\frac{18}{(1.5f'_{ci} - 3)}$	$\frac{19}{(7 + f'_{ci})}$
Size correction factor, K_s	$1.45 - 0.13\left(\frac{V}{S}\right) \geq 1.0$	1.0	$1 + 0.2\left[0.45 - 0.13\left(\frac{V}{S}\right)\right] \geq 1.0$
Time development factor, K_{td}	$\frac{t}{12(\frac{100 - 4f'_{ci}}{f'_{ci} + 20}) + t}$	$\frac{t}{(\frac{300}{f'_{ci} + 30} + 0.8t^{0.98})}$	$\frac{t^{0.6}}{(4 + t^{0.6})}$

Notes:
- H = Humidity, %
- V = Volume, in^3
- S = Surface area, in^2
- t = Time, days
- f'_{ci} = Compressive strength at release, ksi
- k_4 = UHPC material correction factors for shrinkage, assumed to be 1.0 without a physical test. Using the shrinkage test, according to ASTM C157 (2017), k_4 is taken as the ratio of the measured total shrinkage strain to the predicted value.

3.5 TRANSFER LENGTH

A transfer length of 30 d_b may be used for design for the developed UHPC mixture. The details of the research conducted on the transfer length of UHPC for this research program are documented in the Volume 2 report, Section 7.1.5. Note that the bond strength between UHPC and the prestressing strands has been found to be superior to that of typical CC members (Graybeal 2019). The transfer length was found to be less than the value of 60 d_b recommended

by AASHTO (2020), Section 5.9.4.3. FHWA (2022) recommends a transfer length of 24 d_b for UHPC members.

3.6 FLEXURE DESIGN FOR SERVICE LIMIT STATE

3.6.1 General

This section explains the flexure design recommendations for the service limit state for prestressed UHPC bridge girders. These recommendations are based on the project findings and the AASHTO LRFD Bridge Design Specifications (AASHTO 2020) and the draft specifications for UHPC girder design proposed by FHWA (2022) and under consideration by AASTHO.

The Service III limit state is used as per AASHTO (2020) Section 3.4.1 to check the stress limits at each load stage. These stress limits typically govern the feasible number of strands for a given span length, taking into consideration the prestressing losses. Typically, the stresses in a simply supported girder are controlled by the stresses at the beam ends at release and at the midspan section at service. The stress limits and standard service stress checks to be evaluated are described below. Further guidance for calculating the composite deck and girder section properties, including selection of modulus of elasticity values, are provided in the design examples included in this report.

3.6.2 Notation for Stress Checks

The following notation is used for the stress checks provided below.

A_g = gross area of the section, in^2

e_{end} = eccentricity of prestressing force with respect to centroid of girder at the ends, in.

e_{mid} = eccentricity of prestressing force with respect to centroid of girder at midspan, in.

F_e = total prestressing force after losses, kips

F_i = total prestressing force before losses, kips

f_c' = design compressive strength of UHPC at 28 days, ksi

f_{cd}' = design compressive strength of conventional concrete at 28 days, ksi

f_{ci}' = design compressive strength of UHPC at time of prestressing, ksi

f_t' = design tensile strength of UHPC at 28 days, ksi

f'_{ti} = design tensile strength of UHPC at time of prestressing, ksi

M_g = midspan moment due to girder self-weight, kip-in.

M_{gt} = moment at the transfer length due to girder self-weight, kip-in.

M_h = midspan moment due to haunch self-weight, kip-in.

M_{ht} = moment at the transfer length due to haunch self-weight, kip-in.

M_L = factored midspan moment due to live load, kip-in.

M_{Lt} = factored moment at the transfer length due to live load, kip-in.

M_r = midspan moment due to railing self-weight, kip-in.

M_{rt} = moment at the transfer length due to railing self-weight, kip-in.

M_s = midspan moment due to deck slab self-weight, kip-in.

M_{st} = moment at the transfer length due to deck slab self-weight, kip-in.

M_{ws} = midspan moment due to wearing surface self-weight, kip-in.

M_{wst} = moment at the transfer length due to wearing surface self-weight, kip-in.

S_b = section modulus for the extreme bottom fiber of the girder section, in^3

S_{bc} = section modulus for the extreme bottom fiber of the composite section, in^3

S_t = section modulus for the extreme top fiber of the girder section, in^3

S_{tc} = section modulus for the extreme top fiber of the composite section, in^3

S_{tgc} = section modulus for the extreme top fiber of the girder of the composite section, in^3

3.6.3 Flexural Stress Limits

Key to prestressed girder design are the stress limits permitted for various load stages. The limits for the maximum tension and compressive stresses in the concrete under flexure, must be satisfied when selecting the number of prestressing strands and their arrangement. The following stress limits are considered for the prestressing strands and the service stress checks of the UHPC cross-section.

3.6.3.1 Prestressing Strand

The stress limits for prestressing steel should satisfy AASHTO (2020) Table 5.9.2.2-1, where the stress limit for low relaxation steel immediately prior to transfer f_{pbt} is 75 percent of the

specified minimum tensile strength of the prestressing strands f_{pu}. Therefore, for low relaxation Grade 270 prestressing steel, f_{pu} = 270 ksi and f_{pbt} = 202.5 ksi.

3.6.3.2 UHPC

The stress limits recommended by the proposed AASTHO draft specifications for UHPC (FHWA 2022) based on the research conducted by El-Helou and Graybeal (2022) are considered in these guidelines. These higher tensile limits are a deviation from the AASHTO (2020) limits for tension due to the superior tensile strength and performance of UHPC attributed by the steel fibers. These stress limits lead to the advantage of allowing higher prestressing forces for UHPC pretensioned bridge girders relative to standard pretensioned bridge girders. However, the recommended relationships to establish compression stress limits for UHPC girders (FHWA 2022) are the same as those used for conventional concrete girders provided by AASHTO (2020).

3.6.3.2.1 Allowable Stress Limits at Release of Prestress

Compression

The compressive stress limit at release of prestress σ_{ci} for prestressed UHPC bridge girders are based on the recommended draft specifications for UHPC FHWA (2022). This relationship is consistent with that for conventional concrete girders (AASHTO 2020),

$$\sigma_{ci} = 0.65 f'_{ci} \tag{3.20}$$

where:

f'_{ci} = Compressive strength of UHPC at the time of prestressing, ksi

Tension

The recommended tensile stress limit at release σ_{ti} for prestressed UHPC bridge girders is based on the recommendations from FHWA (2022) and El-Helou and Graybeal (2022),

$$\sigma_{ti} = 0.85 f'_{ti} \tag{3.21}$$

where:

f'_{ti} = Tensile strength of UHPC at the time of prestressing, ksi

3.6.3.2.2 Allowable Stress Limits at Service

Compression

The recommended compressive stress limit at service σ_c for prestressed UHPC bridge girders is based on the recommended draft specifications for UHPC (FHWA 2022). This relationship is consistent with that for CC girders (AASHTO 2020) as follows,

$$\sigma_c = 0.60 f'_c \tag{3.22}$$

where:

f'_c = Compressive strength of UHPC for design at service, ksi

Tension

The recommended tensile stress limit for prestressed UHPC bridge girders is consistent with the recommendation from FHWA (2022) and El-Helou and Graybeal (2022),

$$\sigma_t = 0.85 f'_t \tag{3.23}$$

where:

f'_t = Tensile strength of UHPC for design at service, ksi

3.6.4 Flexural Stress Checks

The following stress checks evaluate the maximum stresses due to the prestressing force, eccentricity of the prestressing force, and the effects of loading at different load stages. These expressions are specifically applicable for simply supported pretensioned bridge girders, which are the focus of the design examples in this report volume. The sign convention is negative for compressive stresses and positive for tensile stresses.

3.6.4.1 Stresses at Release of Prestress

Girder Ends

At top (girder):

$$f_{top} = -\frac{F_i}{A_g} + \frac{F_i e_{end}}{S_t} - \frac{M_{gt}}{S_t} \leq 0.85 f'_{ti} \tag{3.24}$$

At bottom (girder):

$$f_{bottom} = -\frac{F_i}{A_g} - \frac{F_i e_{end}}{S_b} + \frac{M_{gt}}{S_b} \geq -0.65 f'_{ci} \tag{3.25}$$

Midspan

At top (girder):

$$f_{top} = -\frac{F_i}{A_g} + \frac{F_i e_{mid}}{S_t} - \frac{M_g}{S_t} \leq 0.85 f'_{ti} \tag{3.26}$$

At bottom (girder):

$$f_{bottom} = -\frac{F_i}{A_g} - \frac{F_i e_{mid}}{S_b} + \frac{M_g}{S_b} \geq -0.65 f'_{ci} \tag{3.27}$$

3.6.4.2 Stresses at Time of Deck Placement

Unshored deck construction is being considered.

Girder Ends

At top (girder):

$$f_{top} = -\frac{F_e}{A_g} + \frac{F_e e_{end}}{S_t} - \frac{M_{gt} + M_{st} + M_{ht}}{S_t} \geq -0.45 f'_c \tag{3.28}$$

At bottom (girder):

$$f_{bottom} = -\frac{F_e}{A_g} - \frac{F_e e_{end}}{S_b} + \frac{M_{gt} + M_{st} + M_{ht}}{S_b} \leq 0.85 f'_t \tag{3.29}$$

Midspan

At top (girder):

$$f_{top} = -\frac{F_e}{A_g} + \frac{F_e e_{mid}}{S_t} - \frac{M_g + M_s + M_h}{S_t} \geq -0.45 f_c' \tag{3.30}$$

At bottom (girder):

$$f_{bottom} = -\frac{F_e}{A_g} - \frac{F_e e_{mid}}{S_b} + \frac{M_g + M_s + M_h}{S_b} \leq 0.85 f_t' \tag{3.31}$$

3.6.4.3 Stresses at Service Due to Effective Prestress and Permanent (Dead) Load

Girder Ends

At top (deck slab):

$$f_{top,deck} = -\frac{M_{wst} + M_{rt}}{S_{tc}} \geq -0.45 f_{cd}' \tag{3.32}$$

At top (girder):

$$f_{top} = -\frac{F_e}{A_g} + \frac{F_e e_{end}}{S_t} - \frac{M_{gt} + M_{st} + M_{ht}}{S_t} - \frac{M_{wst} + M_{rt}}{S_{tgc}} \geq -0.45 f_c' \tag{3.33}$$

At bottom (girder):

$$f_{bottom} = -\frac{F_e}{A_g} - \frac{F_e e_{end}}{S_b} + \frac{M_{gt} + M_{st} + M_{ht}}{S_b} + \frac{M_{wst} + M_{rt}}{S_{bc}} \leq 0.85 f_t' \tag{3.34}$$

Midspan

At top (deck slab):

$$f_{top} = -\frac{M_{ws} + M_r}{S_{tc}} \geq -0.45 f_{cd}' \tag{3.35}$$

At top (girder):

$$f_{top} = -\frac{F_e}{A_g} + \frac{F_e e_{mid}}{S_t} - \frac{M_g + M_s + M_h}{S_t} - \frac{M_{ws} + M_r}{S_{tgc}} \geq -0.45 f_c' \tag{3.36}$$

At bottom (girder):

$$f_{bottom} = -\frac{F_e}{A_g} - \frac{F_e e_{mid}}{S_b} + \frac{M_g + M_s + M_h}{S_b} + \frac{M_{ws} + M_r}{S_{bc}} \leq 0.85 f_t' \tag{3.37}$$

3.6.4.4 Stresses at Service Due to Effective Prestress and Total Load

<u>*Girder Ends*</u>

At top (deck slab):

$$f_{top} = -\frac{M_{wst} + M_{rt} + M_{Lt}}{S_{tc}} \geq -0.60 f_{cd}' \tag{3.38}$$

At top (girder):

$$f_{top} = -\frac{F_e}{A_g} + \frac{F_e e_{end}}{S_t} - \frac{M_{gt} + M_{st} + M_{ht}}{S_t} - \frac{M_{wst} + M_{rt} + M_{Lt}}{S_{tgc}} \geq -0.60 f_c' \tag{3.39}$$

At bottom (girder):

$$f_{bottom} = -\frac{F_e}{A_g} - \frac{F_e e_{end}}{S_b} + \frac{M_{gt} + M_{st} + M_{ht}}{S_b} + \frac{M_{wst} + M_{rt} + M_{Lt}}{S_{bc}} \leq 0.85 f_t' \tag{3.40}$$

<u>*Midspan*</u>

At top (deck slab):

$$f_{top} = -\frac{M_{ws} + M_r + M_L}{S_{tc}} \geq -0.60 f_{cd}' \tag{3.41}$$

At top (girder):

$$f_{top} = -\frac{F_e}{A_g} + \frac{F_e e_{mid}}{S_t} - \frac{M_g + M_s + M_h}{S_t} - \frac{M_{ws} + M_r + M_L}{S_{tgc}} \geq -0.60 f_c' \tag{3.42}$$

At bottom (girder):

$$f_{bottom} = -\frac{F_e}{A_g} - \frac{F_e e_{mid}}{S_b} + \frac{M_g + M_s + M_h}{S_b} + \frac{M_{ws} + M_r + M_L}{S_{bc}} \leq 0.85 f_t' \tag{3.43}$$

3.7 FLEXURE STRENGTH LIMIT STATE

3.7.1 General

In addition to the stress checks outlined above, flexural design for UHPC girders must also consider the ultimate flexure capacity that is evaluated by the Strength I limit state in the AASHTO LRFD Bridge Design Specifications (AASHTO 2020), Section 3.4.1.

3.7.2 Review of UHPC Draft Specifications

Design specifications for UHPC girders recommended by FHWA (2022), which exist in their draft stage at the time of the development of these guidelines, suggest the use of a triangular stress block in the compression zone of the girder as shown in Figure 3.1. This model is consistent with the recommendations of El-Helou and Graybeal (2022). For UHPC girder sections where the UHPC section provides the primary contribution to the compression force for developing the nominal moment strength, it is recommended that the flexural capacity be determined using the model shown in Figure 3.1. In addition, the contribution of the tension force resisted by the UHPC can be determined as shown. The stress distribution across the cross section is considered to be linearly elastic when the strain in compression is less than or equal to the elastic compression strain limit ε_{cp}. The tensile stresses are considered to be elastic until reaching the strain at effective cracking stress $\varepsilon_{t,cr.}$ The limit of strain in tension is denoted by the average localization strain $\varepsilon_{t,loc.}$

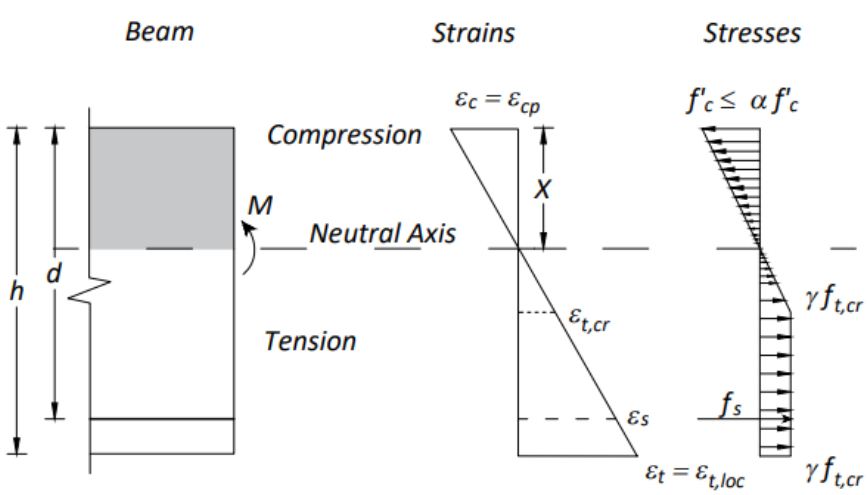

Figure 3.1. Triangular Stress Block for UHPC (adapted from El-Helou and Graybeal (2022)).

3.7.3 Composite UHPC Girders with Conventional Concrete Deck

This research project considered UHPC girders composite with a CC deck. In this case, the CC deck provides the primary contribution to the internal compression force developed in flexure at ultimate conditions. Note that AASHTO (2020) Section 5.6.2.2 indicates the use of a rectangular stress block for modeling CC, which is applicable for the CC deck in compression.

For the girder designs considered in this project, it was found that all or a significant portion of the compression force was resisted by the CC deck concrete. In these cases, the rectangular stress block assumption provided a simple and conservative estimate of the flexural strength. The following approach can be adopted to determine the nominal moment strength in such cases.

- The depth of the equivalent rectangular stress block a is β_1 times the depth of the neutral axis from the compressive fiber, where the factor β_1 is dependent on the compressive strength of the CC concrete as per AASHTO (2020) Section 5.6.2.2.
- When the compression force provided by the UHPC girder is small relative to the compression forces provided by the CC deck, a simple rectangular stress distribution can also be effective in computing the flexural strength of the UHPC portion of the section. In this case, a value of 0.65 may be adopted for β_1 for the UHPC section due to the high strength of UHPC.
- The sum of forces in compression and tension are equated to zero to locate the position of the neutral axis and the moment capacity of the cross-section is determined by multiplying the total compressive force or the total tensile force with the lever arm. The lever arm is the distance between the centroid of the total compression force and the centroid of the total tension force of the composite section. For simplicity, it is conservative to neglect the contribution of the UHPC to the tension force in the section.
- The flexural capacity is calculated using Equation (3.44) based on AASHTO (2020), Section 5.6.3.2. Note that this simple expression neglects the contribution of the tension force provided by the portion of the UHPC girder section in tension.

$$M_n = NA_p f_{ps}\left(d_p - \frac{a}{2}\right) \tag{3.44}$$

where:

N	=	Number of prestressing strands
A_p	=	Area per prestressing strand, in^2
f_{ps}	=	Average stress in prestressing steel at the time for which the nominal resistance of member is required, ksi, according to AASHTO (2020) equation 5.6.3.1.1-1.
d_p	=	Distance from extreme compression fiber to the centroid of the prestressing strands, in.
a	=	Depth of equivalent rectangular stress block, in.

The rectangular stress block approach may be used for the I-shaped girders with a composite CC deck due to simplicity and effectiveness of design for girders similar to those tested in this project. A comparison between the approaches in AASHTO (2020) and FHWA (2022) is documented in Volume 2 report (Section 5.5) for the three experimental girder specimens designed and tested under flexure as a part of this research program. The feasibility design study, documented in the Volume 2 report (Chapter 3), showed that the rectangular stress block was more conservative for girder designs using 0.6 in. diameter strands, while the triangular stress block model was more conservative when using 0.7 in. diameter strands. It is suggested that when the neutral axis extends into the UHPC girder, one should compare the results for both models. If the rectangular stress block model is more conservative, it may be used.

The UHPC draft specifications proposed model in Figure 3.1 can be applied to the UHPC girder section, as well. As discussed in the Volume 2 report, the approach outlined in the UHPC draft specifications gave conservative estimates of the nominal flexure capacity: 3.2% less than the experimental capacity for the Tx34-1 specimen, 7.9% less for the Tx34-2 girder specimen, and 13.4% less for Tx54 girder specimen. Note that only a small portion of the top flange of the UHPC of Tx54 girder was under compression and, in each of these estimates, the tension capacity of the UHPC was considered.

3.8 SHEAR STRENGTH LIMIT STATE

3.8.1 Nominal Shear Strength

The nominal shear capacity of the section is determined by the Equation (3.45), which is consistent with the proposed AASHTO draft specifications for UHPC (FHWA 2022). This expression, along with the accompanying relationships provided below, predicted the shear capacity of the UHPC girder specimens closely based on the experimental research documented in the Volume 2 report with the exception of one girder specimen, where the shear capacity recommendation overpredicted the shear capacity by approximately 20 percent. The AASHTO LRFD Specifications (AASHTO 2020) expressions for the shear contribution of the transverse steel reinforcement and harped prestressed tendons are also used in the AASHTO draft specifications for UHPC (FHWA 2022) and are recommended in these guidelines. The contribution of UHPC to shear capacity is different than that of CC to account for the improved tensile strength and performance of UHPC due to the post-cracking ductility imparted by the steel fibers. Based on the research documented in the Volume 2 report, Section 6.1.3, the shear capacity of the UHPC was found to be directly proportional to the first cracking tensile strength of UHPC measured experimentally from the companion direct uniaxial tension test specimens using the method outlined in the AASHTO T 397 Draft (2022).

$$V_n = V_{UHPC} + V_S + V_P \tag{3.45}$$

where:

V_n = Nominal shear resistance, kips

V_{UHPC} = Nominal shear resistance of UHPC, kips

V_S = Shear resistance provided by transverse steel reinforcement, kips

V_P = Prestressing force component in the direction of the shear force (vertical component), kips

The three components of the shear capacity are computed using the following expressions. Equation (3.46) is based on the formula recommended by El-Helou and Graybeal (2022) and El-Helou and Graybeal (2023). These are also elaborated and compared with other methods in the Volume 2 report, Section 6.1.3.1 and Section 6.6.4.

$$V_{UHPC} = f'_t b_w d_v \cot(\theta) \tag{3.46}$$

$$V_S = \frac{A_v f_y d_v \cot(\theta)}{s} \tag{3.47}$$

$$V_P = N_h A_p f_{pe} \sin(\alpha) \tag{3.48}$$

where:

f'_t	=	First cracking tensile strength of UHPC based on experimental data, ksi
b_w	=	Width of web section, in.
d_v	=	Effective shear depth, in.
θ	=	Shear crack angle, degrees
A_v	=	Area of transverse steel reinforcement, in^2
f_y	=	Yield strength of transverse steel reinforcement, ksi
s	=	Vertical spacing of transverse steel reinforcement, in.
N_h	=	Number of harped strands
A_p	=	Cross-sectional area of an individual prestressing strand, in^2
f_{pe}	=	Effective stress in prestressing strands after losses, ksi
α	=	Angle of harping, degrees

The crack angle is computed using Equation (3.49). The details of this method and the comparison with the experimental test data is documented in the Volume 2 report, Section 6.1.3.4.

$$\theta = \cot^{-1}\left(\sqrt{1 + \left|\frac{F/A}{f_t'}\right|}\right) \tag{3.49}$$

where:

F	=	Prestressing force after losses, kips
A	=	Area of the girder, in^2
f'_t	=	Uniaxial tensile stress, ksi

3.8.2 Minimum Transverse Shear Reinforcement

In general, the use of minimum transverse reinforcement is recommended to enhance the ductility in case of impending shear cracking if the bridge girder is overloaded. The transverse reinforcement can also be extended into the deck and used for interface shear resistance. Application of the minimum shear reinforcement leads to beneficial ductility and higher shear capacity as observed in the full-scale shear testing reported in Volume 2 report, Section 6.6.5.

The minimum transverse shear reinforcement requirement is adapted from the AASHTO LRFD Specifications (AASHTO 2020), Section 5.7.2.3. This requirement states that minimum transverse reinforcement must be provided when the following condition occurs,

$$V_u \geq 0.5\phi\,(V_{UHPC} + V_P) \tag{3.50}$$

where:

ϕ = Shear resistance factor, 0.9

The above expression requires that when the factored design shear force exceeds the 50 percent of the reduced nominal shear strength provided by the UHPC girder and any vertical component of prestressing at the considered section location, minimum transverse steel must be provided. However, as noted earlier, the use of minimum transverse reinforcement is generally recommended for enhanced ductility and shear strength.

The requirements for minimum transverse reinforcement are taken from AASHTO (2020), Section 5.7.2.6, where the minimum transverse reinforcement spacing is as follows:

If $v_u < 0.125f'_c$:

$$s_{max} = 0.8d_v \leq 24 \text{ in.} \tag{3.51}$$

If $v_u \geq 0.125f'_c$:

$$s_{max} = 0.4d_v \leq 12 \text{ in.} \tag{3.52}$$

where:

v_u = Shear stress $= \frac{|V_u - \phi V_P|}{\phi b_w d_v}$

FHWA (2022) recommends that the spacing of the transverse reinforcement shall not exceed the maximum permitted spacing s_{max} given as:

$$s_{max} = 0.25 d_v \cot(\theta) \leq 24 \text{ in.} \tag{3.53}$$

3.8.3 Transverse Reinforcement for Shear Strength

Transverse shear reinforcement is required for strength when the following condition occurs.

$$V_u \geq \phi\,(V_{UHPC} + V_P) \tag{3.54}$$

In this case, one option to strengthen the beam for shear is to design transverse reinforcement (addition of V_S) to provide the required nominal shear strength for the UHPC girder at locations where the shear strength must be increased, similar to CC girder design (see Eq. (3.47)). The requirements for minimum transverse reinforcement, noted above, are also applicable.

3.9 INTERFACE SHEAR DESIGN

3.9.1 Interface Shear Resistance

The minimum interface shear requirements may be computed using Section 5.7.4.3 of AASHTO (2020) where the interface consists of placement of CC on clean, laitance free UHPC without intentional roughening. Interface shear resistance is determined as follows. These recommendations are consistent with FHWA (2022).

$$V_{ni} = cA_{cv} + \mu\left(A_{vf} f_y + P_c\right) \tag{3.55}$$

where:

c = Cohesion factor as per AASHTO (2020), Section 5.7.4.4, ksi (0.075 ksi)

A_{cv} = Area of concrete engaged in interface shear transfer, in^2

μ = Friction factor as per AASHTO (2020), Section 5.7.4.4 (0.6)

A_{vf} = Area of steel reinforcement crossing shear plane within A_{cv}, in^2

f_y = Yield strength of transverse steel reinforcement, ksi

P_c = Permanent net compressive force normal to the shear plane, kips

Effective surface roughening of the top surface of the UHPC girder was found to be difficult due to the self-consolidating nature of UHPC; therefore, it is likely necessary to provide additional reinforcement for interface shear resistance between the CC deck and UHPC girder in additional to the existing minimum transverse shear reinforcement.

3.9.2 Reinforcement for Interface Shear Strength

Shear reinforcement needed for composite action at the interface shear critical region in excess of the required transverse shear reinforcement may be provided by higher diameter hooks (bundled U shaped #5 bars of 12 in. length were used for the tested girders in this project) or high strength steel studs (Crane 2010). Figure 3.2 presents the U composite bar detail provided in the girder specimens.

AASHTO (2020) Section 5.7.4.2 and FHWA (2022) recommend that the cross-sectional area of the interface shear reinforcement A_{vf} that crosses the area resisting the interface shear A_{cv} should satisfy the following condition. More details are provided in the design examples.

$$A_{vf} = \frac{0.05A_{cv}}{f_v} \tag{3.56}$$

where:

A_{vf} = Interface shear reinforcement area crossing the shear plane encompassing the area A_{cv}, in^2

A_{cv} = Area of concrete engaged in interface shear transfer, in^2

f_y = Yield stress of steel reinforcement, 60 ksi

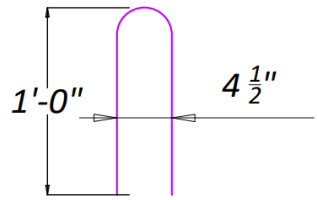

Figure 3.2. U-shaped Composite Bar Detail used for Interface Shear Resistance.

3.10 SPLITTING RESISTANCE

3.10.1 General Recommendations

The unreinforced ends of the tested UHPC girder specimens were not damaged after the release of strands and during application of service and factored demands to the girders. Therefore, the improved tensile strength of the UHPC girder due to the presence of steel fibers was determined to be sufficient to withstand the release of the prestressing strands. Consistent with the guidelines provided by the PCI study on UHPC (Tadros 2021), it is recommended that the splitting reinforcement is reduced because the current limits for CC girders are very conservative when applied to UHPC girders.

Reinforcement is recommended at the ends of the pretensioned beams to resist the bursting stresses occurring due to end zone prestressing operations. Although the superior tensile strength of UHPC is effective in resisting these forces without any reinforcement, it is suggested to provide minimum splitting resistance reinforcement, as described below.

3.10.2 Minimum Splitting Resistance Reinforcement

The approach used in the AASHTO draft specifications for UHPC may be applied to determine the minimum splitting resistance reinforcement, as shown in Equation (3.57). This equation accounts for the tensile strength of UHPC as per FHWA (2022) .

$$f_s A_s + 0.25\gamma_u f'_t h b_v \geq 0.04 P_i \tag{3.57}$$

where:

f_s = Stress in steel, 20 ksi

γ_u = UHPC tensile reduction factor, should not be greater than 0.85, to account for variability in direct tension test results.

A_s = Area of transverse steel located in $h/4$ distance from ends, in^2

h = Total girder depth, in.

b_v = Width of the girder web, in.

f'_t = Uniaxial tensile stress, ksi

P_i = Prestressing force at release, kips

3.10.3 Alternate Method

An alternate mechanics-based method is also provided below based on this research project. The total area of steel to resist the bursting forces may be found such that the following condition is satisfied at prestress transfer.

$$f_s A_s \geq 0.04 P_i \tag{3.58}$$

To determine the equivalent area of transverse reinforcement assumed to be contributed by the steel fibers, the following expression is considered,

$$\frac{\rho_{fiber} f_{fiber}}{3} = \frac{A_{v_eq} f_{stirrup}}{b_v \left(h/4 \right)} \tag{3.59}$$

where:

A_{v_eq} = Equivalent stirrup area contributed by steel fibers, in^2

$f_{stirrup}$ = Yield stress of mild steel transverse reinforcement, ksi

ρ_{fiber} = Volume of steel fibers, percent

f_{fiber} = Tensile strength of steel fibers, ksi

h = Total girder depth, in.

b_v = Width of the girder web, in.

3.10.4 Basic Layout of Mild Steel Reinforcement

Figure 3.3 presents the basic layout of the mild steel reinforcement for shear resistance, interface shear resistance, and splitting resistance for a typical UHPC I-girder. Detailed design drawings will be presented with the respective design examples.

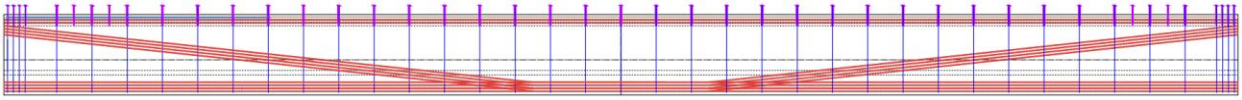

Figure 3.3. Reinforcement Details.

3.11 CAMBER AND DEFLECTION

Camber and deflection are computed using the self-weight of the bridge deck system, prestressing, live load as well as the effect due to creep, shrinkage, and relaxation of steel. Camber calculations include the dead load of the UHPC girder, CC deck and haunch, superimposed dead load, and the effect due to prestressing.

The following creep coefficients at the time of deck placement and service conditions are considered using the proposed creep model as per the Volume 1 report with parameters as follow:

- 60 percent RH
- 11.7 ksi compressive strength at release
- 18 ksi compressive strength at service
- 3.5 volume-to-surface area ratio

Creep coefficient at 90 days (deck placement) $\psi_{CR} = 0.53$

Creep coefficient at 27,375 days (final) $\psi_{CR} = 0.80$

The growth of camber at transfer, before and after deck placement, and final (service) stages are computed as per the recommendations provided by eConstruct (2020), which uses the PCI multipliers method with updated multipliers (eConstruct 2020). Note that this method tends to overestimate camber, while a more accurate prediction can be obtained using the time step method, as discussed in the Volume 2 report Section 7.2.3.

Deflection at transfer,

$$\Delta_{at_transfer} = \left(\Delta_{gtr} + \Delta_{PS}\right) \tag{3.60}$$

Deflection before deck placement,

$$\Delta_{before_deck} = \left(\Delta_{g_{tr}} + \Delta_{PS}\right)(1 + \psi_{CR}) + \left(\Delta_{PS_loss}(1 + 0.7\psi_{CR})\right) \tag{3.61}$$

Deflection after casting deck,

$$\Delta_{after_deck} = \left(\Delta_{g_{tr}} + \Delta_{PS}\right)(1 + \psi_{CR}) + \left(\Delta_{PS_loss}(1 + 0.7\psi_{CR})\right) + \Delta_{sl} \tag{3.62}$$

Final deflection,

$$\Delta_{final} = \left(\Delta_{g_{tr}} + \Delta_{PS}\right)(1 + \psi_{CR}) + \left(\Delta_{PS_loss}(1 + 0.7\psi_{CR})\right) + \Delta_{sl} + \Delta_{SI} \tag{3.63}$$

where:

$\Delta_{g_{tr}}$	=	Deflection due to girder self-weight at transfer, in.
Δ_{PS}	=	Camber due to prestressing, in.
Δ_{PS_loss}	=	Deflection due to prestress losses, in.
Δ_{sl}	=	Deflection due to deck slab and haunch, in.
Δ_{SI}	=	Deflection due to super imposed dead load, in.

The live load deflection check is carried out as per AASHTO (2020) Section 3.6.1.3.2 to ensure that the deflection of the bridge deck is within the recommended limit as per AASHTO (2020), Section 2.5.2.6.2.

4 DESIGN EXAMPLE FOR TX34

4.1 BACKGROUND AND SIGNIFICANCE

There are several advantages of using UHPC for the development of structural designs with slender members and higher capacity. The superior durability of UHPC justifies the high initial cost of the analysis due to the lower maintenance requirements for UHPC structural elements. UHPC is already being used in many applications in connections, overlays, and retrofitting of steel and concrete connections. The use of UHPC in full-scale structural elements such as bridge girders, piers, and deck slabs is known to have significant potential due to the pioneering work done globally and in the US. The Texas Department of Transportation (TxDOT) is interested in evaluating the application of UHPC in standard bridge girders in Texas. Based on the research conducted for the nonproprietary UHPC mixture development from locally sourced materials in Texas and full-scale testing of precast pretensioned UHPC girders, two design examples are developed for the implementation of UHPC Tx-shaped bridge girders. The Texas 34 design example is described in this chapter.

4.2 DETAILED DESIGN EXAMPLE FOR A UHPC TX34 GIRDER

This design example evaluates the use of UHPC Tx34 girders in combination with a conventional concrete deck slab for a 46 ft wide bridge. The objective of this design example is to present the design modifications that need to be made to account for the use of UHPC. This design example highlights the elimination of one girder line to five girder lines while achieving a span length comparable to that with six girder lines for a conventional concrete Tx34 design option. This example shows how the design can be made more economical using UHPC by reducing the volume of the concrete for one girder line and the resulting superstructure weight on the piers.

4.3 BRIDGE GEOMETRY AND MATERIAL PROPERTIES

This section provides geometric details of the bridge superstructure and the material properties of the concrete components, wearing surface, and prestressing steel. Concrete components include the deck slab including the haunch, and the railing, which are composed of reinforced conventional concrete, and the girders that are composed of pretensioned UHPC members.

4.3.1 Geometric Properties

The geometric parameters of the bridge superstructure are listed in Table 4.1 and will be explained in further detail. The bridge superstructure comprises a simply supported UHPC bridge girder with a composite conventional concrete deck slab.

Figure 4.1 presents the bridge cross-section detail for this design example.

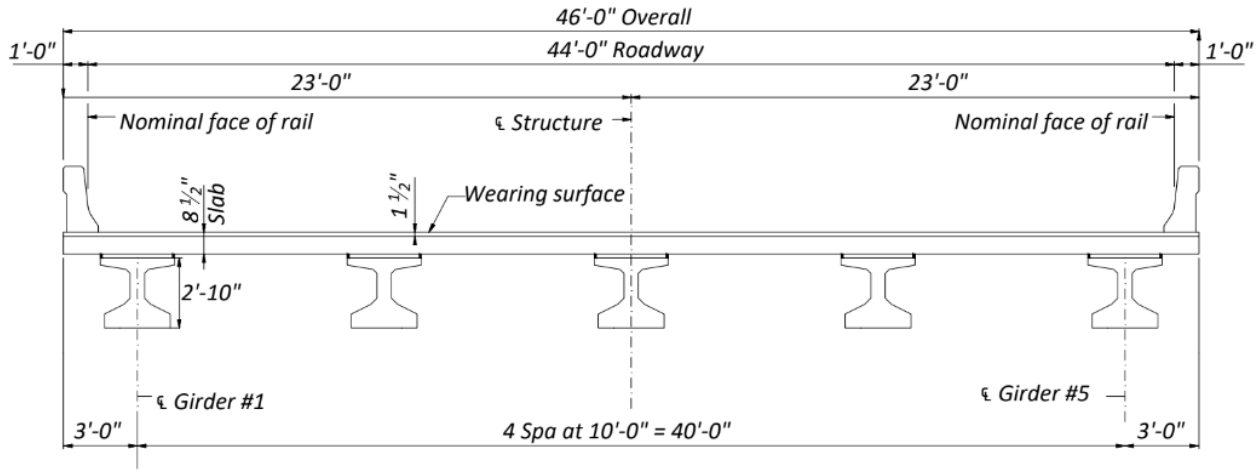

Figure 4.1. Bridge Cross-Section Details.

Table 4.1. Geometric Properties of Tx34 Bridge.

Parameter	**Value**
Bridge width, W	46 ft
Back-wall to back-wall distance, L_{br}	85 ft
Bearing span length, L	83 ft
Number of girders	5
Girder center-to-center spacing, s	10 ft
Overhang beyond the centerline of the exterior girders on each side	3 ft
Thickness of deck slab, t_s	8.5 in.
Thickness of asphalt wearing surface, t_{ws}	2 in.
Thickness of haunch, t_h	2 in.
Number of lanes, N_L	3
Multiple presence factor, m as per Table 3.6.1.1.2-1 of AASHTO LRFD (AASHTO 2020)	0.85

4.3.2 Material Properties

This section lists the material properties of the concrete components such as the deck and haunch, which are composed of conventional concrete, and the girder, composed of UHPC. This section also documents the characteristics of prestressing strands used for the design.

4.3.2.1 Ultra-High Performance Concrete (UHPC)

Owing to the superior mechanical properties of UHPC, when compared to conventional concrete, a higher compressive strength f'_{ci} of 11.7 ksi at release and 28-day compressive strength f'_c of 18 ksi at service are used in this study. These values are selected as the minimum required compressive strengths at release and service and will be checked for adequacy in the design checks provided in this example. Note that the minimum f'_{ci} is recommended to be taken as 0.65 f'_c to minimize early age creep effects. One of the key material properties of UHPC is its improved tensile strength, ductility, and energy absorption capacity due to the presence of steel fibers. The higher tensile strength is attributed to the use of fibers, as mentioned in design guides and codes such as ACI 544.4R-18 (2018), AFGC (2013), and Model Code (2010), and in the research conducted by FHWA (FHWA 2022). The parameters needed for design computations pertaining to UHPC are provided in Table 4.2. These parameters are based on the average typical experimental test results from the full-scale companion specimens fabricated with the Tx54 girder specimen. Note that the lower limits of tensile strengths are chosen to be conservative.

Table 4.2. Properties of UHPC for Tx34 I-Girders.

Parameter	**Value**
Compressive strength at release, f'_{ci}	11.7 ksi
28-day compressive strength at service, f'_c	18.0 ksi
Elastic tensile strength at release, f'_{ti}	0.72 ksi
Elastic tensile strength at service, f'_t	0.85 ksi
Post cracking tensile strength, f'_{tu}	0.85 ksi
MOE at release, E_{gi}	6742 ksi
MOE at service, E_g	7423 ksi
Unit weight of reinforced UHPC, γ_{UHPC}	0.160 kcf

In the absence of experimental data, the modulus of elasticity of UHPC can be computed using one of the available empirical expressions. The expression developed through material level testing of the developed nonproprietary UHPC, as described in the Volume 1 report, is shown in Equation (4.1).

$$E_{UHPC} = 1430\sqrt{f_c'} \tag{4.1}$$

where:

f_c' = Specified compressive strength of UHPC at the given age, ksi

For reference, the equation for analytically predicting MOE recommended by the AASHTO draft specifications for UHPC (FHWA 2022) is as follows:

$$E_{UHPC} = 2500K_1 f_c'^{0.33} \tag{4.2}$$

where:

K_1 = Correction factor of MOE to be considered as 1.0 unless determined experimentally

The modulus of elasticity computed for the two design examples using the empirical equations listed above are compared with the experimental modulus of elasticity. Table 4.3 shows that the experimental modulus of elasticity is higher that the predicted values, with the percentage values relative to the measured value listed in the table. Therefore, the empirical relationships do not overpredict the measured MOE values with the FHWA (2022) expression providing a close prediction of the experimental values. The experimental values are being used in the design example.

Table 4.3. Comparison of Experimental and Computed MOE.

Description		E_{gi}, **ksi**		E_g, **ksi**	
Present Research	Experimental	6742	-	7423	-
	Empirical (Eq. 4.1)	4891	73%	6067	82%
Draft UHPC Specs (Eq. 4.2)		5629	83%	6489	87%

4.3.2.2 Conventional Concrete Deck Slab

The material properties of conventional Class S concrete are considered for the deck of the bridge as summarized in Table 4.4.

Table 4.4. Properties of Conventional Concrete Deck.

Parameter	**Value**
28-day compressive strength at service, f'_{cd}	4.0 ksi
MOE, E_d	3987 ksi
Unit weight of reinforced concrete, γ_{cc}	0.150 kcf

The modulus of elasticity of conventional concrete has been computed using the empirical equation provided in the AASHTO LRFD Specifications (AASHTO 2020) Article 5.4.2.4-1, shown in Equation (4.3).

$$E_c = 120{,}000 K_1 w_c^{2.0} f_c'^{0.33} \tag{4.3}$$

where:

K_1 = Correction factor based on the source of aggregate, unless otherwise found by physical test it is assumed to be 1.0, and as per the owner's approval

w_c = Unit weight of concrete, kcf

f'_c = Characteristic compression strength of UHPC at the given age, ksi

It is to be noted that the unit weight of conventional concrete is assumed to be 0.145 kcf for calculation of E_c, which is consistent with TxDOT practice.

4.3.2.3 Wearing Surface and Barrier Details

It was assumed that the deck slab is topped up with an asphalt wearing surface having the properties listed in Table 3.1. One of the heaviest barriers, T551, was also added as a superimposed dead load. The weight of both the barriers is distributed to all five girders of the bridge, following the guidance provided in the TxDOT *Bridge Design Manual* (TxDOT 2018).

Table 4.5. Properties of Wearing Surface and Barrier (T551 Railing).

Parameter	Value
Unit weight of wearing surface, γ_{ws}	0.140 kcf
Linear weight of railing, T551, w_r	0.382 klf

4.3.2.4 Mechanical and Geometric Properties of Prestressing Strands

The mechanical properties of 0.6 in. diameter, seven-wire, low-relaxation prestressing strands used for this design example are listed in Table 4.6.

Table 4.6. Mechanical and Geometric Properties of Prestressing Strands.

Parameter	Value
Ultimate strength of steel strands, f_{pu}	270 ksi
Yield strength of steel strands, f_{py}	243 ksi
MOE of strands, E_p	28,500 ksi
Diameter of strands, d_b	0.6 in.
Area of prestressing strands, A_t	0.217 in^2

4.4 GIRDER DETAILS AND SECTION PROPERTIES

The section properties of the Tx34 girder are provided in Table 4.7 based on the standard TxDOT bridge drawings (TxDOT 2019).

Table 4.7. Girder Details and Sectional Properties.

Parameter	Value
Length of girder, L_g	84.5 ft
Depth of girder, h_g	34 in.
Thickness of web, b_w	7 in.
Distance of neutral axis from top of girder, y_t	18.5 in.
Distance of neutral axis from bottom of girder, y_b	15.5 in.
Area of girder, A_g	627 in^2
Moment of inertial about x-axis, I_g	88,355 in^4
Section modulus at the top of girder, S_t	4779 in^3
Section modulus at the bottom of girder, S_b	5697 in^3
Modular Ratio, E_g/E_d, η_{UHPC}	1.86

4.5 COMPOSITE SECTION DETAILS AND SECTIONAL PROPERTIES

The section properties of the composite section are obtained by transforming the section using the modular ratio. This approach is consistent with the recommendations in the *TxDOT Bridge Design Manual* (TxDOT 2018). The calculations are shown in Table 4.8

The transformed width of the deck of the composite section $= \frac{1}{\eta_{UHPC}} \times$ effective width

$$= \frac{1}{1.86}(120 \text{ in.}) = 64.5 \text{ in.}$$

Table 4.8. Computation of Properties of Composite Section.

Component	Transformed Area, A (in^2)	y_b (in.)	Ay_b (in^3)	$A(y_{bc}\text{-}y_b)^2$ (in^3)	I (in^4)	$I + A(y_{bc}\text{-}y_b)^2$ (in^4)
Girder	627	15.5	9725	86,946	88,355	175,301
Slab	548	40.3	22,049	92,068	3298	95,366
Haunch	37	35	1278	2,173	12	2185
Σ	1211	-	33,052	-	-	272,852

The properties of the composite section of the Tx34 girder of UHPC and the deck slab of CC are listed in Table 4.9.

Table 4.9. Properties of Tx34 UHPC Girder with CC Deck Slab.

Parameter	**Value**
Total depth of the section, h_c	44.5 in.
Effective width of the section, b_e	120 in.
Distance of neutral axis from top of girder, y_{tc}	17.2 in.
Distance of neutral axis from bottom of girder, y_{bc}	27.3 in.
Transformed area of composite girder, A_{gc}	1211 in^2
Moment of inertia about x-axis, I_{cg}	272,852 in^4
Section modulus of composite section at the top of the composite section, S_{tc}	15,850 in^3
Section modulus of composite section at the top of the girder, S_{tgc}	40,638 in^3
Section modulus of composite section at the bottom of girder, S_{bc}	10,000 in^3

4.6 LOAD DEMANDS

This section documents the computations of the demands on the bridge superstructure due to dead and live loads per the AASHTO LRFD Specifications (AASHTO 2020). This section also mentions the various factors needed to compute the factored loads. Table 4.10 presents the factors considered for load combinations as per Table 3.4.4-1 of the AASHTO LRFD Specifications (AASHTO 2020).

Table 4.10. Load Combinations Considered.

	Dead Load	Wearing Surface Load	Live Load	Impact Load
Service I	1	1	1	1
Service III	1	1	1	1
Strength I	1.25	1.5	1.75	1.75

4.6.1 Dead Loads

The dead loads due to the self-weight of the prestressed girders, the deck slab, and the haunch act on the non-composite prestressed girder, whereas the dead loads due to the superimposed weight of the wearing surface and the railings act on the composite girder section. The self-weights for the components are listed below.

<u>Self-Weight Computations</u>

Girder, w_g $= \gamma_{UHPC} \times A_g$ (4.4)

$$= (0.160\ \text{kip/ft}^3)\left(\frac{627\ \text{in}^2}{144\ \text{in}^2/\text{ft}^2}\right) = 0.697\ \text{klf}$$

Deck slab, w_s $= \gamma_{cc} \times t_s \times b_e$ (4.5)

$$= (0.15\ \text{kip/ft}^3)\left(\frac{8.5\ \text{in.}}{12\ \text{in./ft}}\right)(10\ \text{ft}) = 1.06\ \text{klf}$$

Haunch, w_h $= \gamma_{cc} \times t_h \times b_h$ (4.6)

$$= (0.15\ \text{kip/ft}^3)\left(\frac{2\ \text{in.}}{12\ \text{in./ft}}\right)\left(\frac{34\ \text{in.}}{12\text{in./ft}}\right) = 0.071\ \text{klf}$$

Wearing surface, w_{ws} = $\gamma_{ws} \times t_s \times b_e$ (4.7)

$$= (0.14\ \text{kip/ft}^3)\left(\frac{2\ \text{in.}}{12\ \text{in./ft}}\right)(10\ \text{ft}) = 0.23\ \text{klf}$$

Distributed weight of barrier T551, w_{dr} = $2 \times \left(\frac{w_r}{5\ \text{girders}}\right)$ (4.8)

$$= 2 \times \left(\frac{0.382\ \text{klf}}{5\ \text{girders}}\right) = 0.153\ \text{klf}$$

4.6.2 Live Loads

The live loads are assumed to be the standard HL-93 loading and this load acts on the composite section of the bridge. The combination consists of the maximum of the load contribution from an HS20 truck, as shown in Figure 4.2, or design tandem, as presented in Figure 4.3, and design lane load. The live loads are listed in Table 4.11 and are taken from Article 2 of the AASHTO LRFD Specifications (AASHTO 2020).

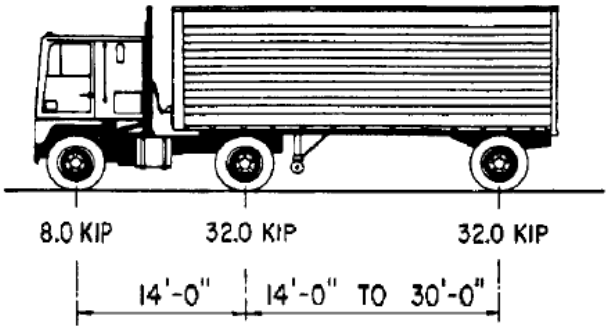

(a) Truck Axle Loadings and Longitudinal Spacings

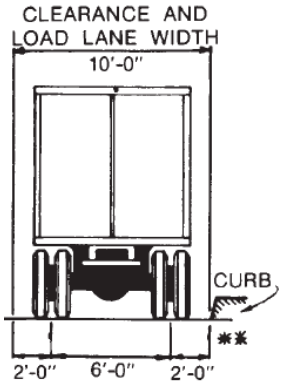

(b) Truck Transverse Spacing

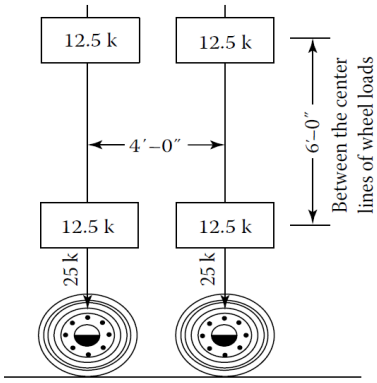

(c) Tandem Axle Loadings and Longitudinal Spacings

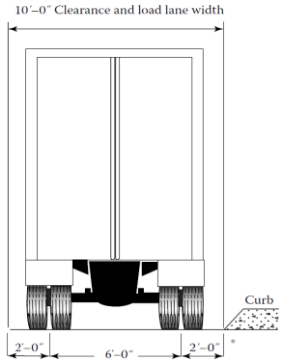

(d) Tandem Transverse Spacing

Figure 4.2. HS20 Truck Loading (AASHTO 2020; Taly 2014).

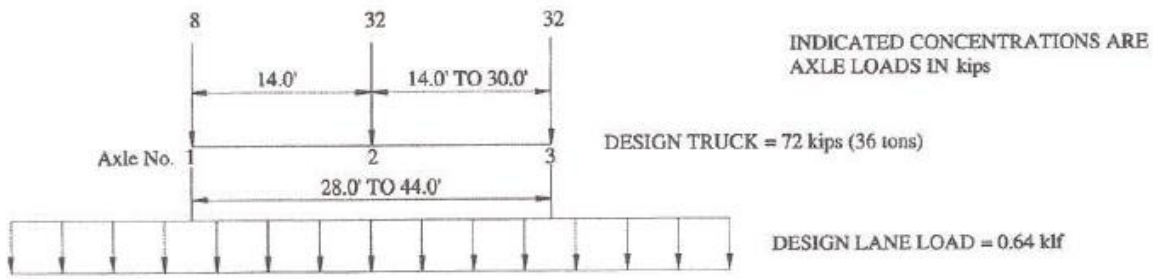

(a) Design Truck and Lane Load

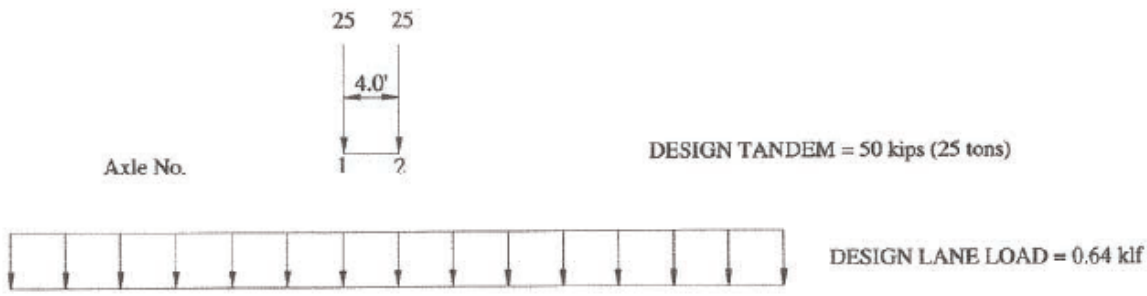

(b) Design Tandem and Lane Load

Figure 4.3. Designated HL-93 Load Model (AASHTO 2018).

Table 4.11. Live Load Details.

Parameter	**Description**
Design truck load	8-kip, 32-kip and 32-kip axles spaced 14 ft apart from each other
Design tandem load	25-kip and 25-kip axles spaced 4 ft apart
Design lane load	0.64 klf across 10 ft width, uniformly distributed longitudinally

4.6.3 Unfactored and Factored Moment Demands

Maximum demand due to moments is calculated using dead loads and vehicular live loads. The process is simplified using a long-standing methodology of live load distribution factors (LLDFs). These were adapted using approximate LLDFs expressions provided in the AASHTO LRFD Specifications (AASHTO 2020) Article 4.6.2.2. In the LLDF method, a multi-girder bridge superstructure can be reduced to a single one-dimensional (1D) beam element. Thus, LLDFs are applied to convert demands on a single 1D beam element into the demands for one of the girders and its associated deck slab in a multi-girder beam-slab bridge. The service and strength limit states specified by AASHTO LRFD Specifications (AASHTO 2020) are

considered including the following load combinations: Service I, Service III, and Strength I. The relevant load factors are provided in Table 3.4.4-1 of the AASHTO LRFD Specifications (AASHTO 2020). Table 4.10 presents the load combinations considered. The dead loads are increased by 25 percent and the live load and impact loads are increased by 75 percent for the Strength I load combination, respectively, and the computations are shown below.

<u>Dead Load Moment Demands Computations</u>

Dead loads include the self-weight of structural components, such as the girder and deck slab including the haunch thickness, and nonstructural components such as wearing surface and railings. The weight of the wearing surface is distributed equally to all girders while the weight of railings is distributed to first three girders from the edge following the recommendations provided in *TxDOT Bridge Design Manual* (TxDOT 2018).

Girder, M_g $$= w_g \frac{L^2}{8} \tag{4.9}$$

$$= (0.697 \text{ klf}) \left(\frac{(83 \text{ ft})^2}{8} \right) = 600 \text{ kip-ft}$$

Deck Slab, M_s $$= w_s \frac{L^2}{8} \tag{4.10}$$

$$= (1.06 \text{ klf}) \left(\frac{(83 \text{ ft})^2}{8} \right) = 915 \text{ kip-ft}$$

Haunch, M_h $$= w_h \frac{L^2}{8} \tag{4.11}$$

$$= (0.071 \text{ klf}) \left(\frac{(83 \text{ ft})^2}{8} \right) = 61 \text{ kip-ft}$$

Wearing surface, M_{ws} $$= w_{ws} \frac{L^2}{8} \tag{4.12}$$

$$= (0.23 \text{ klf}) \left(\frac{(83 \text{ ft})^2}{8} \right) = 201 \text{ kip-ft}$$

Barrier T551, M_r $= w_{dr}\frac{L^2}{8}$ (4.13)

$$= (0.153\text{ klf})\left(\frac{(83\text{ ft})^2}{8}\right) = 132\text{ kip-ft}$$

Self-weight of girder at transfer length, M_{Dt} $= \frac{w_g L_g l_t}{2} - \frac{w_g {l_t}^2}{2}$ (4.14)

$$= \frac{(0.697\text{ klf})(84.5\text{ ft})(1.5\text{ ft})}{2} - \frac{(0.697\text{klf})(1.5\text{ ft})^2}{2}$$

$$= 43.4\text{ kip-ft}$$

For the computation of moment due to self-weight of girder at transfer length M_{Dt} is computed as follows.

Transfer length, l_t $= 30d_b$ (4.15)

$$= (30)(0.6\text{ in.}) = 18\text{ in.} = 1.5\text{ ft}$$

<u>Live Load Moment Demands Computations</u>

The vehicular live loading on the roadways of bridges specified as HL-93 by AASHTO LRFD Specifications (AASHTO 2020) Article 3.6.1.2.1, as described in the previous section, is used for the demand due to live load moments. Absolute maximum moment due to an HS20 truck occurs when the centerline of the span (midspan location) bisects the 32-kip middle axle load and the resultant of the HS20 load group. The maximum moment occurs under the 32-kip middle axle. Similarly, the absolute maximum moment due to tandem load occurs when one of the 25-kip loads and the resultant of the tandem load group are placed equidistant from centerline of the span (midspan location). It occurs under the 25-kip load that is close to midspan. These two methods can be obtained using the influence line method and are “exact methods” of calculating moment demands due to HS20 and tandem loads (Figure 4.2 and Figure 4.3).

Alternatively, the maximum moment at midspan due to HS20 truck can be calculated, without any significant error, by placing the 32-kip middle axle at the midspan. Similarly, the maximum moment at midspan due to tandem load can be calculated by placing one of the 25-kip axle loads

at the midspan. These are simpler approximate methods that may be used for computing maximum moment demands due to AASHTO HS20 or tandem loads. The difference between exact and approximate method is inconsequential (less than 1 percent) and can be ignored for all practical purposes (Taly 2014). Furthermore, the moment due to uniformly distributed loads can be calculated at midspan and superposed with that from vehicular moment demand. This means that the difference between exact and approximate truck moment calculations will be even less significant when added together with the UDL due to all dead loads and vehicular lane load. The maximum moment demand at midspan due to HS20 truck and tandem load can then be calculated as:

Design truck, M_{HS20} $= 18L - 280$ (4.16)

$= (18\text{ kip})(83\text{ ft}) - (280\text{ kip-ft}) = 1214\text{ kip-ft}$

Design tandem, M_{Tandem} $= 12.5L - 50$ (4.17)

$= (12.5\text{ kip})(83\text{ ft}) - 50\text{ kip-ft} = 987.5\text{ kip-ft}$

Design lane load, M_{Lane} $= \dfrac{0.64L^2}{8}$ (4.18)

$= \dfrac{(0.64\text{ klf})(83\text{ ft})^2}{8} = 551.1\text{ kip-ft}$

<u>Live Load Distribution Factor for Interior Beams</u>

The total vehicular moment demand for the critical interior girder can be calculated by multiplying the moment demand from a single one-dimensional beam element with the moment live load distribution factor (LLDF) computed using equations in AASHTO LRFD Specifications (AASHTO 2020) Table 4.6.2.2.2b-1.

For a prestressed concrete I-girder with concrete deck bridge having two or more design lanes loaded:

Live load distribution factor for moment, g_m $= 0.075 + \left(\frac{S}{9.5}\right)^{0.6}\left(\frac{S}{L}\right)^{0.2}\left(\frac{K_g}{12.0Lt_s{}^3}\right)^{0.1}$ (4.19)

$= 0.075 + \left(\frac{10}{9.5}\right)^{0.6}\left(\frac{10}{83}\right)^{0.2} 1.02$

$= 0.766$

$\left(\frac{K_g}{12.0Lt_s{}^3}\right)^{0.1} = 1.02$ AASHTO (2020) - Table 4.6.2.2.1-3

Factored Live Load Moment, M_{LL} $= g_m(1.33 \times \max(M_{HS20}, M_{Tandem}) + M_{Lane})$ (4.20)

$= 0.766(1.33\ (1214) + 551.1) = 1659$ kip-ft

4.6.4 Unfactored and Factored Shear Demands

The maximum demand due to shear is also calculated using dead loads and vehicular live loads. Shear LLDFs were determined using the approximate LLDFs expressions provided in the AASHTO LRFD Specifications (AASHTO 2020) Article 4.6.2.2.

Effective shear depth (d_v) $= \max$ (inner lever arm (z), $\max$ ($0.9d_p$, 0.72h)) (4.21)

$= \max$ (34.2, $\max$ (0.9 (37.30), 0.72 (44.5))

$= \max$(34.2, $\max$ (33.6, 32.0)

$= \max$ (34.2, 33.6)

$= 34.2$ in.

Note: Computation of z and d_p are shown in Section 4.7.10 under flexure resistance at strength limit state.

Critical section for shear calculations (x_s) $= \frac{d_v + 9}{12}$ (4.22)

$= \frac{34.2 + 9}{12}$

$= 3.56$ ft

Shear Demands

Design truck, V_{HS20}

$$= 32\left(\frac{L - x_s}{L}\right) + 32\left(\frac{L - 14 - x_s}{L}\right) + 8\left(\frac{L - 28 - x_s}{L}\right) \quad (4.23)$$

$$= 32\left(\frac{83 - 3.56}{83}\right) + 32\left(\frac{83 - 14 - 3.56}{83}\right) + 8\left(\frac{83 - 28 - 3.56}{83}\right)$$

$$= 60.8 \text{ kips}$$

Design tandem, V_{Tandem}

$$= 25\left(\frac{L - x_s}{L}\right) + 25\left(\frac{L - 4 - x_s}{L}\right) \quad (4.24)$$

$$= 25\left(\frac{83 - 3.56}{83}\right) + 25\left(\frac{83 - 4 - 3.56}{83}\right)$$

$$= 46.7 \text{ kips}$$

Design maximum truck, V_{Truck}

$$= \max(V_{HS20}, V_{Tandem}) \quad (4.25)$$

$$= \max(60.8, 46.8) \text{ kips}$$

$$= 60.8 \text{ kips}$$

Design lane, V_{Lane}

$$= 0.64\frac{L}{2} - 0.64x_s \quad (4.26)$$

$$= 0.64\left(\frac{83}{2}\right) - 0.64(3.56)$$

$$= 24.3 \text{ kips}$$

The shear LLDF is computed using the expressions in AASHTO LRFD Specifications (AASHTO 2020) Table 4.6.2.2.3a-1. For prestressed concrete I-girder with concrete deck and with two or more design lanes loaded:

Live load distribution factor for shear, g_v

$$= 0.2 + \frac{S}{12} - \left(\frac{S}{35}\right)^{2.0} \quad (4.27)$$

$$= 0.2 + \frac{10}{12} - \left(\frac{10}{35}\right)^{2.0}$$

$$= 0.952$$

Factored Live Load Shear, V_{LL}

$$= g_v\,(1.33V_{Truck} + V_{Lane}) \quad (4.28)$$

$$= 0.952((1.33)(60.8) + 24.3)$$

$$= 100.1 \text{ kips}$$

Shear Demand due to Dead Load

Girder, V_g

$$= w_g \frac{L}{2} - w_g x_s \tag{4.29}$$

$$= (0.697)\left(\frac{83}{2}\right) - (0.697)(3.56)$$

$$= 26.4 \text{ kips}$$

Deck slab, V_s

$$= w_s \frac{L}{2} - w_s x_s \tag{4.30}$$

$$= (1.06)\left(\frac{83}{2}\right) - (1.06)(3.56)$$

$$= 40.3 \text{ kips}$$

Haunch, V_h

$$= w_h \frac{L}{2} - w_s x_s \tag{4.31}$$

$$= (0.071)\left(\frac{83}{2}\right) - (0.071)(3.56)$$

$$= 2.7 \text{ kips}$$

Wearing surface, V_{ws}

$$= w_{ws} \frac{L}{2} - w_{ws} x_s \tag{4.32}$$

$$= (0.23)\left(\frac{83}{2}\right) - (0.23)(3.56)$$

$$= 8.9 \text{ kips}$$

Barrier T551, V_r

$$= w_r \frac{L}{2} - w_r x_s \tag{4.33}$$

$$= (0.153)\left(\frac{83}{2}\right) - (0.153)(3.56)$$

$$= 5.8 \text{ kips}$$

Factored Shear Demand, V_u

$$= 1.25\left(\mathrm{V_g} + \mathrm{V_h} + \mathrm{V_s} + \mathrm{V_r}\right) + 1.50(\mathrm{V_{ws}}) + 1.75(\mathrm{V_{LL}}) \tag{4.34}$$

$$= (1.25)(26.4 + 2.7 + 40.3 + 5.8) + (1.50)(8.9) + (1.75)(100.1)$$

$$= 282.5 \text{ kips}$$

4.7 FLEXURAL STRESS DESIGN AT SERVICE LIMIT STATE

4.7.1 General Procedure

This section reports the steps involved in evaluating the flexural capacity of the composite girder section for the service-level flexural demands computed in the previous section. The steps to select the number and arrangement of prestressing strands to meet the service stress limits for a given section geometry and selected material properties are summarized as follows.

1. Stress inequalities at various transportation and loading stages are plotted using assumed values of prestressing losses. The feasible domain, a region that satisfies all the critical limit state inequalities, is considered for selecting an optimal combination of the number of strands and eccentricity of the prestressing force, such that it can be constructed for the Tx34 shape.

2. Once a practical combination that lies within the feasible domain is obtained, the selected combination of strands and eccentricity is used to compute the prestressing losses. The eccentricity of the prestressing force is computed with respect to the centroid of the girder and is denoted by e_{pg}, and the number of strands is denoted by N.

3. The initial and final prestress that were assumed in Step 1 are then modified based on the prestressing loss obtained in Step 2 and then a revised feasibility domain is obtained.

4. This iterative cycle is repeated until the number of strands and the eccentricity combination is optimized.

5. The stresses are checked to verify that the arrangement of strands is suitable. If not, solutions such as harping and/or debonding of strands are considered.

4.7.2 Sign Convention

The compressive forces and stresses are considered negative and tensile forces and stresses are considered positive throughout this design example.

4.7.3 Prestress Losses

Prestressing losses are computed using the AASHTO LRFD Specifications (AASHTO 2020) in Article 5.9.3. The design example incorporates the prestress loss computations from the AASHTO LRFD Specifications (AASHTO 2020) with the modifications recommended by the AASHTO draft specifications for UHPC (FHWA 2022). The creep and shrinkage values are based on the findings of the present research study and listed in Section 3.4.2.2 and 3.4.2.3.

$$\Delta f_{pT} = \Delta f_{pST} + \Delta f_{pLT} \tag{4.35}$$

where:

Δf_{pT} = Total loss, ksi

Δf_{pST} = Short-term losses at transfer due to sum of loss or gains on account of elastic shortening or extension at prestressing and/or load transfer and early age shrinkage, ksi

Δf_{pLT} = Losses on account of long-term shrinkage and creep of concrete, and relaxation of steel, ksi

4.7.3.1 Prestress Losses at Transfer

The total prestress loss at transfer is calculated as follows:

$$\Delta f_{pST} = \Delta f_{pES} + \Delta f_{pSHI} \tag{4.36}$$

where:

Δf_{pST} = Prestress loss at transfer, ksi

Δf_{pES} = Prestress loss due to elastic shortening at transfer, ksi, AASHTO LRFD Equation 5.9.3.2.3a-1 (AASHTO 2020)

Δf_{pshi} = Prestress loss due to autogenous shrinkage occurring during the time between final set and transfer, ksi, using the PCI study equation 5.4.1-2 (eConstruct 2020)

(a) *Prestress Losses due to Elastic Shortening*

Elastic shortening in pretensioned members is computed using the expression in AASHTO LRFD Specifications (AASHTO 2020) Article 5.9.3.2.3a-1.

$$\Delta f_{pES} = \frac{E_p}{E_{ct}} f_{cgp} \tag{4.37}$$

where:

f_{cgp} = Stress in concrete at the centroid of the prestressing tendons due to prestressing force after transfer and the member self-weight at the section of maximum moment, ksi

E_p = Modulus of elasticity of prestressing steel, taken as 28,500 ksi

E_{ct} = Modulus of elasticity of concrete at transfer or at the time of load application, ksi

$$f_{cgp} = NA_t f_{pi}\left(\frac{1}{A_g} + \frac{{e_{pg}}^2}{I_g}\right) - \frac{M_g e_{pg}}{I_g} \tag{4.38}$$

Elastic Shortening Computations:

Effective stress in prestressing steel at transfer, f_{pi} = $(0.9)(0.75)f_{pu}$ (4.39)

$(0.9)(0.75)(270) = 182.3$ ksi

Assume number of strands, N = 48

The above computations are iterated, and the final iteration of calculations is shown.

$$f_{cgp} = NA_t f_{pi}\left(\frac{1}{A_g} + \frac{{e_{pg}}^2}{I_g}\right) - \frac{M_g e_{pg}}{I_g} \tag{4.40}$$

$$= (48)(0.217)(184)\left(\frac{1}{627} + \frac{(9.93)^2}{88{,}355}\right) - \frac{(7199)(9.93)}{88{,}355}$$

$$= 4.38 \text{ ksi}$$

$$\Delta f_{pES} = \frac{E_p}{E_{gi}} f_{cgp} \tag{4.41}$$

$$= \frac{28{,}500}{6742} \quad (4.38)$$

$$= 18.5 \text{ ksi}$$

(b) *<u>Early Age Shrinkage of UHPC</u>*

Loss due to early age shrinkage of UHPC is

$$\Delta f_{pSHI} = \varepsilon_{shi} E_p K_i \quad (4.42)$$

where:

ε_{shi} = Autogenous shrinkage strain occurring between the time between final set and transfer, taken as 200×10^{-6} in./in. (from this study)

K_{di} = Transformed section coefficient that accounts for initial (elastic) interaction between concrete and bonded steel, assumed to be 0.83 according to Section F.1.6.1 of eConstruct (2020)

$$\Delta f_{pSHI} = (200 \times 10^{-6})(28{,}500)(0.83) = 4.73 \text{ ksi}$$

$$\Delta f_{pST} = 18.5 + 4.73 = 23.3 \text{ ksi}$$

Initial stress in prestressing steel just after release, f_{pi}:

$$f_{pi} = 0.75 f_{pu} - \Delta f_{pST} \quad (4.43)$$

$$= (0.75)(270 \text{ ksi}) - 23.3 \text{ ksi}$$

$$= 179.2 \text{ ksi}$$

The value of the initially assumed f_{pi} is varied using trial and error until the difference between the initial and final value of f_{pi} is minimized. The final f_{pi} after several trials is

$$f_{pi} = 179.2 \text{ ksi}$$

4.7.3.2 Time Dependent Prestress Losses

AASHTO LRFD (AASHTO 2020) Article 5.9.3.4. provides the expression for the long-term prestress losses as,

$$\Delta f_{pLT} = \left(\Delta f_{pSR} + \Delta f_{pCR} + \Delta f_{pR1}\right)_{id} + \left(\Delta f_{pSD} + \Delta f_{pCD} + \Delta f_{pR2} - \Delta f_{SS}\right)_{df} \quad (4.44)$$

where:

Δf_{pT} = Total prestress loss, ksi

Δf_{pLT} = Long-term prestress loss, ksi [AASHTO LRFD Equation 5.9.3.4.1-1 (AASHTO 2020)]

Δf_{pSR} = Prestress loss due to shrinkage of girder occurring between transfer and deck placement, ksi [AASHTO LRFD Equation 5.9.3.4.2a-1 (AASHTO 2020)]

Δf_{pCR} = Prestress loss due to creep of girder occurring between transfer and deck placement, ksi [AASHTO LRFD Equation 5.9.3.4.2b-1 (AASHTO 2020)]

Δf_{pR1} = Prestress loss due to relaxation of prestressing strands occurring between transfer and deck placement, 1.2 ksi for low-relaxation strands [AASHTO LRFD Article 5.9.3.4.2c (AASHTO 2020)]

Δf_{pSD} = Prestress loss due to shrinkage of girder occurring between time of deck placement and final time, ksi [AASHTO LRFD Equation 5.9.3.4.3a-1 (AASHTO 2020)]

Δf_{pCD} = Prestress loss due to creep of girder occurring between time of deck placement and final time, ksi [AASHTO LRFD Equation 5.9.3.4.3b-1 (AASHTO 2020)]

Δf_{pR2} = Prestress loss due to relaxation of prestressing strands in composite section between deck placement and final, $\Delta f_{pR2} = \Delta f_{pR1} = 1.2$ ksi for low-relaxation strands [AASHTO LRFD Specifications Article 5.9.3.4.3c (AASHTO 2020)]

Δf_{pSS} = Prestress gain due to shrinkage of deck in composite section, ksi [AASHTO LRFD Equation 5.9.3.4.3d-1 (AASHTO 2020)]

<u>Time Dependent Loss Computation</u>

Prestress Losses between Transfer and Deck Placement

(a) <u>*Shrinkage of UHPC*</u>

$$\Delta f_{pSR} = \varepsilon_{bid} E_p K_{id} \tag{4.45}$$

where:

ε_{bid} = Shrinkage strain $= \varepsilon_{SR} k_{hs} k_f k_s k_{td}$

K_{id} = Transformed section coefficient

$$= \frac{1}{1 + \frac{E_p}{E_{ci}} \frac{A_{ps}}{A_g} \left(1 + \frac{A_g e_{pg}^2}{I_g}\right) \left[1 + 0.7\psi_{b_{(t_f,t_i)}}\right]}$$

$$= \frac{1}{1 + \frac{28{,}500}{6742} \frac{10.42}{627} \left(1 + \frac{627 \times (9.93)^2}{88{,}355}\right) [1 + 0.7(0.8)]} = 0.84$$

ε_{SR} = Ultimate shrinkage strain of UHPC = 700× 10^{-6} (from this study)

k_{hs} = Humidity correction factor for shrinkage for UHPC

$= 1 + 0.2(1 - 0.014H) = 1 + 0.2(1 - 0.014(60)) = 1.032$

k_f = Strength correction factor for UHPC

$$= \frac{19}{7 + f'_{ci}} = 1.016$$

k_s = Size correction factor for UHPC

$$= 1 + 0.2\left[0.45 - 0.13\left({}^{V}/_{S}\right)\right] = 1 + 0.2[0.45 - 0.13(3.5)] = 1.0$$

k_{td} = Time development factor for UHPC

$$= \frac{t^{0.6}}{4 + t^{0.6}} = \frac{90^{0.6}}{4 + 90^{0.6}} = 0.79$$

t = Final time = 90 days

$$\Delta f_{pSR} = (0.000578)(28500)(0.84) = 13.9 \text{ ksi}$$

(b) <u>*Creep of UHPC*</u>

$$\Delta f_{pCR} = \frac{E_p}{E_{gi}} f_{cgp} \psi_{b_{(t_d,t_i)}} K_{id} \tag{4.46}$$

where:

$\psi_{b_{(t_d,t_i)}}$ = Creep coefficient of UHPC girder at time of deck placement due to loading at transfer = $\psi_{ult} k_{hc} k_f k_s k_{td}$

ψ_{ult} = Ultimate creep coefficient $= 0.8$ (from this study)

k_{hc} = Humidity correction factor for creep for UHPC = 1.0

k_{td} = Time development factor for UHPC

$$= \frac{t^{0.6}}{8+t^{0.6}} = \frac{90^{0.6}}{8+90^{0.6}}$$

$$= 0.65$$

$$\psi_{b_{(t_d,t_i)}} = (0.8)(1)(1.016)(1)(0.65) = 0.53$$

$$\Delta f_{pCR} = \frac{28{,}500}{6742}(4.38)(0.53)(0.84) = 8.2 \text{ ksi}$$

(c) <u>Relaxation of Prestressing Strands</u>

$$\Delta f_{pR1} = 1.2 \text{ ksi}$$

$$\left(\Delta f_{pSR} + \Delta f_{pCR} + \Delta f_{pR1}\right)_{id} = 13.9 + 8.2 + 1.2 = 23.3 \text{ ksi}$$

Effective stress in prestressing steel at time of deck placement, f_{ped}:

$$f_{ped} = f_{pi} - \left(\Delta f_{pSR} + \Delta f_{pCR} + \Delta f_{pR1}\right)_{id} \tag{4.47}$$

$$= 179.2 - 23.3$$

$$= 155.9 \text{ ksi}$$

Prestress Losses between Deck Placement to Final Time

(a) *<u>Shrinkage of UHPC</u>*

$$\Delta f_{pSD} = \varepsilon_{bdf} E_p K_{df} \tag{4.48}$$

where:

ε_{bdf} = Shrinkage strain $= (\varepsilon_{SR} k_{hs} k_f k_s k_{td})_{fi} - (\varepsilon_{SR} k_{hs} k_f k_s k_{td})_{id}$

K_{df} = Transformed section coefficient

$$= \frac{1}{1 + \frac{E_p}{E_{ci}}\frac{A_{ps}}{A_c}\left(1 + \frac{A_c e_{pc}^2}{I_c}\right)\left[1 + 0.7\psi_{b_{(t_f,t_i)}}\right]}$$

$$= \frac{1}{1 + \frac{28{,}500}{6742}\frac{10.42}{1211}\left(1 + \frac{1211 \times (21.7)^2}{272{,}852}\right)[1 + 0.7(0.8)]} = 0.85$$

k_{td} = Time development factor for UHPC

$$= \frac{t^{0.6}}{4+t^{0.6}} = \frac{(27{,}285)^{0.6}}{4+(27{,}285)^{0.6}} = 0.99$$

t = Final time = 27,375 days = 75 years

Δf_{pSD} = $(0.000149)(28{,}500)(0.85) = 3.61$ ksi

(b) <u>*Creep of UHPC*</u>

$$\Delta f_{pCD} = \frac{E_p}{E_{gi}} f_{cgp}\left[\psi_{(t_f,t_i)} - \psi_{(t_d,t_i)}\right] K_{df} + \frac{E_p}{E_g}\Delta f_{cd}\psi_{b\,(t_f,t_d)} K_{df} \tag{4.49}$$

where:

Δf_{cd} = Change in concrete stress at centroid of prestressing strands due to long-term losses between transfer and deck placement, ksi

$$= \left(\Delta F_p\right)_{id}\left(\frac{1}{A_g} + \frac{{e_{pg}}^2}{I_g}\right) + \frac{M_d e_{pg}}{I_g}$$

$$= NA_{ps}\left(\Delta f_{pSR} + \Delta f_{pCR} + \Delta f_{pR1}\right)_{id}\left(\frac{1}{A_g} + \frac{{e_{pg}}^2}{I_g}\right) + \frac{M_d e_{pg}}{I_g}$$

$$= 48 \times 0.217 \times 23.3\left(\frac{1}{627} + \frac{9.93^2}{88355}\right) + \frac{15{,}703.5 \times 9.93}{88355}$$

$= 2.26$ ksi

$\psi_{b\,(t_f,t_d)}$ = Creep coefficient of UHPC girder at time of deck placement due to loading at transfer = $\psi_{ult} k_{hc} k_f k_s k_{td}$

k_{td} = Time development factor for UHPC

$$= \frac{t^{0.6}}{8 + t^{0.6}} = \frac{27285^{0.6}}{8 + 27285^{0.6}}$$

$= 0.98$

$\psi_{b\,(t_f,t_i)}$ = $(0.8)(1)(1.016)(1)(0.98) = 0.80$

$$\Delta f_{pCD} = \frac{28{,}500}{6742}(4.38)(0.80 - 0.53)(0.85) + \frac{28{,}500}{7423}(2.26)(0.80 - 0.53)(0.85) = 6.28 \text{ ksi}$$

(c) <u>*Relaxation of Prestressing Strands*</u>

Δf_{pR2} = 1.2 ksi

(d) <u>*Shrinkage of deck*</u>

$$\Delta f_{pSS} = \frac{E_p}{E_g}(\Delta f_{cdf})(K_{df})\left[1 + 0.7\psi_b(t_f, t_d)\right] \tag{4.50}$$

where:

Δf_{cdf} = Change in concrete stress due to shrinkage of deck concrete at centroid of prestressing strands, ksi, AASHTO LRFD Equation 5.9.3.4.3d-2 (AASHTO 2020)

$$= \frac{\varepsilon_{ddf} A_d E_{c\,deck}}{\left[1 + 0.7\psi_d(t_f, t_d)\right]}\left(\frac{1}{A_c} - \frac{e_{pc}e_d}{I_c}\right)$$

$$= \frac{0.000695 \times (1020 + 68) \times 3987}{[1 + 0.7 \times 2.56]}\left(\frac{1}{1211} - \frac{21.7 \times 12.96}{272{,}853}\right)$$

$= -0.22$ ksi

ε_{ddf} = $\varepsilon_{SR} k_{hs} k_f k_s k_{td} = 695$ microstrain

ε_{SR} = Ultimate shrinkage strain of CC = 480 microstrain

k_{hs} = Humidity correction factor for shrinkage for CC

$= (2 - 0.014H) = (2 - 0.014(60)) = 1.16$

k_f = Strength correction factor for CC

$$= \frac{5}{1 + f'_{ci}} = \frac{5}{1 + 3} = 1.25$$

k_s = Size correction factor for CC

$= \left[1.45 - 0.13\left({}^{V}/_{S}\right)\right] = [1.45 - 0.13(3.5)] = 1.0$

k_{td} = Time development factor for CC

$$= \frac{t}{12\left(\frac{100 - 4f'_{ci}}{f'_{ci} + 20}\right) + t} = \frac{27{,}285}{12\left(\frac{100 - 4 \times 3}{3 + 20}\right) + 27{,}285} = 1.0$$

$\psi_{b(t_d,t_i)}$ = Creep coefficient of UHPC girder at time of deck placement due to loading at transfer = $\psi_{ult} k_{hc} k_f k_s k_{td} t_i^{-0.118}$

ψ_{ult} = Ultimate creep coefficient $= 1.9$

k_{hc} = Humidity correction factor for shrinkage for UHPC

= $1.56 - (0.008H) = (1.56 - 0.008(60)) = 1.0$

$t_i^{-0.118}$ = Age of concrete at time of loading application = 1 day

$$\Delta f_{pSS} = \frac{28{,}500}{7423}(-0.22)(0.85)[1 + 0.7(0.80 - 0.53)] \tag{4.51}$$

$$= -0.86 \text{ ksi}$$

$$\left(\Delta f_{pSD} + \Delta f_{pCD} + \Delta_{pR2} - \Delta f_{pSS}\right)_{df} = 3.61 + 6.28 + 1.2 - 0.86 = 10.23 \text{ ksi}$$

$$\Delta f_{pLT} = 23.3 + 10.23$$

$$= 33.53 \text{ ksi}$$

Effective stress in prestressing steel after long term losses, f_{pe}:

$$f_{pe} = f_{pi} - \Delta f_{pLT} \tag{4.52}$$

$$= 179.2 - 33.53$$

$$= 145.7 \text{ ksi}$$

$$\eta_f = \frac{f_{pe}}{f_{pi}} = \frac{145.7}{179.2} = 0.81$$

$$\eta_d = \frac{f_{pe}}{f_{ped}} = \frac{145.7}{155.9} = 0.93$$

The values of f_{pi} and f_{pe} are then used to get the feasible domain and the number of strands, and eccentricity is selected using the feasible region of the inequalities. A combination of $N = 48$ [total area of prestressing strands, $A_{ps} = NA_t = 10.42$ in.^{2}], $e_{pg} = 9.93$ in. (midspan), and $e_{end} = 5.26$ in. (girder ends) is the theoretical set of parameters selected from the plot of the stress inequalities. Finally, the iterative value of $f_{pi} = 179.2$ ksi and $f_{pe} = 145.7$ ksi was obtained using the updated prestress losses.

4.7.3.3 Prestress Losses using Creep and Shrinkage Models from this Study

Other recommendations in the literature are also compared with the method of computing the prestress losses in UHPC girders given by the AASHTO draft specifications for UHPC (FHWA 2022) using the creep and shrinkage models developed as a part of this research project listed in Section 3.4.2.2 and 3.4.2.3. Four methods are summarized as follows.

1. Method 1 uses the recommendations from the AASHTO draft specifications for UHPC (FHWA 2022) that are explained in detail in Section 3.4. This approach is used for the detailed computations provided above for this design example. However, Method 1 uses the creep and shrinkage models developed in this research.

2. Method 2 is the same as Method 1 with the exception of excluding the early age (autogenous) shrinkage from the computations.

3. Method 3 is also similar to Method 1, except the creep and shrinkage models are based on the AASHTO draft specifications for UHPC (FHWA 2022) recommendations

4. Method 4 follows the recommendations of the PCI study for UHPC (eConstruct 2020). However, Method 4 uses the creep and shrinkage models developed in this research.

Table 4.13 presents the comparison of the prestress losses based on the four methods explained above.

Table 4.12. Comparison of Prestress Losses.

Prestress Loss Method	**Method 1**	**Method 2**	**Method 3**	**Method 4**
	FHWA (2022)	**FHWA (2022)**	**FHWA (2022)**	**eConstruct (2020)**
Creep and Shrinkage Models	**Present Research**	**Present Research (without early shrinkage)**	**AASHTO Draft (FHWA models)**	**Present Research**
Elastic Shortening Δf_{ES}, ksi	18.53	18.53	18.53	18.53
Early shrinkage Δf_{pSHI}, ksi	4.73	0	0	4.73
Shrinkage b/w transfer and deck placement Δf_{pSR}, ksi	13.89	13.89	17.99	17.73
Creep b/w transfer and deck placement Δf_{pCR}, ksi	8.23	8.23	25.37	11.60
Δf_{pr1}, Relaxation b/w transfer and deck placement Δf_{pr1}, ksi	1.2	1.2	1.20	1.2
Shrinkage b/w deck placement and final Δf_{pSD}, ksi	3.61	3.61	4.43	0
Creep b/w deck placement and final Δf_{pCD}, ksi	6.28	6.28	9.96	0
Relaxation b/w deck placement and final Δf_{pr2}, ksi	1.2	1.2	1.20	1.2
Prestress gain due to shrinkage of deck in composite section Δf_{SS}, ksi	-0.86	-0.86	-0.86	0
Total prestress losses Δf_{pT}, ksi	56.82	52.08	77.83	54.99
Effective stress in prestressing steel at transfer Δf_{pi}, ksi	179.2	184.0	184.0	179.2
Effective stress in prestressing steel at final Δf_{pe}, ksi	145.7	150.4	124.7	147.5
Percent Prestress losses	28%	26%	38%	27%

Note: b/w: between

4.7.4 Estimating Required Prestressing Force

The required prestressing force is computed at the end of the iterative process. The stress inequalities are computed, and the eccentricities are plotted as a function of the number of strands. The diagram with the plot of all the stress inequalities forms the feasibility domain. The assumptions to initiate the computations are as follows.

Assumptions:

Initial estimate for stress in prestressing steel at transfer, f_{pi}	=	$(0.9)(0.75)f_{pu}$	(4.53)
[Note: 10 percent losses used as per AASHTO LRFD Specifications (AASHTO 2020) C5.9.3.2.3a]	=	$(0.9)\ (0.75)\ (270\text{ ksi})\ =\ 182.3\text{ ksi}$	
Estimated effective stress in prestressing steel after long term losses, f_{pe}	=	$(0.8)\ f_{pi}$	(4.54)
	=	$(0.8)\ (182.3\text{ ksi})\ =\ 145.8\text{ ksi}$	

After carrying out the computations for plotting the feasible domain and computing the prestressing losses as mentioned in the previous section, the following initial and final prestressing forces are obtained. In this case, the estimated f_{pe} is very close to the value of f_{pe} after considering detailed loss calculations. The value shown here is based on Method 1 in Table 4.12.

Final prestress after the computation of losses:

Initial stress in prestressing steel just after release, f_{pi}	=	179.2 ksi
Effective stress in prestressing steel at time of deck placement, f_{ped}	=	155.9 ksi
Effective stress in prestressing steel after long term losses, f_{pe}	=	145.7 ksi

Note: These values are used for computing the final feasible domain in the following sections.

4.7.5 Flexural Stresses at Transfer

4.7.5.1 Compression Stress Limit at Transfer

At transfer, the compression stresses are computed as per the Service I Load Combination in AASHTO LRFD Specifications (AASHTO 2020) Table 3.4.1-1. AASHTO draft specifications for UHPC (FHWA 2022) Article 1.5.2.1.3.a recommends the compressive stress limit before losses as $0.65f'_{ci}$ (ksi), which is consistent with Article 5.9.2.3.1a of the AASHTO LRFD

Specifications (AASHTO 2020). The compressive stress inequality is applicable at the bottom fiber and is computed at the transfer length, l_t. The expression is reduced to a form where the eccentricity can be expressed as a function of the number of strands.

<u>Computation of Compression Limit at Bottom Fiber at Transfer Length</u>

$$-\frac{A_{ps}f_{pi}}{A_g} - \frac{A_{ps}f_{pi}e_{pg}}{S_b} + \frac{M_{Dt}}{S_b} \geq -0.65f'_{ci} \tag{4.55}$$

$$\rightarrow e_{pg} \leq \frac{0.65f'_{ci}S_b}{A_{ps}f_{pi}} - \frac{S_b}{A_g} + \frac{M_{Dt}}{A_{ps}f_{pi}}$$

$$\rightarrow e_{pg} \leq (0.65f'_i S_b + M_{Dt})\frac{1}{F_i} - \frac{S_b}{A_g}$$

$$\rightarrow e_{pg} \leq (0.65(11.7)(5697) + 520)\frac{\eta_f}{F} - \frac{5697}{627}$$

$$\rightarrow e_{pg} \leq (43{,}326 + 520)\frac{0.81}{F} - 9.09$$

$$\rightarrow e_{pg} \leq (35{,}244)\frac{1}{F} - 9.09$$

4.7.5.2 Tension Stress Limit at Transfer

The tensile stress inequality is computed using the load factors as per Service I Load Combination in Table 3.4.1-1 in AASHTO LRFD Specifications (AASHTO 2020). The tensile stress limit is considered to be $0.85f'_{ti}$ as per El-Helou and Graybeal (2022).

Computation of Tension Limit at Top Fiber at Transfer Length

$$-\frac{A_{ps}f_{pi}}{A_g}+\frac{A_{ps}f_{pi}e_{pg}}{S_t}-\frac{M_{Dt}}{S_t}\leq 0.85f'_{ti} \tag{4.56}$$

$$\rightarrow e_{pg}\leq\frac{0.85f'_{ti}S_t}{A_{ps}f_{pi}}+\frac{S_t}{A_g}+\frac{M_{Dt}}{A_{ps}f_{pi}}$$

$$\rightarrow e_{pg}\leq(0.85f'_{ti}S_t+M_{Dt})\frac{1}{F_i}+\frac{S_t}{A_g}$$

$$\rightarrow e_{pg}\leq(0.85(0.72)(4{,}779)+520)\frac{\eta_f}{F}+\frac{(4{,}779)}{627}$$

$$\rightarrow e_{pg}\leq(2935+520)\frac{0.81}{F}+7.62$$

$$\rightarrow e_{pg}\leq(2777)\frac{1}{F}+7.62$$

4.7.6 Flexural Stresses after Deck Placement

4.7.6.1 Compression Stress Limit as Deck Placement

At the time of deck placement, the effective prestress and the superimposed dead loads are considered using unshored construction. The compression stress limit as per the AASHTO LRFD Specifications (AASHTO 2020) Table 5.9.2.3.2a-1 is $0.45f'_c$, which is also provided in the AASHTO draft specifications for UHPC (FHWA 2022). The stress is determined for the noncomposite section at the top fiber.

Initial force in prestressing steel just after release, F_i	=	$A_{ps}f_{pi}$
Effective force in prestressing steel at time of deck placement, F_{ed}	=	$A_{ps}f_{ped}$
Effective force in prestressing steel after long term losses, F	=	$A_{ps}f_{pe}$

Computation of Tension Limit at Top Fiber at Midspan

$$-\frac{A_{ps}f_{ped}}{A_g}+\frac{A_{ps}f_{ped}e_{pg}}{S_t}-\frac{M_g+M_s+M_h}{S_t}\geq -0.45f_c' \tag{4.57}$$

$$\rightarrow e_{pg}\geq -\frac{0.45f_c'S_t}{A_{ps}f_{ped}}+\frac{S_t}{A_g}+\frac{M_g+M_s+M_h}{A_{ps}f_{ped}}$$

$$\rightarrow e_{pg}\geq \left(-0.45f_c'S_t+(M_g+M_s+M_h)\right)\frac{1}{F_{ed}}+\frac{S_t}{A_g}$$

$$\rightarrow e_{pg}\geq (-0.45(18)(4779)+(7199+10{,}979+732))\frac{\eta_d}{F}+\frac{4779}{627}$$

$$\rightarrow e_{pg}\geq (-38{,}710+18{,}910)\frac{0.93}{F}+7.62$$

$$\rightarrow e_{pg}\geq (-18{,}414)\frac{1}{F}+7.62$$

4.7.6.2 Tension Stress Limit at Deck Placement

The tension stress limit is computed when the non-composite section is subjected to the effective prestress and the superimposed dead loads. The tensile stress limit at the bottom fiber at midspan is $-0.85f_t'$ based on El-Helou and Graybeal (2022) and the AASHTO draft specifications (FHWA 2022).

Computation of Tension Limit at Bottom Fiber at Midspan

$$-\frac{A_{ps}f_{ped}}{A_g}-\frac{A_{ps}f_{ped}e_{pg}}{S_b}+\frac{M_g+M_s+M_h}{S_b}\leq 0.85f_t' \tag{4.58}$$

$$\rightarrow e_{pg}\geq -\frac{0.85f_t'S_b}{A_{ps}f_{ped}}-\frac{S_b}{A_g}+\frac{M_g+M_s+M_h}{A_{ps}f_{ped}}$$

$$\rightarrow e_{pg} \geq \left(-0.85 f_t' S_b + (M_g + M_s + M_h)\right)\frac{1}{F_{ed}} - \frac{S_b}{A_g}$$

$$\rightarrow e_{pg} \geq (-0.85(0.85)(5697) + (7{,}199 + 10{,}979 + 732))\frac{\eta_d}{F} - \frac{5{,}697}{627}$$

$$\rightarrow e_{pg} \geq (-4116 + 18{,}910)\frac{0.93}{F} - 9.09$$

$$\rightarrow e_{pg} \geq 13{,}758\frac{1}{F} - 9.09$$

4.7.7 Flexural Stresses at Service Limit State

4.7.7.1 Compressive Stress after Losses

The stress limit at the top fiber of the girder at the midspan of the composite section due to the effective prestress after losses, superimposed dead loads and the transient loads (inclusive of the shipping and handling loads) given as $0.60\phi_w f_c'$ in AASHTO LRFD Specifications (AASHTO 2020) Table 5.9.2.3.2a-1, where ϕ_w is the reduction factor based on the web and flange slenderness ratios. Because the slenderness ratios are not greater than 15, $\phi_w = 1$.

<u>Computation of Compression Limit at Top Fiber at Midspan</u>

$$-\frac{A_{ps} f_{pe}}{A_g} + \frac{A_{ps} f_{pe} e_{pg}}{S_t} - \frac{M_g + M_s + M_h}{S_t} - \frac{M_{ws} + M_r + M_L}{S_{tgc}} \geq -0.60 f_c' \tag{4.59}$$

$$\rightarrow e_{pg} \geq -\frac{0.6 f_c' S_t}{A_{ps} f_{pe}} + \frac{S_t}{A_g} + \frac{M_g + M_s + M_h}{A_{ps} f_{pe}} + \frac{(M_{ws} + M_r + M_L) S_t}{S_{tgc} A_{ps} f_{pe}}$$

$$\rightarrow e_{pg} \geq \left(-0.6 f_c' S_t - \left(M_g + M_s + M_h\right) + \frac{(M_{ws} + M_r + M_L) S_t}{S_{tgc}}\right)\frac{1}{F} + \frac{S_t}{A_g}$$

$$\rightarrow e_{pg} \geq \left(-0.6(18)(4{,}779) + (7{,}199 + 10{,}979 + 732) + \frac{(2411 + 1581 + 19{,}906)4779}{(40{,}638)}\right)\frac{1}{F} + \frac{4{,}779}{627}$$

$$\rightarrow e_{pg} \geq (-51{,}613 + 18{,}910 + 2810)\frac{1}{F} + 7.62$$

$$\rightarrow e_{pg} \geq (-29{,}893)\frac{1}{F} + 7.62$$

The compressive stress inequality when the composite section is subjected to the effective prestressing force due to losses and the permanent dead loads is computed at the top fiber of the girder at the midspan.

<u>Computation of Compression Limit at Top Fiber at Midspan</u>

$$-\frac{A_{ps}f_{pe}}{A_g} + \frac{A_{ps}f_{pe}e_{pg}}{S_t} - \frac{M_g + M_s + M_h}{S_t} - \frac{M_{ws} + M_r}{S_{tgc}} \geq -0.45f_c' \tag{4.60}$$

$$\rightarrow e_{pg} \geq -\frac{0.45f_c'S_t}{A_{ps}f_{pe}} + \frac{S_t}{A_g} + \frac{M_g + M_s + M_h}{A_{ps}f_{pe}} + \frac{(M_{ws} + M_r)S_t}{S_{tgc}A_{ps}f_{pe}}$$

$$\rightarrow e_{pg} \geq \left(-0.45f_c'S_t + (M_g + M_s + M_h) + \frac{(M_{ws} + M_r)S_t}{S_{tgc}}\right)\frac{1}{F} + \frac{S_t}{A_g}$$

$$\rightarrow e_{pg} \geq \left(-0.45(18)(4{,}779) + (7{,}199 + 10{,}979 + 732) + \frac{(2411 + 1581)4{,}779}{(40{,}638)}\right)\frac{1}{F} + \frac{4{,}779}{627}$$

$$\rightarrow e_{pg} \geq (-38{,}710 + 18{,}910 + 469)\frac{1}{F} + 7.62$$

$$\rightarrow e_{pg} \geq (-19{,}331)\frac{1}{F} + 7.62$$

4.7.7.2 Tension Stress after Losses

The tension stress limit at the bottom fiber at the midspan due the effective prestress after losses for Service III Load combination from AASHTO LRFD Specifications (AASHTO 2020) Table 3.4.1-1 is considered. The tensile limit for the composite section is $0.85f_t'$ as per AASHTO draft specifications for UHPC (FHWA 2022).

<u>Computation of Tension Limit at Bottom Fiber at Midspan</u>

$$-\frac{A_{ps}f_{pe}}{A_g}-\frac{A_{ps}f_{pe}e_{pg}}{S_b}+\frac{M_g+M_s+M_h}{S_b}+\frac{M_{ws}+M_r+M_L}{S_{bc}}\leq 0.85f_t' \tag{4.61}$$

$$\rightarrow e_{pg}\geq -\frac{0.85f_t'S_b}{A_{ps}f_{pe}}-\frac{S_b}{A_g}+\frac{M_g+M_s+M_h}{A_{ps}f_{pe}}+\frac{(M_{ws}+M_r+M_L)S_b}{S_{bc}A_{ps}f_{pe}}$$

$$\rightarrow e_{pg}\geq \left(-0.85f_t'S_b+(M_g+M_s+M_h)+\frac{(M_{ws}+M_r+M_L)S_b}{S_{bc}}\right)\frac{1}{F}-\frac{S_b}{A_g}$$

$$\rightarrow e_{pg}\geq \left(-0.85(0.85)(5{,}697)+(7{,}199+10{,}979+732)\right.$$
$$\left.+\frac{(2{,}411+1{,}581+19{,}906)5{,}697}{10{,}000}\right)\frac{1}{F}-\frac{5{,}697}{627}$$

$$\rightarrow e_{pg}\geq (-4116+18{,}910+13{,}614)\frac{1}{F}-9.09$$

$$\rightarrow e_{pg}\geq (28{,}408)\frac{1}{F}-9.09$$

Figure 4.4 presents the stress blocks for the inequalities derived. The shape of the stress diagrams represents the actual stress distribution, while the final values provided are the stress limits. It is to be noted that the eccentricity is recorded in inches and is plotted against the inverse of the prestressing force. The optimal number of strands that satisfies the feasible domain is derived from a series of iterations of prestress loss computation. A harped section is designed using 48 strands with 9.93 in. eccentricity at midspan and 5.26 in. eccentricity at the ends. The

selection will be evaluated by checking the stresses within the section with e_{end} or e_{pg} and N combination. For this combination, the prestressing forces are shown.

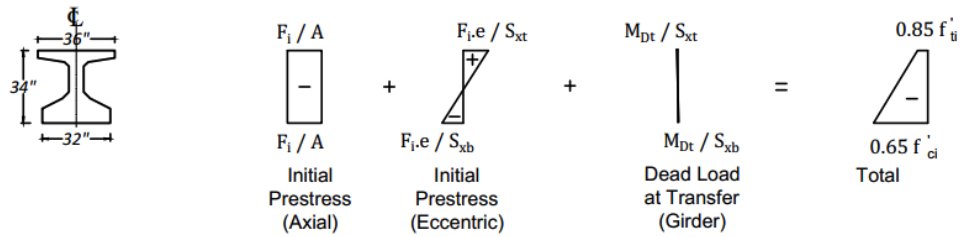

(a) Stress checks at transfer

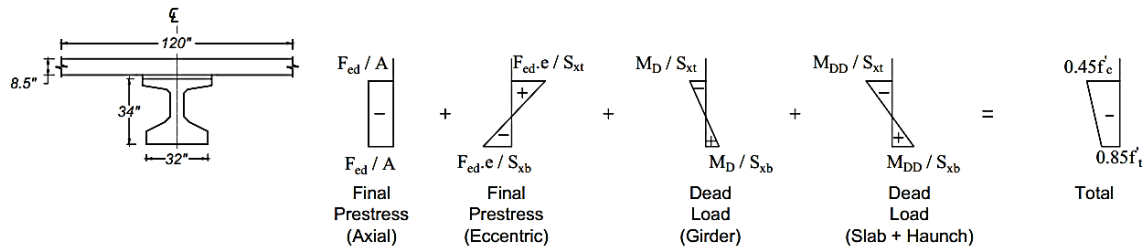

(b) Stress checks at deck placement

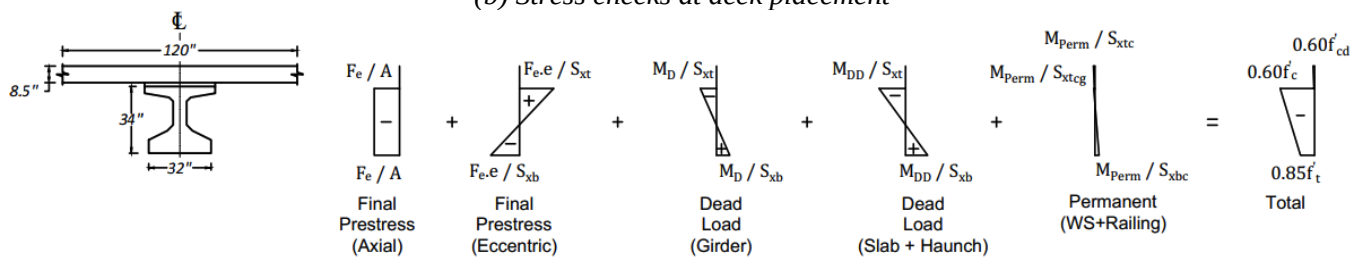

(c) Stress checks at service due to effective prestress and permanent (dead) loads

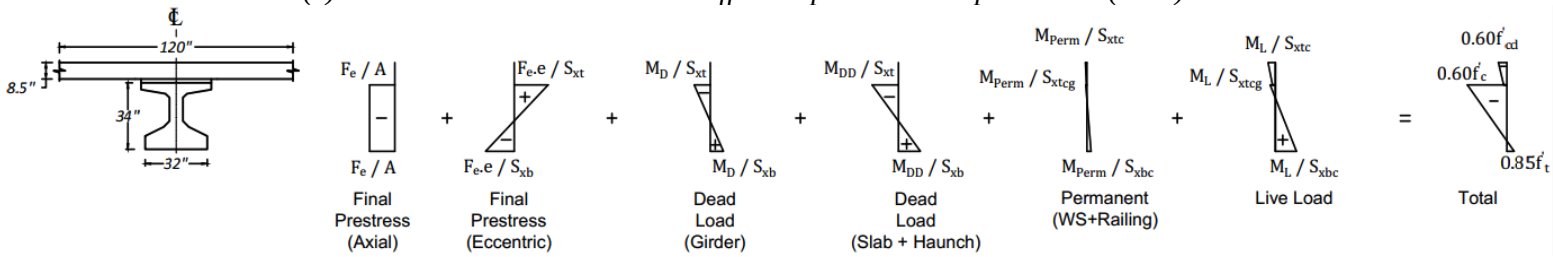

(d) Stress checks at service due to total and effective prestress

Figure 4.4. Stress Blocks for the Derived Inequalities.

Force in Prestressing

Force in prestressing strand at transfer, F_i = $NA_t(0.75f_{pu} - \Delta f_{pST})$ (4.62)

= (48) (0.217) (179.2) = 1867 kips

Force in prestressing strand after losses at deck placement, F_{ed} = $NA_t f_{ped}$ (4.63)

= (48) (0.217) (155.9) = 1624 kips

Force in prestressing strand after losses, F_e = $NA_t f_{pe}$ (4.64)

= (48) (0.217) (145.7) = 1517 kips

Figure 4.5 presents the feasible domain with the eccentricity on the y-axis and the inverse of the prestress force on the x-axis. Note that the top cross-sectional view represents the midspan section and the bottom cross section represents the girder end section. Unlike the girder specimen tested, no straight strands in the top flange were needed by design for this specimen. The transverse reinforcement R-bars are tied to the two non-stressed straight strands at the top of the girder cross-section that are present in the precast bed by default for the purpose of guiding and tying the transverse shear reinforcement bars.

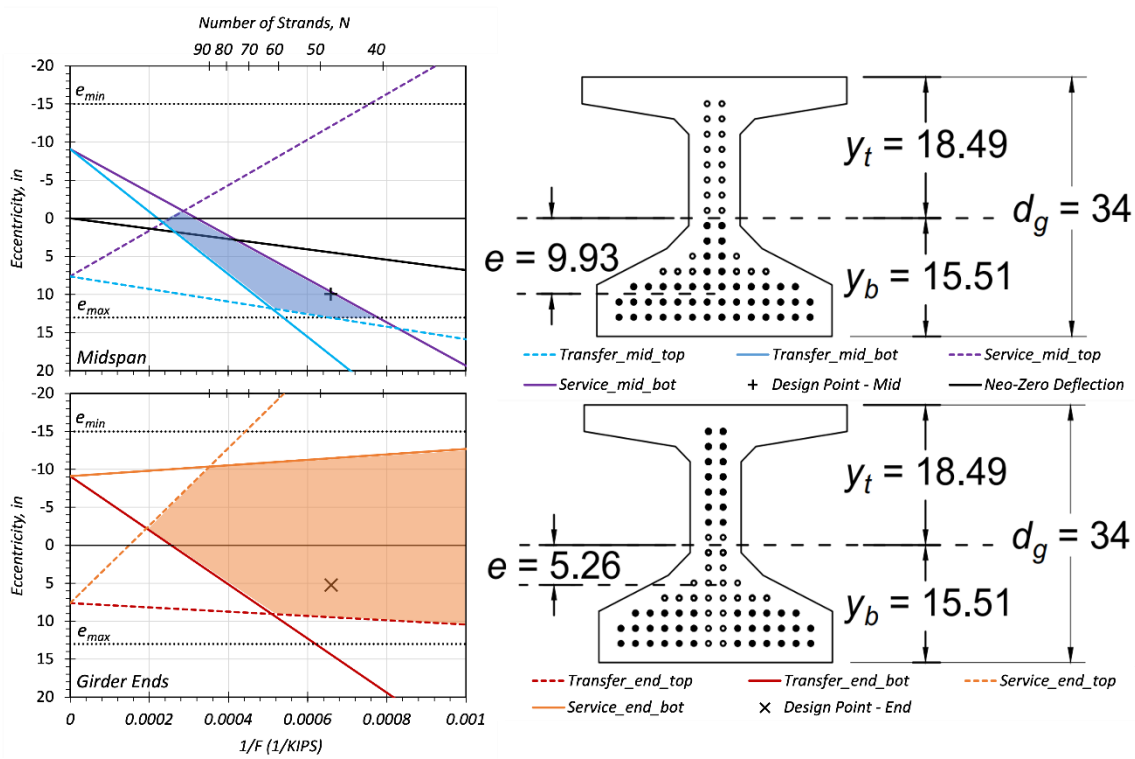

Figure 4.5. Feasible Domain for Flexure Design.

4.7.7.3 Stress Checks

The stresses will be evaluated at each of the critical stages within the bridge construction.

<u>Computation at Prestress Transfer</u>

Stress at bottom fiber at transfer length, f_{bottom}

$$= -\frac{F_i}{A_g} - \frac{F_i e_{end}}{S_b} + \frac{M_{Dt}}{S_b} \geq -0.65 f'_{ci} \tag{4.65}$$

$$= -\frac{1867}{627} - \frac{(1867)(5.26)}{5697} + \frac{520}{5697} \geq -(0.65)(11.7)$$

$$= -2.98 - 1.72 + 0.09 = -4.61 \text{ ksi} \geq -7.61 \text{ ksi [Check OK]}$$

Stress at top fiber at transfer length, f_{top}

$$= -\frac{F_i}{A_g} + \frac{F_i e_{end}}{S_t} - \frac{M_{Dt}}{S_t} \leq 0.85 f'_{ti} \tag{4.66}$$

$$= -\frac{1866}{627} + \frac{(1866)(5.26)}{4779} - \frac{520}{4779} \leq (0.85)(0.72)$$

$$= -2.98 + 2.06 - 0.11 = -1.03 \text{ ksi} \leq 0.61 \text{ ksi [Check OK]}$$

Computation at Deck Placement

Stress at top fiber at midspan, f_{top}

$$= -\frac{F_{ed}}{A_g} + \frac{F_{ed}e_{pg}}{S_t} - \frac{M_g + M_s + M_h}{S_t} \geq -0.45f_c' \quad (4.67)$$

$$= -\frac{1624}{627} + \frac{(1624)(9.93)}{4779} - \frac{(7{,}199 + 10{,}979 + 732)}{4779} \geq -(0.45)(18)$$

$$= -2.59 + 3.37 - 3.96 = -3.18 \text{ ksi} \geq -8.1 \text{ ksi [Check OK]}$$

Stress at bottom fiber at midspan, f_{bottom}

$$= -\frac{F_{ed}}{A_g} - \frac{F_{ed}e_{pg}}{S_b} + \frac{M_g + M_s + M_h}{S_b} \leq 0.85f_t' \quad (4.68)$$

$$= -\frac{1624}{627} - \frac{(1624)(9.93)}{5697} + \frac{(7{,}199 + 10{,}979 + 732)}{5697} \leq (0.85)(0.85)$$

$$= -2.59 - 2.83 + 3.32 = -2.10 \text{ ksi} \leq 0.72 \text{ ksi [Check OK]}$$

Computation at Final

Stress at top fiber at midspan (Permanent), $f_{top.perm}$

$$= -\frac{F_e}{A_g} + \frac{F_e e_{pg}}{S_t} - \frac{M_g + M_s + M_h}{S_t} - \frac{M_{ws} + M_r}{S_{tg}} \geq -0.45f_c' \quad (4.69)$$

$$= -\frac{1517}{627} + \frac{(1517)(9.93)}{4779} - \frac{(7{,}199 + 10{,}979 + 732)}{4779} - \frac{(2411 + 1581)}{40{,}638} \geq -(0.45)(18)$$

$$= -2.42 + 3.15 - 3.96 - 0.10 = -3.33 \text{ ksi} \geq -8.1 \text{ ksi [Check OK]}$$

Stress at top fiber at midspan, f_{top}

$$= -\frac{F_e}{A_g} + \frac{F_e e_{pg}}{S_t} - \frac{M_g + M_s + M_h}{S_t} - \frac{M_{ws} + M_r + M_L}{S_{tg}} \geq -0.6f_c' \quad (4.70)$$

$$= -\frac{1517}{627} + \frac{(1517)(9.93)}{4779} - \frac{(7{,}199 + 10{,}979 + 732)}{4779} - \frac{(2411 + 1581 + 19848)}{40{,}638} \geq -(0.60)(18)$$

$$= -2.42 + 3.15 - 3.96 - 0.59 = -3.82 \text{ ksi} \geq -10.8 \text{ ksi [Check OK]}$$

Stress at bottom fiber at midspan, f_{bottom}

$$= -\frac{F_e}{A_g} - \frac{F_e e_{pg}}{S_b} + \frac{M_g + M_s + M_h}{S_b} + \frac{M_{ws} + M_r + M_L}{S_{bc}} \leq 0.85 f_t' \quad (4.71)$$

$$= -\frac{1517}{627} - \frac{(1517)(9.93)}{5697} + \frac{(7{,}199 + 10{,}979 + 732)}{5697} + \frac{(2411 + 1581 + 19{,}848)}{10{,}000} \leq (0.85)(0.85)$$

$$= -2.42 - 2.64 + 3.32 + 2.39 = 0.65 \text{ ksi}$$

$$\leq 0.72 \text{ ksi [Check OK]}$$

The section passes all the stress checks. Therefore, the selection of 48 strands with 9.93 in. eccentricity at midspan and 5.26 in. eccentricity at the girder ends (14 strands harped) may be used based on the service stress checks. Figure 4.6 presents the strand layout selected. Figure 4.7 presents the stress block diagrams of the critical sections at transfer and service.

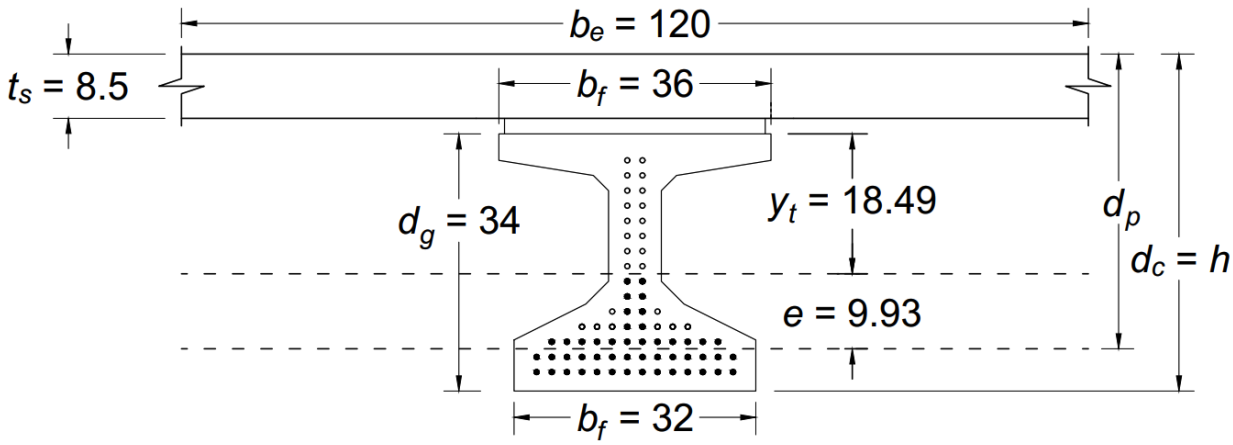

(a) Midspan

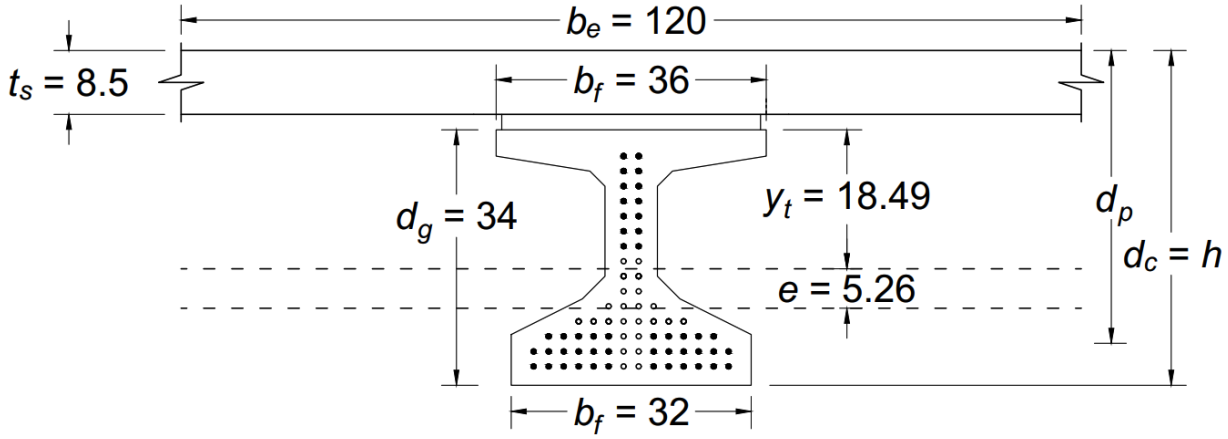

(b) End

Figure 4.6. Strand Layout.

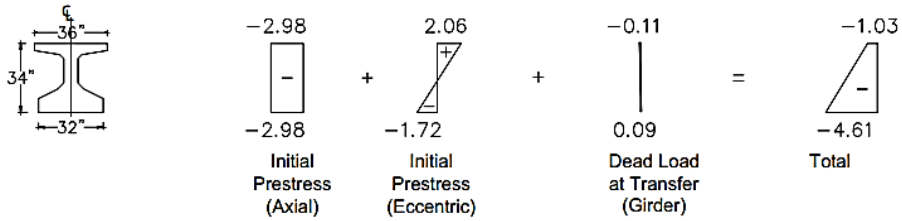

(a) Stress checks at transfer

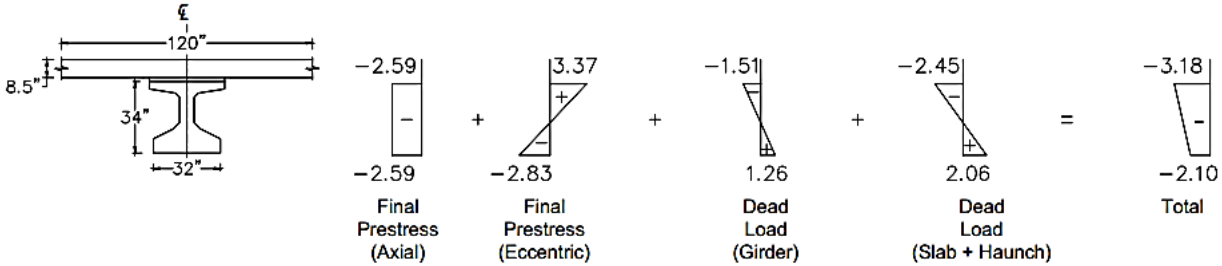

(b) Stress checks at deck placement

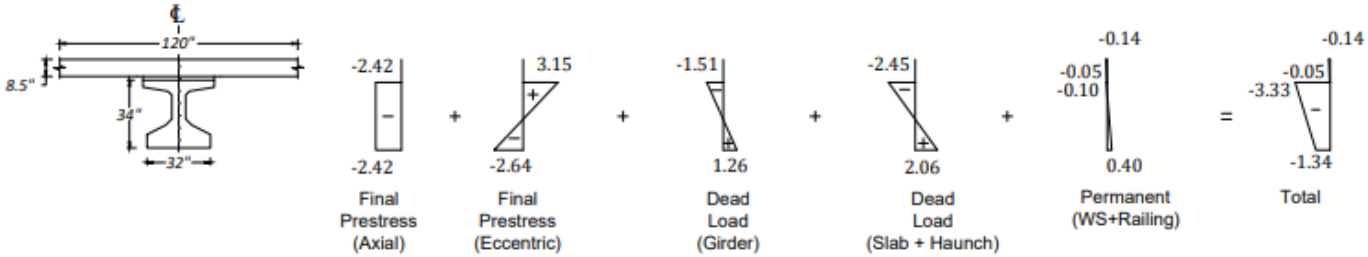

(c) Stress checks at service due to effective prestress and permanent (dead) loads

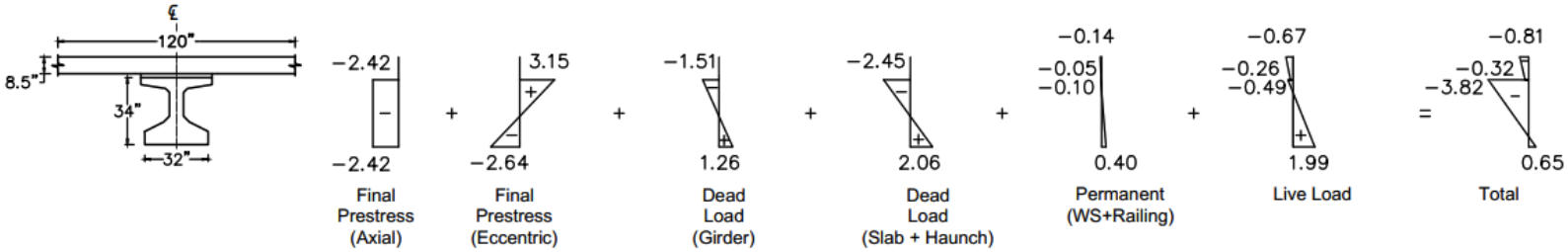

(d) Stress checks at service due to total and effective prestress

Figure 4.7. Stress Checks.

4.7.8 Camber Calculation

<u>Computation of Deflections</u>

Girder self-weight at transfer, Δ_{gtr}

$$= \frac{5w_g {L_g}^4}{384E_{gi}I_g}$$

$$= \frac{(5)(0.697)(84.5^4)}{(384)(6742)\left(\frac{88{,}355}{144\ \text{in}^2/\text{ft}^2}\right)} \times 12\ \text{in./ft}$$

$$= 1.34\ \text{in.}$$

Girder self-weight at erection, Δ_{ger}

$$= \frac{5w_g L^4}{384E_{gi}I_g}$$

$$= \frac{(5)(0.697)(83.0^4)}{(384)(6742)\left(\frac{88{,}355}{144\ \text{in.}^2/\text{ft}^2}\right)} \times 12\ \text{in./ft}$$

$$= 1.25\ \text{in.}$$

Harp point (a)

$$= \frac{L_g}{2} - \max\left(\frac{L_g}{20}, 5\right) = \frac{84.5}{2} - 5 = 37.25\ \text{ft}$$

Prestressing strands, Δ_{PS}

$$= -\frac{F_i}{E_{gi}I_g}\left(\frac{e{L_g}^2}{8} - \frac{(e - e_{end})(a)^2}{6}\right)$$

$$= -\frac{(1867)}{(6742)(88{,}355)}\left(\frac{(9.93)(84.5 \times 12\ \text{in./ft})^2}{8} - \frac{(9.93 - 5.26)(37.25 \times 12\ \text{in./ft})^2}{6}\right)$$

$$= -3.51\ \text{in.}$$

Deck and haunch, Δ_{sl} $= \dfrac{5(w_s + w_h)L^4}{384E_g I_{gc}}$

$$= \frac{(5)(1.062 + 0.071)(83^4)}{(384)(7423)\left(\dfrac{272{,}852}{144\ \text{in}^2/\text{ft}^2}\right)} \times 12\ \text{in./ft}$$

$= 0.60$ in.

Superimposed dead load, Δ_{SI} $= \dfrac{5(w_{ws} + w_{rl})L^4}{384E_g I_{gc}}$

$$= \frac{(5)(0.23 + 0.15)(83^4)}{(384)(7423)\left(\dfrac{272{,}852}{144\ \text{in}^2/\text{ft}^2}\right)} \times 12\ \text{in./ft}$$

$= 0.20$ in.

Prestress Loss, $\Delta_{PS_{loss}}$ (90 days) $= \dfrac{A_{ps}\Delta f_{pLT}}{E_g I_g}\left(\dfrac{eL^2}{8} - \dfrac{(e - e_{end})(a)^2}{6}\right)$

$$= \frac{(9.98)(23.3)}{(7423)(88{,}355)}\left(\frac{(9.93)(83 \times 12\ \text{in./ft})^2}{8} - \frac{(4.67)(37.25 \times 12\ \text{in./ft})^2}{6}\right)$$

$= 0.38$ in.

Prestress Loss, $\Delta_{PS_{loss}}$ (27,375 days) $= \dfrac{A_{ps}\Delta f_{pLT}}{E_g I_g}\left(\dfrac{eL^2}{8} - \dfrac{(e - e_{end})(a)^2}{6}\right)$

$$= \frac{(9.98)(33.55)}{(7423)(88{,}355)}\left(\frac{(9.93)(83 \times 12\ \text{in./ft})^2}{8} - \frac{(4.67)(37.25 \times 12\ \text{in./ft})^2}{6}\right)$$

$= 0.55$ in.

The creep coefficient is computed as per the experimental study conducted and noted in the Volume 1 report and in Section 3.4.2.2 of this report:

Creep coefficient at 90 days (deck placement) $\psi_{CR} = 0.53$

Creep coefficient at 27,375 days (final) $\psi_{CR} = 0.80$

Deflection at transfer, $\Delta_{at_transfer}$

$$= \left(\Delta_{gtr} + \Delta_{PS}\right)$$
$$= (1.34 - 3.51)$$
$$= -2.17 \text{ in.}$$

Deflection before deck placement, Δ_{before_deck}

$$= \left(\Delta_{g_{tr}} + \Delta_{PS}\right)(1 + \psi_{CR}) + \left(\Delta_{PS_loss}(1 + 0.7\psi_{CR})\right)$$
$$= (1.34 - 3.51)\ (1 + 0.53) + \left(0.38\left(1 + 0.7(0.53)\right)\right)$$
$$= -2.80 \text{ in.}$$

Deflection after casting deck, Δ_{after_deck}

$$= \left(\Delta_{g_{tr}} + \Delta_{PS}\right)(1 + \psi_{CR}) + \left(\Delta_{PS_loss}(1 + 0.7\psi_{CR})\right) + \Delta_{sl}$$
$$= (1.34 - 3.51)\ (1 + 0.53) + \left(0.38\left(1 + 0.7(0.53)\right)\right) + 0.60$$
$$= -2.20 \text{ in.}$$

Final deflection, Δ_{final}

$$= \left(\Delta_{g_{tr}} + \Delta_{PS}\right)(1 + \psi_{CR}) + \left(\Delta_{PS_loss}(1 + 0.7\psi_{CR})\right) + \Delta_{sl} + \Delta_{SI}$$
$$= (1.34 - 3.51)\ (1 + 0.80) + \left(0.55\left(1 + 0.7(0.80)\right)\right) + 0.60 + 0.20$$
$$= -2.25 \text{ in.}$$

4.7.9 Live Load Deflection Check

For the preliminary analysis and design purposes, this example considers the maximum allowable deflection limit to be span length *L* divided by 800 (AASHTO 2020).

<u>Maximum allowable deflection limit</u>

Maximum deflection limit, Δ_{limit}

$$= \frac{L}{800} \tag{4.72}$$
$$= \frac{83}{800} = 0.104 \text{ ft} = 1.25 \text{ in.}$$

Deflection due to uniformly distributed load, Δ_{UDL}

$$= mN_L \frac{5qL^4}{384E_gI_{br}} \tag{4.73}$$

$$= (0.85)(3)\left(\frac{(5)(0.64)(83^4)}{(384)(7423)\left(\frac{1{,}287{,}969}{144\ \text{in.}^2/\text{ft}^2}\right)}\right) \times 12\ \text{in./ft}$$

$$= 0.18\ \text{in.}$$

Deflection due to HS20 truck, Δ_{HS20}

$$= 1.33mN_L \frac{\left(32L^3 + 40\left(\frac{L}{2} - 14\right)\left(3L^2 - 4\left(\frac{L}{2} - 14\right)^2\right)\right)}{48E_gI_{br}} \tag{4.74}$$

$$= (1.33)(0.85)(3)\left(\frac{\left(32(83)^3 + (40)\left(\frac{83}{2} - 14\right)\left(3 * 83^2 - 4\left(\frac{83}{2} - 14\right)^2\right)\right)}{(48)(7423)\left(\frac{1{,}287{,}969}{144\ \text{in}^2/\text{ft}^2}\right)}\right)$$

$$\times 12\ \text{in./ft}$$

$$= 0.48\ \text{in.}$$

<u>Computation of Governing Live Load Deflection, Δ_{LL}</u>

Deflection due to live load, Δ_{LL}

$$= \max\left(\Delta_{HS20}, (\Delta_{UDL} + 0.25\Delta_{HS20})\right) \tag{4.75}$$

$$= 0.48\ \text{in.} \leq 1.25\ \text{in.}\ [\text{Check OK}]$$

4.7.10 Flexural Resistance at Strength Limit State

This section documents the ultimate strength check of the prestressed members based on the approach used in the AASHTO LRFD Specifications (AASHTO 2020). The load combination of Strength I is used for this check. The approach provided in the AASHTO draft specifications for UHPC (FHWA 2022) are also shown below for reference.

$$M_u = 1.25\left(M_g + M_s + M_h + M_r\right) + 1.50(M_{ws}) + 1.75(M_{LL}) \tag{4.76}$$

where:

M_u	=	Ultimate factored moment demand
M_g	=	Moment at midspan due to self-weight of the girder, kip-ft
M_s	=	Moment at midspan due to weight of the deck slab, kip-ft
M_h	=	Moment at midspan due to weight of the haunch, kip-ft
M_{ws}	=	Moment at midspan due to weight of the wearing surface, kip-ft
M_r	=	Moment at midspan due to weight of the railing, kip-ft
M_{LL}	=	Moment at midspan due to live loads, kip-ft

Moment Demand, M_u

$$= 1.25\left(M_g + M_s + M_h + M_r\right) + 1.50(M_{ws}) + 1.75(M_{LL}) \quad (4.77)$$

$$= 1.25(600 + 915 + 61 + 132) + 1.50(201) + 1.75(1659)$$

$$= 5339 \text{ kip-ft}$$

The method of AASHTO LRFD Specifications (AASHTO 2020) from Article 5.6.3 using a rectangular stress distribution is shown below. This method is chosen for the composite CIP CC deck and UHPC girder in this example due to the large contribution of the deck to the internal compression force in bending. The nominal flexure capacity computed using the AASHTO LRFD Specifications (AASHTO 2020) assumes a rectangular distribution of stress in the compression zone and neglects the tensile strength of the concrete.

k = 0.28 [for low relaxation strands]

Distance between extreme compression fiber and centroid of strands, d_p

$$= y_t + e + t_s \quad (4.78)$$

$$= 18.49 + 9.93 + 8.5$$

$$= 36.9 \text{ in.}$$

Note: The haunch is conservatively being neglected when determining d_p.

Flexural resistance factor, ϕ

$$= 1.0 \quad (4.79)$$

Stress block parameter, α_1 $= 0.85$ for $f_{cd} \leq 10$ (4.80)

$= \max(0.85 - 0.02(f_{cd} - 10), 0.75)$ for $f_{cd} > 10$

$= 0.85$ $f_{cd} = 4 \leq 10$

Stress block parameter, α_2 $= \max\ (0.85 - 0.02(f_c - 10), 0.75)$ (4.81)

$= \max\ (0.85 - 0.02(18 - 10), 0.75)$

$= 0.75$

Stress block parameter for deck, β_1 $= \max\ (0.85 - 0.05(f_{cd} - 4), 0.65)$ (4.82)

$= \max\ (0.85 - 0.05(4 - 4), 0.65)$

$= 0.85$

Stress block parameter for UHPC girder, β_2 $= \max\ (0.85 - 0.05(f_c - 4), 0.65)$ (4.83)

$= \max\ (0.85 - 0.05(18 - 4), 0.65)$

$= 0.65$

Assuming $a < t_s$

Distance from the extreme compression fiber to the neutral axis, c

$$= \frac{A_{ps}f_{pu} + A_s f_s + A_s' f_s'}{\alpha_1 f_c' \beta_1 b + kA_{ps}\left(\frac{f_{pu}}{d_p}\right)} \quad (4.84)$$

$$= \frac{(10.42)(270)}{(0.85)(4)(0.85)(120) + (0.28)(10.42)\left(\frac{270}{36.9}\right)}$$

$= 7.64$ in.

Depth of equivalent rectangular stress block, a $= \beta_1 c$ (4.85)

$= (0.85)(7.64)$

$= 6.49$ in.

$a = 6.49$ in. $\leq t_s = 8.5$ in. [Check OK]

The compression force is within the CIP CC deck. Therefore, a rectangular stress block assumption is appropriate.

When $f_{pe} \geq 0.5 f_{pu}$ $\quad f_{ps} = f_{pu}\left(1 - k\dfrac{c}{d_p}\right)$ (4.86)

$$f_{ps} = 270\left(1 - 0.28\frac{7.64}{36.9}\right)$$

$$f_{ps} = 254.35 \text{ ksi}$$

Inner lever arm, z $\quad = d_p - \dfrac{1}{2}a$ (4.87)

$$= 36.92 - 3.25$$

$$= 33.67 \text{ in.}$$

Nominal moment, M_n $\quad = A_{ps} f_{ps} z$ (4.88)

$$= (10.42)(254.35)(33.67)$$

$$= 89{,}204 \text{ kip-in.} = 7434 \text{ kip-ft}$$

Reduced nominal moment, M_r $\quad = \phi M_n$ (4.89)

$$= (1.0)(7434)$$

$$= 7434 \text{ kip-ft}$$

$$M_r = 7434 \text{ kip-ft} \geq M_u = 5339 \text{ kip-ft}$$

[Check OK]

The section passes the flexural resistance check for the strength limit state.

The method for computing the nominal moment capacity of a given section recommended as per AASHTO draft specifications for UHPC (FHWA 2022) is applied below. The formulation for computing the moment capacity is explained in Section 3.7.3. The calculations for the approach provided in the AASHTO draft specifications for UHPC (FHWA 2022) are as follows.

Assuming $a < t_s$

Distance from the extreme compression fiber to the neutral axis, c

$$= \frac{A_{ps}f_{pu} + 0.5f'_t(2b_{tf1}h_{tf1} + b_{tf2}h_{tf2} - t_s b_w)}{\alpha_1 f'_c \beta_1 b + kA_{ps}\left(\frac{f_{pu}}{d_p}\right) - 0.5f'_t 3b_w} \quad (4.90)$$

$$= \frac{(10.42)(270) + 0.5(0.85)(2(14.5)(3.5) + (9.25)(4) - (8.5)(7))}{(0.85)(4)(0.85)(120) + (0.28)(10.42)\left(\frac{270}{36.9}\right) - 0.5(0.85)(3)(7)}$$

$$= 7.92 \text{ in.}$$

$c = 7.92$ in. $\leq t_s = 8.5$ in. [Check OK]

The compression force is within the CIP CC deck. Therefore, a rectangular stress block assumption is appropriate.

Inner lever arm, z

$$= d_p - \frac{1}{2}\beta_1 c \quad (4.91)$$

$$= 36.92 - \left({}^{1}/_{2}\right)0.85(7.92)$$

$$= 33.55 \text{ in.}$$

Nominal moment, M_n

$$= \alpha_1 f'_c \beta_1 cbz - 0.5f'_t\left(2b_{tf1}h_{tf1}\right) * \left(d_p - t_s - h_{tf1}/2\right) \quad (4.92)$$

$$- 0.5f'_t(b_{tf2}h_{tf2})$$

$$* \left(d_p - t_s - h_{tf1} - h_{tf2}/3\right)$$

$$- 0.5f'_t(3c - t_s)b_w$$

$$* \left(d_p - t_s - (3c - t_s)/2\right)$$

$$= 0.85 * 4 * 0.85 * 7.92 * 120 * 33.55 - 0.5$$

$$* 0.85(2 * 14.5 * 3.5) * \left(36.92 - 8.5 - \frac{3.5}{2}\right)$$

$$- 0.5 * 0.85(9.25 * 4)$$

$$* \left(36.92 - 8.5 - 3.5 - \frac{4}{3}\right) - 0.5 * 0.85(3$$

$$* 7.92 - 8.5)7$$

$$* (36.92 - 8.5 - (3 * 7.92 - 8.5)/2)$$

$$= 89{,}716 \text{ kip-in.} = 7476 \text{ kip-ft}$$

Reduced nominal moment, M_r $= \phi M_n$ (4.93)

$= (0.9)(7476)$

$= 6729$ kip-ft

$M_r = 6729$ kip-ft $\geq M_u = 5339$ kip-ft

[Check OK]

The section passes the flexural resistance check for the strength limit state.

Table 4.13 compares the nominal moment capacity, neutral axis depth, and the lever arm calculated by the two approaches, AASHTO LRFD Specifications (AASHTO 2020) and the proposed UHPC draft specifications. Note that for this example the simplified approach based on the AASHTO LRFD Specifications provides a value close to that of the proposed UHPC draft specifications but is slightly more conservative.

Table 4.13. Comparison of Nominal Moment Capacity.

Description	AASHTO LRFD	FHWA (2022)	Ratio
Nominal Moment M_n, k-ft	7434	7476	0.99
Neutral Axis c, in.	7.64	7.92	0.96
Lever Arm z, in.	33.67	33.55	1.00

4.8 SHEAR RESISTANCE AT STRENGTH LIMIT STATE

Shear design of the UHPC bridge considers the additional strength due to the presence of steel fibers. The recommendations from El-Helou and Graybeal (2022) are used for computing the design shear strength.

4.8.1 Critical Section for Shear

The critical section for the maximum design V_u is computed as per the AASHTO LRFD Specifications (AASHTO 2020) Article 5.7.3.2 and is taken at a distance d_v from the inside face of the support.

4.8.2 Nominal Shear Resistance

Factored Shear Demand, V_u $= 1.25(V_g + V_h + V_s + V_r) + 1.50(V_{ws}) + 1.75(V_{LL})$

$= (1.25)(26.4 + 2.7 + 40.3 + 5.8) + (1.50)(8.9) + (1.75)(100.1)$ (4.94)

$= 282.5$ kips

Ultimate shear resistance of UHPC, V_{Rd} $= V_{Rd,UHPC} + V_{Rd,S} + V_{Rd,P}$ (4.95)

Based on the empirical results documented in the Appendix B of the AASHTO draft specifications for UHPC (FHWA 2022):

Shear failure angle, θ $=27.3^{o}$

d_v is computed as per Section 4.6.4.

Effective shear depth (d_v) $= \max$ (inner lever arm (z), $\max(0.9d_p, 0.72h)$) (4.96)

$= \max(33.67, \max(0.9\ (37.30), 0.72\ (44.50))$

$= \max(33.67, \max(33.60, 32.00)$

$= \max(33.67, 33.60)$

$= 33.67$ in.

Note: Computation of z and d_p are shown in Section 4.7.10 under flexure resistance at strength limit state.

UHPC contribution term, $V_{Rd,UHPC}$ $= f'_t b_w d_v cot(\theta)$ (4.97)

$= (0.85)(7)(33.67)\cot(27.3)$

$= 388.1$ kips

Transverse steel contribution, $V_{Rd,S}$ $= \dfrac{A_v f_y d_v \cot(\theta)}{s}$

where:

A_v = Area of transverse steel = (2)(0.20) = 0.40 in^2

f_y = Yield strength of transverse steel = 60 ksi

s = Spacing between transverse steel

= $0.25d_v \cot(\theta) \leq 24$ in. = $0.25(34.2)\cot(27.3) = 16.5$ in.

Use #4 R bars at 24 in. spacing for minimum transverse reinforcement.

$V_{Rd,S}$ $= \frac{(0.40)(60)(33.67)\cot(27.3)}{16.5}$

$= 94.9$ kips

Harped strands contribution, $V_{Rd,P}$ $= N_H A_p f_{pe} \sin(\alpha)$ (4.98)

where:

N_H = Number of strands harped = 14

α = Angle of harped strands

$= \tan^{-1}\left({(d_{s_top} - d_s)}/{a}\right)$

$= \tan^{-1}\left({(30.5 - 14.5)}/{(37.25 \times 12)}\right)$

$= 2.05^{o}$

where:

d_{s_top} = The distance from the bottom of girder to the centerline of the uppermost harped strand at the girder end, in.

d_s = The distance from the bottom of girder to the centerline of the uppermost harped strand at the location where harping begins near the girder midspan, in.

$V_{Rd,P}$ $=(14)(0.217)(145.7)\sin(2.05)$ (4.99)

$= 15.83$ kips

With no transverse reinforcement

$\therefore\ V_{Rd}$ $= V_{Rd,UHPC} + V_{Rd,P}$ (4.100)

$= 388.1 + 15.83$

$= 404$ kips

Factored shear resistance $= \phi_v V_{Rd}$

$= 0.9 \times 404$

$= 363.6$ kips

Because $V_u = 282.5 \text{ kips} \geq (0.5)(363.6) \text{ kips} = 181.8 \text{ kips}$,

$V_u \geq 0.5\, V_{Rd}$

therefore, minimum shear reinforcement is required per AASHTO (2020). Note that the AASHTO draft specifications for UHPC (FHWA 2022) does not require minimum shear reinforcement in this case. However, based on the results of this research project it is recommended that minimum shear reinforcement be used.

With minimum transverse reinforcement

$$\therefore\ V_{Rd} = V_{Rd,UHPC} + V_{Rd,S} + V_{Rd,P} \tag{4.101}$$

$$= 388.1 + 94.9 + 15.83$$

$$= 498.9 \text{ kips}$$

Factored shear resistance $= \phi_v V_{Rd}$

$$= 0.9 \times 498.9$$

$$= 449 \text{ kips} \geq V_u = 282.5 \text{ kips} \quad \text{[Check OK]}$$

4.9 SPLITTING RESISTANCE

Splitting resistance of the end anchorage zone is checked based on the AASHTO draft specifications for UHPC (FHWA 2022). The splitting resistance of pretensioned anchorage zones is computed as follows:

$$P_r = 0.04 P_i = 0.04 \times 1867 \tag{4.102}$$

$$= 74.7 \text{ kips}$$

To account for the resistance, a steel stress f_s of 20 ksi is assumed and the reinforcement zone is limited to a distance of $h/4$ from the end of the girder. To consider the effects of steel fibers two options are explored.

Option 1: The resistance to splitting forces contributed by the steel fibers of UHPC are assumed as per the AASHTO draft specifications for UHPC (FWHA 2022) and the formula is listed below.

$$f_s A_s + 0.25\gamma_u f'_t h b_v \geq 0.04 P_i \tag{4.103}$$

Rewriting the above expression, the area of transverse steel located within a distance of $h/4$ from the girder ends is determined as:

$$\begin{aligned} A_s &\geq \frac{(0.04P_i - 0.25\gamma_u f'_t h b_v)}{f_s} \\ &\geq \frac{(74.7 - 0.25 \times 0.85 \times 0.72 \times 34 \times 7)}{20} \\ &= 1.91 \text{ in}^2 \end{aligned}$$

Using #5 R-bars (two legs), the number of bars, $N_{stirrups} = A_s/A_v$

$$N_{stirrups} = 1.91/(0.31 \times 2) = 3.08 \sim 3$$

$$\text{Spacing, } s = \frac{\frac{h}{4} - \text{cover}}{N_{stirrups} - 1} = \frac{34/4 - 2.5}{(3-1)} = 3 \text{ in.}$$

Option 2: The alternate mechanics-based method explained in Section 3.10.3 of this report is demonstrated. The resistance to splitting forces contributed by the steel fibers of UHPC are assumed based on the orientation of fibers. The fiber orientation is assumed to be in three directions. Therefore, 1/3 is considered as a reasonable reduction factor to account for the orientation of fibers in the vertical direction. The equivalent area of transverse reinforcement provided by the steel fibers is determined as follows.

$$\begin{aligned} & f_s A_s \geq 0.04 P_i \\ A_{s,req.} &\geq 0.04 P_i / f_s \\ &\geq 0.04 \times 1867/20 \\ &\geq 3.73 \text{ in}^2 \end{aligned} \tag{4.104}$$

Contribution of fiber:

Volume of steel fibers, ρ_{fiber} $= 1.5\% = 0.015$

Tensile strength of steel fibers, f_{fiber} $= 406$ ksi

Yield strength of stirrups, $f_{stirrup}$ $= 60$ ksi

To determine the equivalent area of transverse reinforcement:

$$\frac{\rho_{fiber} f_{fiber}}{3} = \frac{A_{v_eq} f_{stirrup}}{b_v \, {}^{h}/_{4}}$$

$$A_{v_eq} = \frac{\rho_{fiber} f_{fiber} \left(b_v \, {}^{h}/_{4}\right)}{3 f_{stirrup}}$$

$$A_{v_eq} = \frac{0.015 \times 406 \times 7 \times {}^{34}/_{4}}{3 \times 60}$$

$$= 1.86 \text{ in}^2$$

Total area of stirrups may be calculated as follows:

$$A_{s,req.} = A_s + A_{v_eq}$$

$$A_s = A_{s,req.} - A_{v_eq}$$

$$A_s = 3.73 - 1.86$$

$$= 1.87 \text{ in}^2$$

Using #5 R-bars, the number of bars, $N_{stirrups} = A_s / A_v$

$$N_{stirrups} = 1.87/(0.31 \times 2) = 3.02 \sim 3$$

Spacing, s $= \dfrac{\frac{h}{4} - \text{cover}}{N_{stirrups} - 1} = \dfrac{34/4 - 2.5}{(3 - 1)} = 3$ in.

4.10 INTERFACE SHEAR DESIGN

As discussed in Section 3.9.1, the interface shear design approach below follows Section 5.7.4.3 of the AASHTO LRFD Specifications (AASHTO (2020) where the interface consists of

placement of CC on clean, laitance free concrete without intentional roughening. These recommendations are consistent with those of FHWA (2022) for CC on clean, laitance free UHPC. The interface shear resistance is determined as follows.

The factored shear force at the critical section (at a distance d_v from the inside face of the support) is considered:

Factored vertical shear	$V_1 = V_u = 283.95$ kips
Distance between the centroid of the tension steel and the mid-thickness of the slab	$d_{v1} = \frac{t_s}{2} + Y_t + e = 32.67$ in.
Factored horizontal shear per unit length of girder (AASHTO LRFD 5.7.4.5):	$V_{h1} = \frac{V_u}{d_{v1}} = 8.7$ kips/in.
Area of interface per unit length	$A_{cv} = b_{vi} \times 1 = 36 \frac{\text{in.}^2}{\text{in.}}$

Note: b_{vi} = top flange width, b_f = 36 in. in this case.

Provide at least the minimum interface shear reinforcement as per the recommendations of the AASHTO draft specifications for UHPC (FHWA 2022).

Try providing #5 UC bars at a 6 in. center-to-center spacing at the interface.

$$A_{vf} = \frac{2 \text{ legs} \times 2 \text{ UC bars} \times 0.31}{6} = 0.206 \text{ in.}^2/\text{in.}$$

According to AASHTO LRFD 5.7.4.2, the minimum shear interface reinforcement is given as follows:

$$A_{vf} \geq \frac{0.05 A_{cv}}{f_y} = 0.027 \text{ in.}^2/\text{in.}$$

The values for concrete placed against a clean concrete surface, free of laitance, but not intentionally roughened provided in AASHTO LRFD Art. 5.7.4.4 are used as recommended by FHWA (2022).

Cohesion factor, $c = 0.075$ ksi

Friction factor, $\mu = 0.6$

Fraction of concrete strength available to resist interface shear, $K_1 = 0.2$

Limiting interface shear resistance, $K_2 = 0.8$ ksi

Compressive force, $P_c = 0$ kips

According to AASHTO LRFD Eq. 5.7.4.3-3:

$$V_{ni} = cA_{cv} + \mu\left(A_{vf}f_y + P_c\right)$$

$$= 0.075 \times 36 + 0.6\left(\frac{0.31 \times 2 \text{ legs} \times 2 \text{ UC bars}}{6 \text{ in. spacing}} \times 60 + 0\right)$$

$$= 0.075 \times 36 + 0.6(0.206 \times 60 + 0)$$

$$= 10.12 \text{ kip/in.}$$

The nominal shear resistance shall not exceed either of the following:

$V_{ni} \leq K_1 f'_c A_{cv} = 0.2 \times 4 \times 36 = 28.8$ kip/in. [Check OK]

$V_{ni} \leq K_2 A_{cv} = 0.8 \times 36 = 28.8$ kip/in. [Check OK]

$\phi_v V_{ni} = 0.9 \times 10.12 = 9.1$ kip/in.

The factored horizontal shear per unit length of girder is calculated at different sections along the span length of the girder. The spacing between the UC bars is changed to ensure that the factored horizontal shear force per unit length (V_{h1}) does not exceed the reduced nominal shear resistance ($\phi_v V_{ni}$). Based on the interface shear demand computed as per AASHTO LRFD Art. 5.7.4.5 along the span length, the spacing is adjusted and the following layout is suggested.

Provide additional interface shear reinforcement in the form of bundled UC bars, with the following arrangement:

- two (bundled) #5 UC bars at a center-to-center spacing of 6 in. up to 12 ft from each girder end, with end cover of 2.5 in.
- followed by two (bundled) #5 UC bars at a center-to-center spacing of 9 in. up to 18 ft from each girder end
- followed by two (bundled) #5 UC bars at a center-to -center spacing of 12 in. up to 29 ft from each girder end
- followed by two (bundled) #5 UC bars at a center-to-center spacing of 24 in. from each girder end

4.11 END BLOCK REINFORCEMENT

End block reinforcement to be provided as per TxDOT standard detailing for I-girders (TxDOT 2017). The detailed drawings of the design example are enclosed in the Appendix.

4.12 DESIGN SUMMARY

The following Table 4.14 summarizes the key aspects of the design example.

Table 4.14. Summary of Design Details.

Design Details	**Value**
Bridge Geometry:	
Bridge Width, W	46 ft
Back-wall to back-wall distance, L_{br}	85 ft
Number of girders	5
UHPC:	
Compressive strength at release, f'_{ci}	11.7 ksi
28-day compressive strength at service, f'_c	18 ksi
Elastic tensile strength at release, f'_{ti}	0.72 ksi
Elastic tensile strength at service, f'_t	0.85 ksi
Post cracking tensile strength, f'_{tu}	0.85 ksi
MOE at release, E_{gi}	6742 ksi
MOE at release, E_g	7423 ksi
Conventional Concrete:	
28-day compressive strength at service, f'_{cd}	4.0 ksi
MOE at release, E_d	3986 ksi
Prestressing Strand Details:	
Ultimate strength of steel strands, f_{pu}	270 ksi
Yield strength of steel strands, f_{py}	243 ksi
MOE of strands, E_p	28,500 ksi
Diameter of strands, d_b	0.6 in.
Girder Section:	
Length of girder, L_g	84.5 ft
Depth of girder, h_g	34 in.

Table 4.14. (Continued).

Composite Section:	
Total Height, H	44.5 in.
Effective width of the section, B_e	120 in.
Distance of neutral axis from top of girder, y_{tc}	17.2 in.
Distance of neutral axis from bottom of girder, y_{bc}	27.3 in.
Area of girder, A_{gc}	1211 in^2
Moment of inertial about x-axis, I_{cg}	272,852 in^4
Dead Load Moment Demand:	
Girder, M_g	600 kip-ft
Deck Slab, M_s	915 kip-ft
Haunch, M_h	61 kip-ft
Wearing surface, M_{ws}	201 kip-ft
Barrier T551, M_r	132 kip-ft
Self-weight of girder at transfer length, M_{Dt}	43.4 kip-ft
Live Load Moment Demand:	
Factored Live Load Moment, M_{LL}	1659 kip-ft
Dead Load Shear Demand:	
Girder, V_g	26.4 kips
Deck slab, V_s	40.3 kips
Haunch, V_h	2.7 kips
Wearing surface, V_{ws}	8.9 kips
Barrier T551, V_r	5.8 kips
Factored Shear Demand, V_u	282.5 kips
Live Load Shear Demand:	
Factored Live Load Shear, V_{LL}	100.1 kips

Table 4.14. (Continued).

Prestressing Losses:	
Initial, f_{pi}	179.2 ksi
Final, f_{pe}	145.7 ksi
Flexure Design:	
Number of strands, N	48
Force in prestressing strand immediately, F_i	1867 kips
Force in prestressing strand after losses, F	1517 kips
All stress checks pass in flexure.	
Camber and Deflection:	
Camber with deck, Δ_{final}	2.25 in.
Design passes the deflection check, Δ_{LL}	0.48 in. < 1.25 in.
Flexural resistance at strength limit state:	
Moment demand, M_u	5339 kip-ft
Reduced nominal moment, ϕM_n	7434 kip-ft
$\phi M_n > M_u$ → section has sufficient flexural resistance for strength limit state	
Shear Design:	
Shear demand, V_u	282.5 kips
Reduced nominal shear, ϕV_n	449 kips
Nominal shear reinforcement is recommended.	
Splitting resistance reinforcement	Provide #5 R bars at 3 in. spacing c/c up to $h/4$ (8.5 in.) distance from the ends (a total of 3 #5 R bars)
Interface Shear Resistance	Provide 2 (bundled) #5 UC bars with c/c spacing of 6 in. up to 12 ft from the end with end cover of 2.5 in., followed by 2 (bundled) #5 UC bars with c/c spacing of 9 in. up to 18 ft, followed by 2 (bundled) #5 UC bars with c/c spacing of 12 in. up to 29 ft, followed by 2 (bundled) #5 UC bars at c/c spacing of 24 in.
End block reinforcement to be provided as per TxDOT (2017)	

5 DESIGN EXAMPLE FOR TX54

5.1 DETAILED DESIGN EXAMPLE FOR A UHPC TX54 GIRDER

This design example evaluates the use of UHPC Tx54 girders in combination with a conventional concrete deck slab for a 46 ft wide bridge. The objective of this design example is to present the design modifications that need to be made to account for the use of UHPC. This design example highlights the potential to achieve longer span lengths due to the superior tensile and compressive strengths of UHPC with a shallow cross-section compared to conventional concrete. The Tx54 design example is described in this chapter.

5.2 BRIDGE GEOMETRY AND MATERIAL PROPERTIES

This section provides geometric details of the bridge superstructure and the material properties of the concrete components, wearing surface, and prestressing steel. Concrete components include the deck slab including the haunch, and the railing, which are composed of reinforced conventional concrete, and the girders that are composed of pretensioned UHPC members.

5.2.1 Geometric Properties

The geometric parameters of the bridge superstructure are listed in Table 5.1 and will be explained in further detail. The bridge superstructure comprises a simply supported UHPC bridge girder with a composite conventional concrete deck slab. Figure 5.1 presents the bridge cross-section detail for this design example.

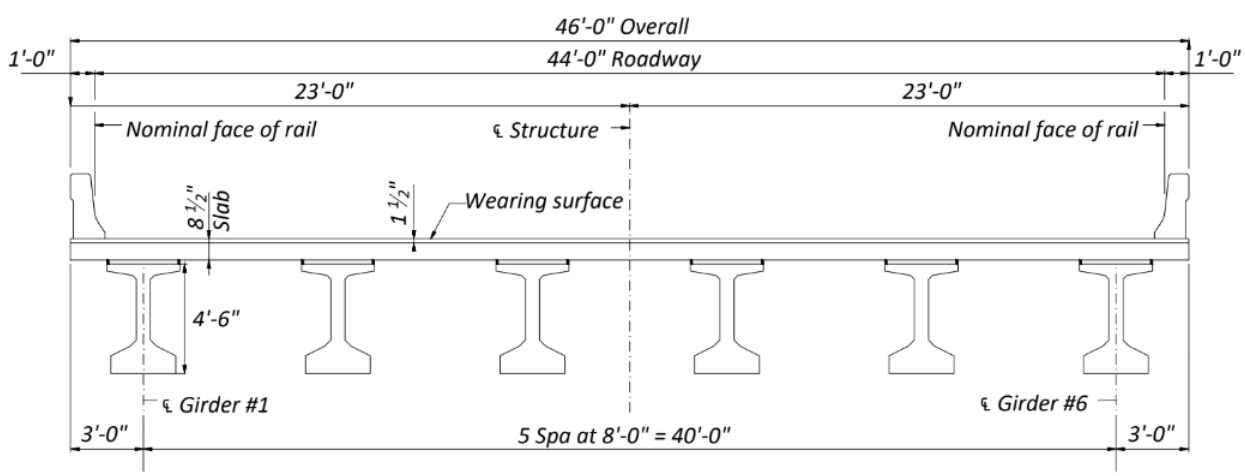

Figure 5.1. Bridge Cross-Section Details.

Table 5.1. Geometric Properties of Tx54 Bridge.

Parameter	Value
Bridge width, W	46 ft
Back-wall to back-wall distance, L_{br}	144 ft
Bearing span length, L	142 ft
Number of girders	6
Girder center-to-center spacing, s	8 ft
Overhang beyond the centerline of the exterior girders on each side	3 ft
Thickness of deck slab, t_s	8.5 in.
Thickness of asphalt wearing surface, t_{ws}	2 in.
Thickness of haunch, t_h	2 in.
Number of lanes, N_L	3
Multiple presence factor, m as per Table 3.6.1.1.2-1 of AASHTO LRFD (AASHTO 2020)	0.85

5.2.2 Material Properties

This section lists the material properties of the concrete components such as the deck and haunch, which are composed of conventional concrete, and the girder, composed of UHPC. This section also documents the characteristics of prestressing strands used for the design.

5.2.2.1 Ultra-High Performance Concrete (UHPC)

Owing to the superior mechanical properties of UHPC, when compared to conventional concrete, a higher compressive strength f'_{ci} of 11.7 ksi at release and 28-day compressive strength f'_c of 18 ksi at service are used in this study. These values are selected as the minimum required compressive strengths at release and service and will be checked for adequacy in the design checks provided in this example. Note that the minimum f'_{ci} is recommended to be taken as 0.65 f'_c to minimize early age creep effects. One of the key material properties of UHPC is its improved tensile strength, ductility, and energy absorption capacity due to the presence of steel fibers. The higher tensile strength is attributed to the use of fibers, as mentioned in design guides and codes such as ACI 544.4R-18 (2018), AFGC (2013), and Model Code (2010), and in the research conducted by FHWA (FHWA 2022). The parameters needed for design computations pertaining to UHPC are provided in Table 5.2. These parameters are based on the average typical

experimental test results from the full-scale companion specimens fabricated with Tx54 girder specimen.

Table 5.2. Properties of UHPC for Tx54 I-Girders.

Parameter	**Value**
Compressive strength at release, f'_{ci}	11.7 ksi
28-day compressive strength at service, f'_c	18 ksi
Elastic tensile strength at release, f'_{ti}	0.72 ksi
Elastic tensile strength at service, f'_t	0.85 ksi
Post cracking tensile strength, f'_{tu}	0.85 ksi
MOE at release, E_{gi}	6742 ksi
MOE at service, E_g	7423 ksi
Unit weight of reinforced UHPC, γ_{UHPC}	0.160 kcf

In the absence of experimental data, the modulus of elasticity of UHPC can be computed using one of the available empirical expressions. The expression developed through material level testing of the developed nonproprietary UHPC, as described in the Volume 1 report, is shown in Equation (5.1). This is similar to the expression recommended in the FHWA 18-036 Report (Haber et al. 2018), which uses a coefficient of 1430.

$$E_{UHPC} = 1430\sqrt{f'_c} \tag{5.1}$$

where:

f'_c = Specified compressive strength of UHPC at the given age, ksi

For reference, the equation for analytically predicting MOE recommended by the AASHTO draft specifications for UHPC (FHWA 2022) is as follows:

$$E_c = 2500K_1 f'^{0.33}_c \tag{5.2}$$

where:

f'_c = Specified compressive strength of UHPC at the given age, ksi

K_1 = Correction factor of MOE to be considered as 1.0 unless determined experimentally

The modulus of elasticity computed for the two design examples using the empirical equations listed above are compared with the experimental modulus of elasticity. Table 5.4 shows that the experimental modulus of elasticity is higher that the predicted values, with the percentage values relative to the measured value listed in the table. Therefore, the empirical relationships do not overpredict the measured MOE values with the FHWA (2022) expression providing a close prediction of the experimental values. The experimental values are being used in the design example.

Table 5.3. Comparison of Experimental and Computed MOE.

Description		E_{gi}, **ksi**		E_g, **ksi**	
Present Research	Experimental	6742	-	7423	-
	Empirical (Eq. 4.1)	4891	73%	6067	82%
Draft UHPC Specs (Eq. 4.2)		5629	83%	6489	87%

5.2.2.2 Conventional Concrete Deck Slab

The material properties of conventional Class S concrete are considered for the deck of the bridge as summarized in Table 5.4.

Table 5.4. Properties of Conventional Concrete Deck.

Parameter	**Value**
28-day compressive strength at service, f'_{cd}	4.0 ksi
MOE, E_d	3987 ksi
Unit weight of reinforced concrete, γ_{cc}	0.150 kcf

The modulus of elasticity of conventional concrete has been computed using the empirical equation provided in the AASHTO LRFD Specifications (AASHTO 2020) Article 5.4.2.4-1 as shown in Equation (5.3)(4.3).

$$E_c = 120{,}000 K_1 w_c^{2.0} f_c'^{0.33} \tag{5.3}$$

where:

K_1 = Correction factor based on the source of aggregate, unless otherwise found by physical test it is assumed to be 1.0, and as per the owner's approval

w_c = Unit weight of concrete, kcf

f_c' = Characteristic compression strength of UHPC at the given age, ksi

It is to be noted that the unit weight of conventional concrete is assumed to be 0.145 kcf, which is consistent with TxDOT practice.

5.2.2.3 Wearing Surface and Barrier Details

It was assumed that the deck slab is topped up with an asphalt wearing surface having the properties listed in Table 3.1. One of the heaviest barriers, T551, was also added as a superimposed dead load. The weight of both the barriers is distributed to all five girders of the bridge, following the guidance provided in the TxDOT *Bridge Design Manual* (TxDOT 2018).

Table 5.5. Properties of Wearing Surface and Barrier (T551 Railing).

Parameter	**Value**
Unit weight of wearing surface, γ_{ws}	0.140 kcf
Linear weight of railing, T551, w_r	0.382 kcf

5.2.2.4 Mechanical and Geometric Properties of Prestressing Strands

The mechanical properties of 0.6 in. diameter, seven-wire, low-relaxation prestressing strands used for this design example are listed in Table 5.6.

Table 5.6. Mechanical and Geometric Properties of Prestressing Strands.

Parameter	Value
Ultimate strength of steel strands, f_{pu}	270 ksi
Yield strength of steel strands, f_{py}	243 ksi
MOE of strands, E_p	28,500 ksi
Diameter of strands, d_b	0.6 in.
Area of prestressing strands, A_t	0.217 in^2

5.3 GIRDER DETAILS AND SECTION PROPERTIES

The section properties of the Tx54 girder are provided in Table 5.7 based on the standard TxDOT bridge drawings (TxDOT 2019).

Table 5.7. Girder Details and Sectional Properties.

Parameter	Value
Length of girder, L_g	143.5 ft
Depth of girder, h_g	54 in.
Thickness of web, b_w	7 in.
Distance of neutral axis from top of girder, y_t	30.5 in.
Distance of neutral axis from bottom of girder, y_b	23.5 in.
Area of girder, A_g	817 in^2
Moment of inertial about x-axis, I_g	299,740 in^4
Section modulus at the top of girder, S_t	9831 in^3
Section modulus at the bottom of girder, S_b	12,749 in^3
Modular Ratio, E_g/E_d, η_{UHPC}	1.86

5.4 COMPOSITE SECTION DETAILS AND SECTIONAL PROPERTIES

The section properties of the composite section are obtained by transforming the section using the modular ratio. This approach is consistent with the recommendations in the *TxDOT Bridge Design Manual* (TxDOT 2018). The calculations are shown in Table 5.8

The transformed width of the deck of the composite section $= \dfrac{1}{\eta_{UHPC}} \times$ effective width

$$= \frac{1}{1.86}(96 \text{ in.}) = 51.6 \text{ in.}$$

Table 5.8. Computation of Properties of Composite Section.

Component	Transformed Area, A (in^2)	y_b (in.)	Ay_b (in^3)	$A(y_{bc}\text{-}y_b)^2$ (in^3)	I (in^4)	$I + A(y_{bc}\text{-}y_b)^2$ (in^4)
Girder	817	23.5	19,208	145,707	299,740	445,447
Slab	438	60.3	26,404	239,662	2639	242,301
Haunch	37	55	2009	12,011	12	12,023
Σ	1292	-	47,620	-	-	699,771

The properties of the composite section of the Tx54 girder of UHPC and the deck slab of CC are listed in Table 5.9.

Table 5.9. Properties of Tx54 UHPC Girder with CC Deck Slab.

Parameter	Value
Total depth of the section, h_c	64.5 in.
Effective width of the section, b_e	96 in.
Distance of neutral axis from top of girder, y_{tc}	27.6 in.
Distance of neutral axis from bottom of girder, y_{bc}	36.9 in.
Transformed area of composite girder, A_{gc}	1292 in^2
Moment of inertia about x-axis, I_{cg}	699,771 in^4
Section modulus of composite section at the top of the composite section, S_{tc}	25,321 in^3
Section modulus of composite section at the top of the girder, S_{tgc}	40,838 in^3
Section modulus of composite section at the bottom of girder, S_{bc}	18,982 in^3

5.5 LOAD DEMANDS

This section documents the computations of the demands on the bridge superstructure due to dead and live loads per the AASHTO LRFD Specifications (AASHTO 2020). This section also mentions the various factors needed to compute the factored loads. Table 5.10 presents the factors considered for load combinations as per Table 3.4.4-1 of the AASHTO LRFD Specifications (AASHTO 2020)

Table 5.10. Load Combination Factors.

	Dead Load	Wearing Surface Load	Live Load	Impact Load
Service I	1	1	1	1
Service III	1	1	1	1
Strength I	1.25	1.5	1.75	1.75

5.5.1 Dead Loads

The dead loads due to the self-weight of the prestressed girders, the deck slab, and the haunch act on the non-composite prestressed girder whereas the dead loads due to the superimposed weight of the wearing surface and the railings act on the composite girder section. The self-weights for the components are listed below.

Self-Weight Computations

Girder, w_g $= \gamma_{UHPC} \times A_g$ (5.4)

$$= (0.160\ \text{kip/ft}^3)\left(\frac{817\ \text{in.}^2}{144\ \text{in.}^2/\text{ft}^2}\right) = 0.908\ \text{klf}$$

Deck slab, w_s $= \gamma_{cc} \times t_s \times b_e$ (5.5)

$$= \left(0.15\frac{\text{kip}}{\text{ft}^3}\right)\left(\frac{8.5\ \text{in.}}{12\ \text{in./ft}}\right)(8\ \text{ft}) = 0.85\ \text{klf}$$

Haunch, w_h $= \gamma_{cc} \times t_h \times b_h$ (5.6)

$$= (0.15\ \text{kip/ft}^3)\left(\frac{2\ \text{in.}}{12\ \text{in./ft}}\right)\left(\frac{34\ \text{in.}}{12\ \text{in./ft}}\right) = 0.071\ \text{klf}$$

Wearing surface, w_{ws} $= \gamma_{ws} \times t_s \times b_e$ (5.7)

$$= (0.14\ \text{kip/ft}^3)\left(\frac{2\ \text{in.}}{12\text{in./ft}}\right)(8\ \text{ft}) = 0.19\ \text{klf}$$

Distributed weight of barrier T551, w_{dr} $= 2 \times \left(\frac{w_r}{6\ \text{girders}}\right)$ (5.8)

$$= 2 \times \left(\frac{0.382\ \text{klf}}{6\ \text{girders}}\right) = 0.127\ \text{klf}$$

5.5.2 Live Loads

The live loads are assumed to be the standard HL-93 loading and this load acts on the composite section of the bridge. The combination consists of the maximum of the load contribution from an HS20 truck, as shown in Figure 5.2, or design tandem, as presented in Figure 5.3, and design lane load. The live loads are listed in Table 5.11 and are taken from Article 2 of the AASHTO LRFD Specifications (AASHTO 2020).

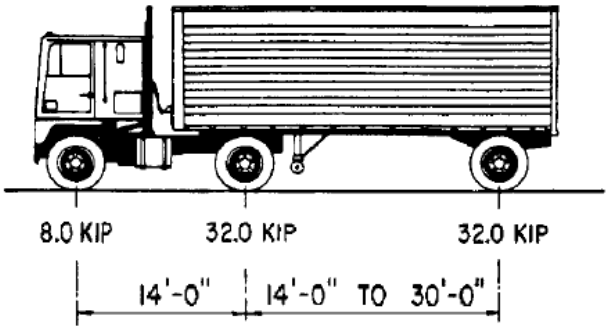

(a) Truck Axle Loadings and Longitudinal Spacings

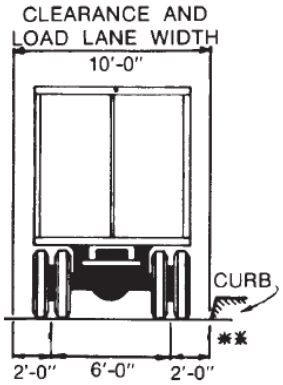

(b) Truck Transverse Spacing

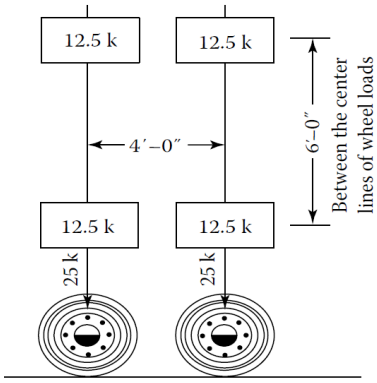

(c) Tandem Axle Loadings and Longitudinal Spacings

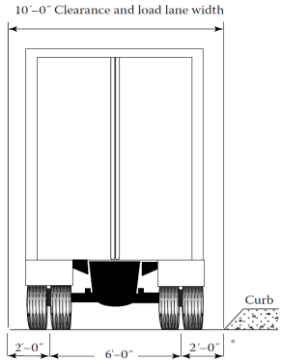

(d) Tandem Transverse Spacing

Figure 5.2. HS20 Truck Loading (AASHTO 2020; Taly 2014).

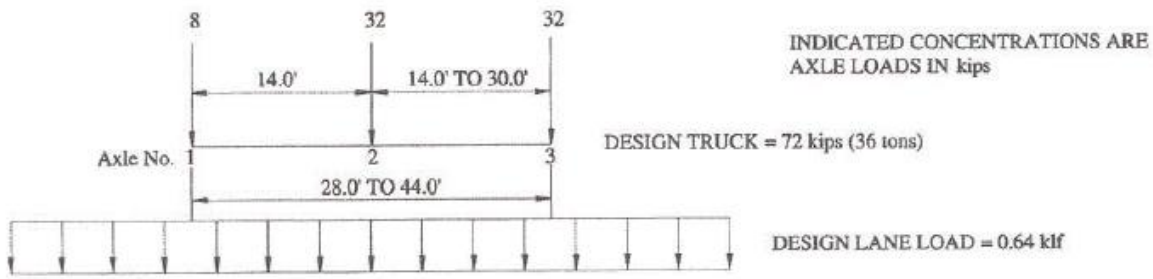

(a) Design Truck and Lane Load

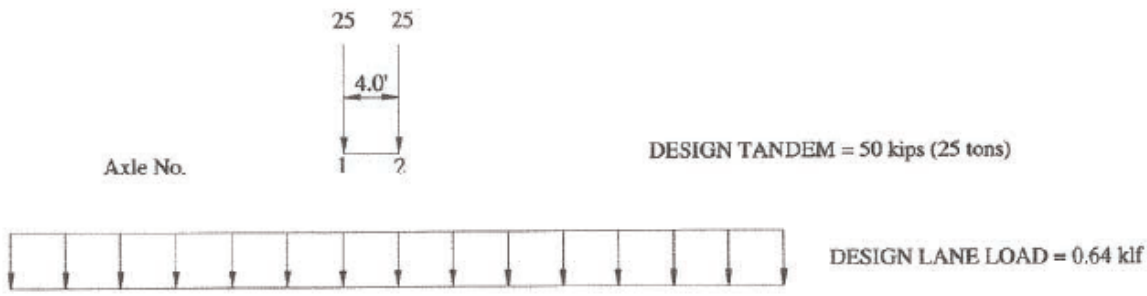

(b) Design Tandem and Lane Load

Figure 5.3. Designated HL-93 Load Model (AASHTO 2018).

Table 5.11. Live Load Details.

Parameter	**Description**
Design truck load	8-kip, 32-kip and 32-kip axles spaced 14 ft apart from each other
Design tandem load	25-kip and 25-kip axles spaced 4 ft apart
Design lane load	0.64 klf across 10 ft width, uniformly distributed longitudinally

5.5.3 Unfactored and Factored Moment Demands

Maximum demand due to moments is calculated using dead loads and vehicular live loads. The process is simplified using a long-standing methodology of live load distribution factors (LLDFs). These were adapted using approximate LLDFs expressions provided in the AASHTO LRFD Specifications (AASHTO 2020) Article 4.6.2.2. In the LLDF method, a multi-girder bridge superstructure can be reduced to a single one-dimensional (1D) beam element. Thus, LLDFs are applied to convert demands on a single 1D beam element into the demands for one of the girders and its associated deck slab in a multi-girder beam-slab bridge.

The service and strength limit states specified by AASHTO LRFD Specifications (AASHTO 2020) are considered including the following load combinations: Service I, Service III, and Strength I. The relevant load factors are provided in Table 3.4.4-1 of the AASHTO LRFD Specifications (AASHTO 2020). The load combination factors considered are listed in Table 5.10. The dead loads are increased by 25 percent and the live load and impact loads are increased by 75 percent for the Strength I load combination, respectively, and the computations are shown below.

<u>Dead Load Moment Demands Computations</u>

Dead loads include the self-weight of structural components, such as the girder and deck slab including the haunch thickness, and nonstructural components such as wearing surface and railings. The weight of the wearing surface is distributed equally to all girders while the weight of railings is distributed to first three girders from the edge following the recommendations provided in *TxDOT Bridge Design Manual* (TxDOT 2018).

Girder, M_g

$$= w_g \frac{L^2}{8} \tag{5.9}$$

$$= (0.908 \text{ klf}) \left(\frac{(142 \text{ ft})^2}{8} \right) = 2288 \text{ kip-ft}$$

Deck Slab, M_s

$$= w_s \frac{L^2}{8} \tag{5.10}$$

$$= (0.85 \text{ klf}) \left(\frac{(142 \text{ ft})^2}{8} \right) = 2142 \text{ kip-ft}$$

Haunch, M_h

$$= w_h \frac{L^2}{8} \tag{5.11}$$

$$= (0.071 \text{ klf}) \left(\frac{(144 \text{ ft})^2}{8} \right) = 178.5 \text{ kip-ft}$$

Wearing surface, M_{ws} $= w_{ws}\frac{L^2}{8}$ (5.12)

$$= (0.19\text{ klf})\left(\frac{(144\text{ ft})^2}{8}\right) = 470.5\text{ kip-ft}$$

Barrier T551, M_r $= w_{dr}\frac{L^2}{8}$ (5.13)

$$= (0.127\text{ klf})\left(\frac{(144\text{ ft})^2}{8}\right) = 321\text{ kip-ft}$$

Self-weight of girder at transfer length, M_{Dt} $= \frac{w_g L_g l_t}{2} - \frac{w_g {l_t}^2}{2}$ (5.14)

$$= \frac{(0.908\text{ klf})(143.5\text{ ft})(1.5\text{ ft})}{2} - \frac{(0.908\text{ klf})(1.5\text{ ft})^2}{2}$$

$$= 96.7\text{ kip-ft}$$

For the computation of moment due to self-weight of girder at transfer length M_{Dt} is computed as follows.

Transfer length, l_t $= 30d_b$ (5.15)

$$= (30)(0.6\text{ in.}) = 18\text{ in.} = 1.5\text{ ft}$$

<u>Live Load Moment Demands Computations</u>

The vehicular live loading on the roadways of bridges specified as HL-93 by AASHTO LRFD Specifications (AASHTO 2020) Article 3.6.1.2.1, as described in the previous section, is used for the demand due to live load moments. Absolute maximum moment due to an HS20 truck occurs when the centerline of the span (midspan location) bisects the 32-kip middle axle load and the resultant of the HS20 load group. The maximum moment occurs under the 32-kip middle axle. Similarly, the absolute maximum moment due to tandem load occurs when one of the 25-kip loads and the resultant of the tandem load group are placed equidistant from centerline of the span (midspan location). It occurs under the 25-kip load that is close to midspan. These two methods can be obtained using the influence line method and are “exact methods” of calculating moment demands due to HS20 and tandem loads (Figure 5.2 and Figure 5.3).

Alternatively, the maximum moment at midspan due to HS20 truck can be calculated, without any significant error, by placing the 32-kip middle axle at the midspan. Similarly, the maximum moment at midspan due to tandem load can be calculated by placing one of the 25-kip axle loads at the midspan. These are simpler approximate methods that may be used for computing maximum moment demands due to AASHTO HS20 or tandem loads. The difference between exact and approximate method is inconsequential (less than 1 percent) and can be ignored for all practical purposes (Taly 2014). This alternate, simple method is used in the design example. Furthermore, the moment due to uniformly distributed loads can be calculated at midspan and superposed with that from vehicular moment demand. This means that the difference between exact and approximate truck moment calculations will be even less significant when added together with the uniformly distributed load (UDL) due to all dead loads and vehicular lane load. The maximum moment demand at midspan due to HS20 truck and tandem load can then be calculated as:

Design truck, M_{HS20} $= 18L - 280$ (5.16)

$= (18\text{ kip})(142\text{ ft}) - (280\text{ kip-ft}) = 2276\text{ kip-ft}$

Design tandem, M_{Tandem} $= 12.5L - 50$ (5.17)

$= (12.5\text{ kip})(142\text{ ft}) - 50\text{ kip-ft} = 1725\text{ kip-ft}$

Design lane load, M_{Lane} $= \dfrac{0.64L^2}{8}$ (5.18)

$= \dfrac{(0.64\text{ klf})(142\text{ ft})^2}{8} = 1613\text{ kip-ft}$

<u>Live Load Distribution Factor for Interior Beams</u>

The total vehicular moment demand for the critical interior girder can be calculated by multiplying the moment demand from a single one-dimensional beam element with the moment live load distribution factor (LLDF) computed using the expressions in AASHTO LRFD Specifications Table 4.6.2.2.2b-1 (AASHTO 2020).

For a prestressed concrete I-girder with concrete deck bridge having two or more design lanes loaded:

Live load distribution factor for moment, g_m

$$= 0.075 + \left(\frac{S}{9.5}\right)^{0.6}\left(\frac{S}{L}\right)^{0.2}\left(\frac{K_g}{12.0Lt_s{}^3}\right)^{0.1} \quad (5.19)$$

$$= 0.075 + \left(\frac{8}{9.5}\right)^{0.6}\left(\frac{8}{142}\right)^{0.2} 1.09$$

$$= 0.626$$

$$\left(\frac{K_g}{12.0Lt_s{}^3}\right)^{0.1} = 1.09$$

AASHTO (2020) - Table 4.6.2.2.1-3

Factored Live Load Moment, M_{LL}

$$= g_m(1.33 \times \max(M_{HS20}, M_{Tandem}) + M_{Lane}) \quad (5.20)$$

$$= 0.626(1.33\ (2276) + 1613) = 2906 \text{ kip-ft}$$

5.5.4 Unfactored and Factored Shear Demands

The maximum girder demand due to shear is also calculated using dead loads and vehicular live loads. Shear LLDFs were determined using the approximate LLDFs expressions provided in the AASHTO LRFD Specifications (AASHTO 2020) Article 4.6.2.2.

Effective shear depth (d_v)

$$= \max\ (\text{inner lever arm (z)}, \max\ (0.9d_p, 0.72\text{h})) \quad (5.21)$$

$$= \max\ (44.9, \max\ (0.9\ (52.1), 0.72\ (64.5))$$

$$= \max(44.9, \max\ (46.9, 46.4)$$

$$= \max\ (44.9, 46.9)$$

$$= 46.9 \text{ in.}$$

Note: Computation of z and d_p are shown in Section 5.6.10 under flexure resistance at strength limit state.

Critical section for shear calculations (x_s)

$$= \frac{d_v + 9}{12} \quad (5.22)$$

$$= \frac{46.9 + 9}{12}$$

$$= 4.7 \text{ ft}$$

Shear Demands

Design truck, V_{HS20}

$$= 32\left(\frac{L - x_s}{L}\right) + 32\left(\frac{L - 14 - x_s}{L}\right) + 8\left(\frac{L - 28 - x_s}{L}\right) \quad (5.23)$$

$$= 32\left(\frac{142 - 4.7}{142}\right) + 32\left(\frac{142 - 14 - 4.7}{142}\right) + 8\left(\frac{142 - 28 - 4.7}{142}\right)$$

$$= 64.9 \text{ kips}$$

Design tandem, V_{Tandem}

$$= 25\left(\frac{L - x_s}{L}\right) + 25\left(\frac{L - 4 - x_s}{L}\right) \quad (5.24)$$

$$= 25\left(\frac{142 - 4.7}{142}\right) + 25\left(\frac{142 - 4 - 4.7}{142}\right)$$

$$= 47.7 \text{ kips}$$

Design maximum truck, V_{Truck}

$$= \max(V_{HS20}, V_{Tandem}) \quad (5.25)$$

$$= \max(64.9, 47.7) \text{ kips}$$

$$= 64.9 \text{ kips}$$

Design lane, V_{Lane}

$$= 0.64\frac{L}{2} - 0.64x_s \quad (5.26)$$

$$= 0.64\left(\frac{142}{2}\right) - 0.64(4.7)$$

$$= 42.5 \text{ kips}$$

The shear LLDR is computed using the expression in AASHTO LRFD Specifications (AASHTO 2020) Table 4.6.2.2.3a-1. For prestressed concrete I-girder with concrete deck and with two or more design lanes loaded:

Live load distribution factor for shear, g_v

$$= 0.2 + \frac{S}{12} - \left(\frac{S}{35}\right)^{2.0} \quad (5.27)$$

$$= 0.2 + \frac{8}{12} - \left(\frac{8}{35}\right)^{2.0}$$

$$= 0.814$$

Factored Live Load Shear, V_{LL}

$$= g_v\,(1.33V_{Truck} + V_{Lane}) \quad (5.28)$$

$$= 0.814((1.33)(64.9) + 42.5)$$

$$= 104.9 \text{ kips}$$

Shear Demand due to Dead Load

Girder, V_g

$$= w_g \frac{L}{2} - w_g x_s \tag{5.29}$$

$$= (0.908)\left(\frac{142}{2}\right) - (0.908)(4.7)$$

$$= 60.2 \text{ kips}$$

Deck slab, V_s

$$= w_s \frac{L}{2} - w_s x_s \tag{5.30}$$

$$= (0.85)\left(\frac{142}{2}\right) - (0.85)(4.7)$$

$$= 56.4 \text{ kips}$$

Haunch, V_h

$$= w_h \frac{L}{2} - w_h x_s \tag{5.31}$$

$$= (0.071)\left(\frac{142}{2}\right) - (0.071)(4.7)$$

$$= 4.7 \text{ kips}$$

Wearing surface, V_{ws}

$$= w_{ws} \frac{L}{2} - w_{ws} x_s \tag{5.32}$$

$$= (0.19)\left(\frac{142}{2}\right) - (0.19)(4.7)$$

$$= 12.4 \text{ kips}$$

Barrier T551, V_r

$$= w_r \frac{L}{2} - w_r x_s \tag{5.33}$$

$$= (0.127)\left(\frac{142}{2}\right) - (0.127)(4.7)$$

$$= 8.4 \text{ kips}$$

Factored Shear Demand, V_u

$$= 1.25\left(\mathrm{V_g} + \mathrm{V_h} + \mathrm{V_s} + \mathrm{V_r}\right) + 1.50(\mathrm{V_{ws}}) + 1.75(\mathrm{V_{LL}}) \tag{5.34}$$

$$= (1.25)(60.2 + 4.7 + 56.4 + 8.4) + (1.50)(12.4) + (1.75)(104.9)$$

$$= 364.3 \text{ kips}$$

5.6 FLEXURAL STRESS DESIGN AT SERVICE LIMIT STATE

5.6.1 General Procedure

This section reports the steps involved in evaluating the flexural capacity of the composite girder section for the service-level flexural demands computed in the previous section. The steps to select the number and arrangement of prestressing strands to meet the service stress limits for a given section geometry and selected material properties are summarized as follows.

1. Stress inequalities at various transportation and loading stages are plotted using assumed values of prestressing losses. The feasible domain, a region that satisfies all the critical limit state inequalities, is considered for selecting an optimal combination of the number of strands and eccentricity of the prestressing force, such that it can be constructed for the Tx54 shape.

2. Once a practical combination that lies within the feasible domain is obtained, the selected combination of strands and eccentricity is used to compute the prestressing losses. The eccentricity of the prestressing force is computed with respect to the centroid of the girder and is denoted by e_{pg}, and the number of strands is denoted by N.

3. The initial and final prestress that were assumed in step 1 are then modified based on the prestressing loss obtained in step 2 and then a revised feasibility domain is obtained.

4. This iterative cycle is repeated until the number of strands and the eccentricity combination is optimized.

5. The stresses are checked to verify that the arrangement of strands is suitable. If not, solutions such as harping and/or debonding of strands are considered.

5.6.2 Sign Convention

The compressive forces and stresses are considered negative and tensile forces and stresses are considered positive throughout this design example.

5.6.3 Prestress Losses

Prestressing losses are computed using the AASHTO LRFD Specifications (AASHTO 2020) in Article 5.9.3. The design example incorporates the prestress loss computations from the AASHTO LRFD Specifications (AASHTO 2020) with the modifications recommended by the AASHTO draft specifications for UHPC (FHWA 2022). The creep and shrinkage values are based on the findings of the present research study and listed in Section 3.4.2.2 and 3.4.2.3.

$$\Delta f_{pT} = \Delta f_{pST} + \Delta f_{pLT} \tag{5.35}$$

where:

Δf_{pT} = Total loss, ksi

Δf_{pST} = Short-term losses at transfer due to sum of loss or gains on account of elastic shortening or extension at prestressing and/or load transfer and early age shrinkage, ksi

Δf_{pLT} = Losses on account of long-term shrinkage and creep of concrete, and relaxation of steel, ksi

5.6.3.1 Prestress Losses at Transfer

The total prestress loss at transfer is calculated as follows:

$$\Delta f_{pST} = \Delta f_{pES} + \Delta f_{pSHI} \tag{5.36}$$

where:

Δf_{pST} = Prestress loss at transfer, ksi

Δf_{pES} = Prestress loss due to elastic shortening at transfer, ksi, AASHTO LRFD Equation 5.9.3.2.3a-1 (AASHTO 2020)

Δf_{pshi} = Prestress loss due to autogenous shrinkage occurring during the time between final set and transfer, ksi, using the PCI study equation 5.4.1-2 (eConstruct 2020)

(c) <u>*Prestress Losses due to Elastic Shortening*</u>

Elastic shortening in pretensioned members is computed using the expression in AASHTO LRFD Specifications (AASHTO 2020) Article 5.9.3.2.3a-1.

$$\Delta f_{pES} = \frac{E_p}{E_{ct}} f_{cgp} \tag{5.37}$$

where:

f_{cgp} = Stress in concrete at the centroid of the prestressing tendons due to prestressing force after transfer and the member self-weight at the section of maximum moment, ksi

E_p = Modulus of elasticity of prestressing steel, taken as 28,500 ksi

E_{ct} = Modulus of elasticity of concrete at transfer or at the time of load application, ksi

$$f_{cgp} = NA_t f_{pi}\left(\frac{1}{A_g} + \frac{{e_{pg}}^2}{I_g}\right) - \frac{M_g e_{pg}}{I_g} \tag{5.38}$$

<u>Elastic Shortening Computations:</u>

Effective stress in prestressing steel at transfer, f_{pi} = $(0.9)(0.75)f_{pu}$ (5.39)

$(0.9)(0.75)(270) = 182.3$ ksi

Assume number of strands, N = 86

The above computations are iterated and the final iteration of calculations is shown.

$$f_{cgp} = NA_t f_{pi}\left(\frac{1}{A_g} + \frac{{e_{pg}}^2}{I_g}\right) \pm \frac{M_g e_{pg}}{I_g} \tag{5.40}$$

$$= (86)(0.217)(181.8)\left(\frac{1}{817} + \frac{(13.1)^2}{299{,}740}\right) - \frac{(27457)(13.1)}{299{,}740}$$

$$= 4.9 \text{ ksi}$$

$$\Delta f_{pES} = \frac{E_p}{E_{gi}} f_{cgp} \tag{5.41}$$

$$= \frac{28{,}500}{6742}(4.9)$$

$$= 20.7 \text{ ksi}$$

(d) *<u>Early Age Shrinkage of UHPC</u>*

Loss due to early age shrinkage of UHPC is

$$\Delta f_{pSHI} = \varepsilon_{shi} E_p K_i \quad (5.42)$$

where:

ε_{shi} = Autogenous shrinkage strain occurring between the time between final set and transfer, taken as 200×10^{-6} in./in. (from this study)

K_d = Transformed section coefficient that accounts for initial (elastic) interaction between concrete and bonded steel, assumed to be 0.83 according to Section F.1.6.1 of eConstruct (2020)

$$\Delta f_{pSHI} = (200 \times 10^{-6})(28{,}500)(0.83) = 4.73 \text{ ksi}$$

$$\Delta f_{pST} = 20.7 + 4.73 = 25.4 \text{ ksi}$$

$$f_{pi} = 0.75 f_{pu} - \Delta f_{pST} \quad (5.43)$$

$$= (0.75)(270 \text{ ksi}) - 25.4 \text{ ksi}$$

$$= 177.1 \text{ ksi}$$

The value of the initially assumed f_{pi} is varied using trial and error until the difference between the initial and final value of f_{pi} is minimized. The final f_{pi} after several trials is

$$f_{pi} = 177.1 \text{ ksi}$$

5.6.3.2 Time Dependent Prestress Losses

AASHTO LRFD (AASHTO 2020) Article 5.9.3.4. provides the expression for the long-term prestress losses as,

$$\Delta f_{pLT} = \left(\Delta f_{pSR} + \Delta f_{pCR} + \Delta f_{pR1}\right)_{id} + \left(\Delta f_{pSD} + \Delta f_{pCD} + \Delta f_{pR2} - \Delta f_{SS}\right)_{df} \quad (5.44)$$

where:

Δf_{pT} = Total prestress loss, ksi

Δf_{pLT} = Long-term prestress loss, ksi, [AASHTO LRFD Equation 5.9.3.4.1-1 (AASHTO 2020)

Δf_{pSR} = Prestress loss due to shrinkage of girder occurring between transfer and deck placement, ksi, [AASHTO LRFD Equation 5.9.3.4.2a-1 (AASHTO 2020)]

Δf_{pCR} = Prestress loss due to creep of girder occurring between transfer and deck placement, ksi, AASHTO LRFD Equation 5.9.3.4.2b-1 (AASHTO 2020)

Δf_{pR1} = Prestress loss due to relaxation of prestressing strands occurring between transfer and deck placement, 1.2 ksi for low-relaxation strands [AASHTO LRFD Article 5.9.3.4.2c (AASHTO 2020)]

Δf_{pSD} = Prestress loss due to shrinkage of girder occurring between time of deck placement and final time, ksi [AASHTO LRFD Equation 5.9.3.4.3a-1 (AASHTO 2020)]

Δf_{pCD} = Prestress loss due to creep of girder occurring between time of deck placement and final time, ksi [AASHTO LRFD Equation 5.9.3.4.3b-1 (AASHTO 2020)]

Δf_{pR2} = Prestress loss due to relaxation of prestressing strands in composite section between deck placement and final, $\Delta f_{pR2} = \Delta f_{pR1} = 1.2$ ksi for low-relaxation strands [AASHTO LRFD Bridge Specifications Article 5.9.3.4.3c (AASHTO 2020)]

Δf_{pSS} = Prestress gain due to shrinkage of deck in composite section, ksi [AASHTO LRFD Equation 5.9.3.4.3d-1 (AASHTO 2020)]

<u>Time Dependent Loss Computation</u>

Prestress Losses between Transfer and Deck Placement

(a) <u>*Shrinkage of UHPC*</u>

$$\Delta f_{pSR} = \varepsilon_{bid} E_p K_{id} \tag{5.45}$$

where:

ε_{bid} = Shrinkage strain $= \varepsilon_{SR} k_{hs} k_f k_s k_{td}$

K_{id} = Transformed section coefficient

$$= \frac{1}{1 + \frac{E_p}{E_{ci}} \frac{A_{ps}}{A_g} \left(1 + \frac{A_g e_{pg}^2}{I_g}\right) \left[1 + 0.7\psi_{b_{(t_f,t_i)}}\right]}$$

$$= \frac{1}{1 + \frac{28{,}500}{6742} \frac{18.66}{817} \left(1 + \frac{817 \times (13.1)^2}{299{,}740}\right) [1 + 0.7(0.8)]} = 0.82$$

ε_{SR} = Ultimate shrinkage strain of UHPC = 700 microstrain

k_{hs} = Humidity correction factor for shrinkage for UHPC

$= 1 + 0.2(1 - 0.014H) = 1 + 0.2(1 - 0.014(60)) = 1.032$

k_f = Strength correction factor for UHPC

$$= \frac{19}{7 + f'_{ci}} = 1.016$$

k_s = Size correction factor for UHPC

$$= 1 + 0.2\left[0.45 - 0.13\left({}^{V}/_{S}\right)\right] = 1 + 0.2[0.45 - 0.13(3.5)] = 1.0$$

k_{td} = Time development factor for UHPC

$$= \frac{t^{0.6}}{4 + t^{0.6}} = \frac{(90)^{0.6}}{4 + (90)^{0.6}} = 0.79$$

t = Final time = 90 days

Δf_{pSR} = $(0.000578)(28500)(0.82) = 13.5$ ksi

(b) <u>*Creep of UHPC*</u>

$$\Delta f_{pCR} = \frac{E_p}{E_{gi}} f_{cgp} \psi_{b_{(t_d,t_i)}} K_{id} \tag{5.46}$$

where:

$\psi_{b_{(t_d,t_i)}}$ = Creep coefficient of UHPC girder at time of deck placement due to loading at transfer = $\psi_{ult} k_{hc} k_f k_s k_{td}$

ψ_{ult} = Ultimate creep coefficient $= 0.8$ (from this study)

k_{hc} = Humidity correction factor for creep for UHPC = 1.0

k_{td} = Time development factor for UHPC

$$= \frac{t^{0.6}}{8 + t^{0.6}} = \frac{(90)^{0.6}}{8 + (90)^{0.6}}$$

$$= 0.65$$

$$\psi_{b_{(t_d,t_i)}} = (0.8)(1)(1.016)(1)(0.65) = 0.53$$

$$\Delta f_{pCR} = \frac{28{,}500}{6742}(4.9)(0.53)(0.82) = 8.93 \text{ ksi}$$

(c) <u>Relaxation of Prestressing Strands</u>

$$\Delta f_{pR1} = 1.2 \text{ ksi}$$

$$\left(\Delta f_{pSR} + \Delta f_{pCR} + \Delta f_{pR1}\right)_{id} = 13.5 + 8.9 + 1.2 = 23.6 \text{ ksi}$$

Prestress Losses between Deck Placement to Final Time

(a) *<u>Shrinkage of UHPC</u>*

$$\Delta f_{pSD} = \varepsilon_{bdf} E_p K_{df} \tag{5.47}$$

where:

ε_{bdf} = Shrinkage strain $= (\varepsilon_{SR} k_{hs} k_f k_s k_{td})_{fi} - (\varepsilon_{SR} k_{hs} k_f k_s k_{td})_{id}$

K_{df} = Transformed section coefficient

$$= \frac{1}{1 + \frac{E_p}{E_{ci}} \frac{A_{ps}}{A_c}\left(1 + \frac{A_c e_{pc}^2}{I_c}\right)\left[1 + 0.7\psi_{b_{(t_f,t_i)}}\right]}$$

$$= \frac{1}{1 + \frac{28{,}500}{6742} \frac{18.66}{1292}\left(1 + \frac{1292 \times (26.46)^2}{699{,}771}\right)[1 + 0.7(0.8)]} = 0.82$$

k_{td} = Time development factor for UHPC

$$= \frac{t^{0.6}}{4 + t^{0.6}} = \frac{(27285)^{0.6}}{4 + (27285)^{0.6}} = 0.99$$

t = Final time = 27,375 days = 75 years

Δf_{pSD} = $(0.000149)(28500)(0.82) = 3.5$ ksi

(b) <u>*Creep of UHPC*</u>

$$\Delta f_{pCD} = \frac{E_p}{E_{gi}} f_{cgp}\left[\psi_{(t_f,t_i)} - \psi_{(t_d,t_i)}\right] K_{df} + \frac{E_p}{E_g}\Delta f_{cd}\psi_{b\,(t_f,t_d)} K_{df} \tag{5.48}$$

where:

Δf_{cd} = Change in concrete stress at centroid of prestressing strands due to long-term losses between transfer and deck placement, ksi

$$= \left(\Delta F_p\right)_{id}\left(\frac{1}{A_g} + \frac{{e_{pg}}^2}{I_g}\right) + \frac{M_d e_{pg}}{I_g}$$

$$= NA_{ps}\left(\Delta f_{pSR} + \Delta f_{pCR} + \Delta f_{pR1}\right)_{id}\left(\frac{1}{A_g} + \frac{{e_{pg}}^2}{I_g}\right) + \frac{M_d e_{pg}}{I_g}$$

$$= 86 \times 0.217 \times 23.6\left(\frac{1}{817} + \frac{13.1^2}{299{,}740}\right) + \frac{37{,}349 \times 13.1}{299{,}740}$$

= 3.15 ksi

$\psi_{b\,(t_f,t_d)}$ = Creep coefficient of UHPC girder at time of deck placement due to loading at transfer = $\psi_{ult} k_{hc} k_f k_s k_{td}$

k_{td} = Time development factor for UHPC

$$= \frac{t^{0.6}}{8 + t^{0.6}} = \frac{27285^{0.6}}{8 + 27285^{0.6}}$$

= 0.98

$\psi_{b\,(t_f,t_i)}$ = $(0.8)(1)(1.016)(1)(0.98) = 0.80$

$$\Delta f_{pCD} = \frac{28{,}500}{6742}(4.38)(0.80 - 0.53)(0.82) + \frac{28{,}500}{7423}(3.15)(0.80 - 0.53)(0.82) = 7.30 \text{ ksi}$$

(c) <u>*Relaxation of Prestressing Strands*</u>

Δf_{pR2} = 1.2 ksi

(d) <u>*Shrinkage of deck*</u>

$$\Delta f_{pSS} = \frac{E_p}{E_g}(\Delta f_{cdf})(K_{df})\left[1 + 0.7\psi_b(t_f, t_d)\right] \tag{5.49}$$

where:

Δf_{cdf} = Change in concrete stress due to shrinkage of deck concrete at centroid of prestressing strands, ksi, AASHTO LRFD Equation 5.9.3.4.3d-2 (AASHTO 2020)

$$= \frac{\varepsilon_{ddf} A_d E_{c\ deck}}{\left[1 + 0.7\psi_d(t_f, t_d)\right]}\left(\frac{1}{A_c} - \frac{e_{pc}e_d}{I_c}\right)$$

$$= \frac{0.000695 \times (816 + 68) \times 3987}{[1 + 0.7 \times 2.56]}\left(\frac{1}{1292} - \frac{26.46 \times 23.4}{699{,}771}\right)$$

$$= -0.096 \text{ ksi}$$

ε_{ddf} = $\varepsilon_{SR} k_{hs} k_f k_s k_{td} = 695$ microstrain

ε_{SR} = Ultimate shrinkage strain of CC = 480 microstrain

k_{hs} = Humidity correction factor for shrinkage for CC

$$= (2 - 0.014H) = (2 - 0.014(60)) = 1.16$$

k_f = Strength correction factor for CC

$$= \frac{5}{1 + f'_{ci}} = \frac{5}{1 + 3} = 1.25$$

k_s = Size correction factor for CC

$$= \left[1.45 - 0.13\left({}^{V}/_{S}\right)\right] = [1.45 - 0.13(3.5)] = 1.0$$

k_{td} = Time development factor for CC

$$= \frac{t}{12\left(\frac{100 - 4f'_{ci}}{f'_{ci} + 20}\right) + t} = \frac{27285}{12\left(\frac{100 - 4 \times 3}{3 + 20}\right) + 27285} = 1.0$$

$\psi_{b(t_d, t_i)}$ = Creep coefficient of UHPC girder at time of deck placement due to loading at transfer = $\psi_{ult} k_{hc} k_f k_s k_{td} t_i^{-0.118}$

ψ_{ult} = Ultimate creep coefficient $= 1.9$

k_{hc} = Humidity correction factor for shrinkage for UHPC

= $1.56 - (0.008H) = (1.56 - 0.008(60)) = 1.08$

$t_i^{-0.118}$ = Age of concrete at time of loading application = 1 day

$$\Delta f_{pSS} = \frac{28{,}500}{7423}(-0.096)(0.82)[1 + 0.7(0.80 - 0.53)] \quad (5.50)$$

$$= -0.36 \text{ ksi}$$

$$\left(\Delta f_{pSD} + \Delta f_{pCD} + \Delta f_{pR2} - \Delta f_{pSS}\right)_{df} = 3.5 + 7.3 + 1.2 - 0.36 = 11.6 \text{ ksi}$$

$$\Delta f_{pLT} = 23.6 + 11.6$$

$$= 35.25 \text{ ksi}$$

$$f_{pe} = f_{pi} - \Delta f_{pLT} \quad (5.51)$$

$$= 177.1 - 35.25$$

$$= 141.8 \text{ ksi}$$

$$\eta_f = \frac{f_{pe}}{f_{pi}} = \frac{141.8}{177.1} = 0.80$$

$$\eta_d = \frac{f_{pe}}{f_{ped}} = \frac{141.8}{153.5} = 0.92$$

The values of f_{pi} and f_{pe} are then used to get the feasible domain and the number of strands, and eccentricity is selected using the feasible region of the inequalities. A combination of $N = 86$ [total area of prestressing strands, $A_{ps} = NA_t = 18.66 \text{ in}^2$] , $e_{pg} = 13.10$ in. (midspan) and $e_{end} = 6.41$ in. (girder ends) is the theoretical set of parameters selected from the plot of the stress inequalities. Finally, and the iterative value of $f_{pi} = 177.10$ ksi and $f_{pe} = 141.8$ ksi was obtained using the updated prestress losses.

5.6.3.3 Prestress Losses using Creep and Shrinkage Models from this Study

Similar to the comparison of prestress losses presented for the Tx34 design example, computed based on various methods in the literature, a comparison of the method of computing the prestress losses in UHPC girders given by the AASHTO draft specifications for UHPC (FHWA 2022) using the creep and shrinkage models developed as a part of this research project listed in Section 3.4.2.2 and 3.4.2.3 is conducted for this example. Four methods are summarized as follows.

1. Method 1 uses the recommendations from the AASHTO draft specifications for UHPC (FHWA 2022) that are explained in detail in Section 3.4. This approach is used for the detailed computations provided above for this design example. However, Method 1 uses the creep and shrinkage models developed in this research listed in Sections 3.4.2.2 and 3.4.2.3.

2. Method 2 is similar to Method 1 with the exception of excluding the early age (autogenous) shrinkage from the computations.

3. Method 3 is also similar to Method 1, except the creep and shrinkage models are based on the AASHTO draft specifications for UHPC (FHWA 2022) recommendations

4. Method 4 follows the recommendations of the PCI study for UHPC (eConstruct 2020). However, Method 4 uses the creep and shrinkage models developed in this research.

Table 5.12 presents the comparison of the prestress losses based on the four methods explained above.

Table 5.12. Comparison of Prestress Losses.

Prestress Loss Method	**Method 1**	**Method 2**	**Method 3**	**Method 4**
	FHWA (2022)	**FHWA (2022)**	**FHWA (2022)**	**eConstruct (2020)**
Creep and Shrinkage Models	**Present Research**	**Present Research (without early shrinkage)**	**AASHTO Draft (FHWA models)**	**Present Research**
Elastic Shortening Δf_{ES}, ksi	20.70	20.70	20.70	20.70
Early shrinkage Δf_{pSHI}, ksi	4.73	0	0	4.73
Shrinkage b/w transfer and deck placement Δf_{pSR}, ksi	13.49	13.49	17.23	17.73
Creep b/w transfer and deck placement Δf_{pCR}, ksi	8.93	8.93	27.14	12.95
Δf_{pr1}, Relaxation b/w transfer and deck placement Δf_{pr1}, ksi	1.2	1.2	1.20	1.2
Shrinkage b/w deck placement and final Δf_{pSD}, ksi	3.49	3.49	4.20	0
Creep b/w deck placement and final Δf_{pCD}, ksi	7.30	7.30	11.89	0
Relaxation b/w deck placement and final Δf_{pr2}, ksi	1.2	1.2	1.20	1.2
Prestress gain due to shrinkage of deck in composite section Δf_{SS}, ksi	-0.36	-0.36	-0.36	0
Total prestress losses Δf_{pT}, ksi	60.7	55.9	83.2	58.5
Effective stress in prestressing steel at transfer Δf_{pi}, ksi	177.1	181.8	181.8	177.1
Effective stress in prestressing steel at final Δf_{pe}, ksi	141.8	146.6	119.3	144.0
Percent Prestress losses	30%	28%	41%	29%

Note: b/w: between

5.6.4 Estimating Required Prestressing Force

The required prestressing force is computed at the end of the iterative process. The stress inequalities are computed, and the eccentricities are plotted as a function of the number of strands. The diagram with the plot of all the stress inequalities forms the feasibility domain. The assumptions to initiate the computations are as follows.

Assumptions:

Initial estimate for effective stress in prestressing steel at transfer, f_{pi}	=	$(0.9)(0.75)f_{pu}$	(5.52)
[Note: 10 percent losses used as per AASHTO LRFD Specifications (AASHTO 2020) C5.9.3.2.3a]	=	$(0.9)\ (0.75)\ (270\ \text{ksi})\ =\ 182.3\ \text{ksi}$	
Effective stress in prestressing steel after long term losses, f_{pe}	=	$(0.8)\ f_{pi}$	(5.53)
	=	$(0.8)\ (182.3\ \text{ksi})\ =\ 145.8\ \text{ksi}$	

After carrying out the computations for plotting the feasible domain and computing the prestressing losses as mentioned in the previous section, the following initial and final prestressing forces are obtained. In this case, the estimated f_{pe} is very close to the value of f_{pe} after considering detailed loss calculations. The value shown here is based on Method 1 in Table 5.12.

Final prestress after the computation of losses:

Initial stress in prestressing steel just after release, f_{pi}	=	177.1 ksi
Effective stress in prestressing steel at time of deck placement, f_{ped}	=	153.5 ksi
Effective stress in prestressing steel after long term losses, f_{pe}	=	141.8 ksi

Note: These values are used for computing the final feasible domain in the following sections.

5.6.5 Flexural Stresses at Transfer

5.6.5.1 Compression Stress Limit at Transfer

At transfer, the compression stresses are computed as per the Service I Load Combination in AASHTO LRFD Specifications (AASHTO 2020) Table 3.4.1-1. AASHTO draft specifications for UHPC (FHWA 2022) Article 1.5.2.1.3.a recommends the compressive stress limit before losses as $0.65f'_{ci}$ (ksi), which is consistent with Article 5.9.2.3.1a of the AASHTO LRFD Specifications (AASHTO 2020). The compressive stress inequality is applicable at the bottom

fiber and is computed at the transfer length, l_t. The expression is reduced to a form where the eccentricity can be expressed as a function of the number of strands.

<u>Computation of Compression Limit at Bottom Fiber at Transfer Length</u>

$$-\frac{A_{ps}f_{pi}}{A_g}-\frac{A_{ps}f_{pi}e_{pg}}{S_b}+\frac{M_{Dt}}{S_b}\geq -0.65f'_{ci} \tag{5.54}$$

$$\rightarrow e_{pg}\leq \frac{0.65f'_{ci}S_b}{A_{ps}f_{pi}}-\frac{S_b}{A_g}+\frac{M_{Dt}}{A_{ps}f_{pi}}$$

$$\rightarrow e_{pg}\leq (0.65f'_{ci}S_b+M_{Dt})\frac{1}{F_i}-\frac{S_b}{A_g}$$

$$\rightarrow e_{pg}\leq (0.65(11.7)(12{,}749)+1160)\frac{\eta_f}{F}-\frac{12{,}749}{817}$$

$$\rightarrow e_{pg}\leq (96{,}956+1160)\frac{0.8}{F}-15.61$$

$$\rightarrow e_{pg}\leq (78{,}493)\frac{1}{F}-15.61$$

5.6.5.2 Tension Stress Limit at Transfer

The tensile stress inequality is computed using the load factors as per Service I Load Combination in Table 3.4.1-1 in the AASHTO LRFD Specifications (AASHTO 2020). The tensile stress limit is considered to be $0.85f'_{ti}$ as per El-Helou and Graybeal (2022).

<u>Computation of Tension Limit at Top Fiber at Transfer Length</u>

$$-\frac{A_{ps}f_{pi}}{A_g}+\frac{A_{ps}f_{pi}e_{pg}}{S_t}-\frac{M_{Dt}}{S_t}\leq 0.85f'_{ti} \tag{5.55}$$

$$\rightarrow e_{pg}\leq \frac{0.85f'_{ti}S_t}{A_{ps}f_{pi}}+\frac{S_t}{A_g}+\frac{M_{Dt}}{A_{ps}f_{pi}}$$

$$\rightarrow e_{pg} \leq (0.85 f'_{ti} S_t + M_{Dt}) \frac{1}{F_i} + \frac{S_t}{A_g}$$

$$\rightarrow e_{pg} \leq (0.85(0.72)(9831) + 1160) \frac{\eta_f}{F} + \frac{(9831)}{817}$$

$$\rightarrow e_{pg} \leq (6016.6 + 1160) \frac{0.8}{F} + 12.03$$

$$\rightarrow e_{pg} \leq (5741) \frac{1}{F} + 12.03$$

5.6.6 Flexural Stresses after Deck Placement

5.6.6.1 Compression Stress Limit as Deck Placement

At the time of deck placement, the effective prestress and the superimposed dead loads are considered using unshored construction. The compression stress limit as per the AASHTO LRFD Specifications (AASHTO 2020) Table 5.9.2.3.2a-1 is $0.45f'_c$, which is also provided in the AASHTO draft specifications for UHPC (FHWA 2022). The stress is determined for the noncomposite section at the top fiber.

Initial force in prestressing steel just after release, F_i	=	$A_{ps} f_{pi}$
Effective force in prestressing steel at time of deck placement, F_{ed}	=	$A_{ps} f_{ped}$
Effective force in prestressing steel after long term losses, F	=	$A_{ps} f_{pe}$

<u>Computation of Tension Limit at Top Fiber at Midspan</u>

$$-\frac{A_{ps} f_{pe}}{A_g} + \frac{A_{ps} f_{ped} e_{pg}}{S_t} - \frac{M_g + M_s + M_h}{S_t} \geq -0.45 f'_c \tag{5.56}$$

$$\rightarrow e_{pg} \geq -\frac{0.45 f'_c S_t}{A_{ps} f_{ped}} + \frac{S_t}{A_g} + \frac{M_g + M_s + M_h}{A_{ps} f_{ped}}$$

$$\rightarrow e_{pg} \geq \left(-0.45 f'_c S_t + (M_g + M_s + M_h)\right) \frac{1}{F_{ed}} + \frac{S_t}{A_g}$$

$$\rightarrow e_{pg} \geq (-0.45(18)(9831) + (27{,}457 + 25{,}709 + 2142))\frac{0.92}{F} + \frac{9831}{817}$$

$$\rightarrow e_{pg} \geq (-79{,}631 + 55{,}308)\frac{0.92}{F} + 12.03$$

$$\rightarrow e_{pg} \geq (-22{,}377)\frac{1}{F} + 12.03$$

5.6.6.2 Tension Stress Limit at Deck Placement

The tension stress limit is computed when the non-composite section is subjected to the effective prestress and the superimposed dead loads. The tensile stress limit at the bottom fiber at midspan is $-0.85f_t'$ based on El-Helou and Graybeal (2022) and the AASHTO draft specifications (FHWA 2022).

<u>Computation of Tension Limit at Bottom Fiber at Midspan</u>

$$-\frac{A_{ps}f_{ped}}{A_g} - \frac{A_{ps}f_{ped}e_{pg}}{S_b} + \frac{M_g + M_s + M_h}{S_b} \leq 0.85f_t' \tag{5.57}$$

$$\rightarrow e_{pg} \geq -\frac{0.85f_t'S_b}{A_{ps}f_{ped}} - \frac{S_b}{A_g} + \frac{M_g + M_s + M_h}{A_{ps}f_{ped}}$$

$$\rightarrow e_{pg} \geq \left(-0.85f_t'S_b + (M_g + M_s + M_h)\right)\frac{1}{F_{ed}} - \frac{S_b}{A_g}$$

$$\rightarrow e_{pg} \geq (-0.85(0.85)(12{,}749) + (27{,}457 + 25{,}709 + 2142))\frac{0.92}{F} - \frac{12{,}749}{817}$$

$$\rightarrow e_{pg} \geq (-9211 + 55{,}308)\frac{0.92}{F} - 15.61$$

$$\rightarrow e_{pg} \geq 42{,}409\frac{1}{F} - 15.61$$

5.6.7 Flexural Stresses at Service Limit State

5.6.7.1 Compressive Stress after Losses

The stress limit at the top fiber of the girder at the midspan of the composite section due to the effective prestress after losses, superimposed dead loads and the transient loads (inclusive of the shipping and handling loads) given as $0.60\phi_w f_c'$ in AASHTO LRFD Specifications (AASHTO 2020) Table 5.9.2.3.2a-1, where ϕ_w is the reduction factor based on the web and flange slenderness ratios. Because the slenderness ratios are not greater than 15, $\phi_w = 1$.

<u>Computation of Compression Limit at Top Fiber at Midspan</u>

$$-\frac{A_{ps}f_{pe}}{A_g} + \frac{A_{ps}f_{pe}e_{pg}}{S_t} - \frac{M_g + M_s + M_h}{S_t} - \frac{M_{ws} + M_r + M_L}{S_{tgc}} \geq -0.60f_c' \tag{5.58}$$

$$\rightarrow e_{pg} \geq -\frac{0.6f_c'S_t}{A_{ps}f_{pe}} + \frac{S_t}{A_g} + \frac{M_g + M_s + M_h}{A_{ps}f_{pe}} + \frac{(M_{ws} + M_r + M_L)S_t}{S_{tgc}A_{ps}f_{pe}}$$

$$\rightarrow e_{pg} \geq \left(-0.6f_c'S_t - \left(M_g + M_s + M_h\right) + \frac{(M_{ws} + M_r + M_L)S_t}{S_{tgc}}\right)\frac{1}{F} + \frac{S_t}{A_g}$$

$$\rightarrow e_{pg} \geq \left(-0.6(18)(9831) + (27{,}457 + 25{,}709 + 2142) + \frac{(5646 + 3851 + 34{,}869)9831}{(40{,}838)}\right)\frac{1}{F} + \frac{9831}{817}$$

$$\rightarrow e_{pg} \geq (-106{,}175 + 55{,}308 + 10{,}680)\frac{1}{F} + 12.03$$

$$\rightarrow e_{pg} \geq (-40{,}187)\frac{1}{F} + 12.03$$

The compressive stress inequality when the composite section is subjected to the effective prestressing force due to losses and the permanent dead loads is computed at the top fiber of the girder at the midspan.

Computation of Compression Limit at Top Fiber at Midspan

$$-\frac{A_{ps}f_{pe}}{A_g}+\frac{A_{ps}f_{pe}e_{pg}}{S_t}-\frac{M_g+M_s+M_h}{S_t}-\frac{M_{ws}+M_r}{S_{tgc}}\geq -0.45f_c' \tag{5.59}$$

$$\rightarrow e_{pg}\geq -\frac{0.45f_c'S_t}{A_{ps}f_{pe}}+\frac{S_t}{A_g}+\frac{M_g+M_s+M_h}{A_{ps}f_{pe}}+\frac{(M_{ws}+M_r)S_t}{S_{tgc}A_{ps}f_{pe}}$$

$$\rightarrow e_{pg}\geq \left(-0.45f_c'S_t+(M_g+M_s+M_h)+\frac{(M_{ws}+M_r)S_t}{S_{tgc}}\right)\frac{1}{F}+\frac{S_t}{A_g}$$

$$\rightarrow e_{pg}\geq \left(-0.45(18)(9831)+(27{,}457+25{,}709+2142)+\frac{(5646+3851)9831}{(40{,}838)}\right)\frac{1}{F}+\frac{9831}{817}$$

$$\rightarrow e_{pg}\geq (-79{,}631+55{,}308+2286)\frac{1}{F}+12.03$$

$$\rightarrow e_{pg}\geq (-22{,}037)\frac{1}{F}+12.03$$

5.6.7.2 Tension Stress after Losses

The tension stress limit at the bottom fiber at the midspan due the effective prestress after losses for Service III Load combination from AASHTO LRFD Specifications (AASHTO 2020) Table 3.4.1-1 is considered. The tensile limit for the composite section is $0.85f_t'$ as per AASHTO draft specifications for UHPC (FHWA 2022).

Computation of Tension Limit at Bottom Fiber at Midspan

$$-\frac{A_{ps}f_{pe}}{A_g}-\frac{A_{ps}f_{pe}e_{pg}}{S_b}+\frac{M_g+M_s+M_h}{S_b}+\frac{M_{ws}+M_r+M_L}{S_{bc}}\leq 0.85f_t' \tag{5.60}$$

$$\rightarrow e_{pg}\geq -\frac{0.85f_t'S_b}{A_{ps}f_{pe}}-\frac{S_b}{A_g}+\frac{M_g+M_s+M_h}{A_{ps}f_{pe}}+\frac{(M_{ws}+M_r+M_L)S_b}{S_{bc}A_{ps}f_{pe}}$$

$$\rightarrow e_{pg} \geq \left(-0.85 f_t' S_b + (M_g + M_s + M_h) + \frac{(M_{ws} + M_r + M_L) S_b}{S_{bc}}\right)\frac{1}{F} - \frac{S_b}{A_g}$$

$$\rightarrow e_{pg} \geq \left(-0.85(0.85)(12{,}749) + (27{,}457 + 25{,}709 + 2142) + \frac{(5646 + 3851 + 34{,}869)12{,}749}{18{,}982}\right)\frac{1}{F} - \frac{12{,}749}{817}$$

$$\rightarrow e_{pg} \geq (-9211 + 55{,}308 + 29{,}798)\frac{1}{F} - 15.61$$

$$\rightarrow e_{pg} \geq (75{,}985)\frac{1}{F} - 15.61$$

Figure 5.4 presents the stress blocks for the inequalities derived. The shape of the stress diagrams represents the actual stress distribution, while the final values provided are the stress limits. It is to be noted that the eccentricity is recorded in inches and is plotted against the inverse of the prestressing force. The optimal number of strands that satisfies the feasible domain is derived from a series of iterations of prestress loss computation. A harped section is designed using 86 strands with 13.10 in. eccentricity at midspan and 6.41 in. eccentricity at the ends. The selection will be evaluated by checking the stresses within the section with e_{end} or e_{pg} and N combination. For this combination, the prestressing forces are shown in Figure 5.4.

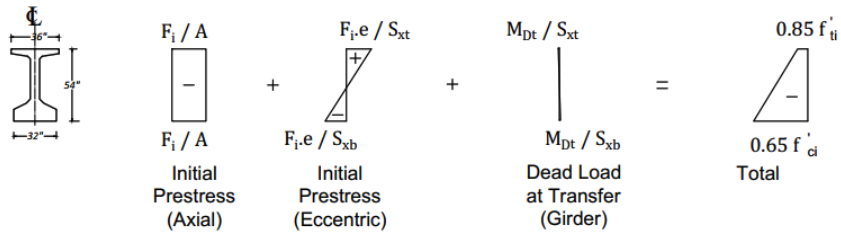

(a) Stress checks at transfer

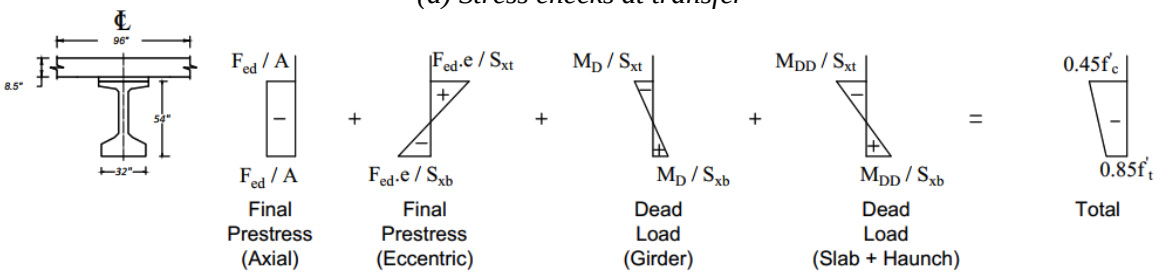

(b) Stress checks at deck placement

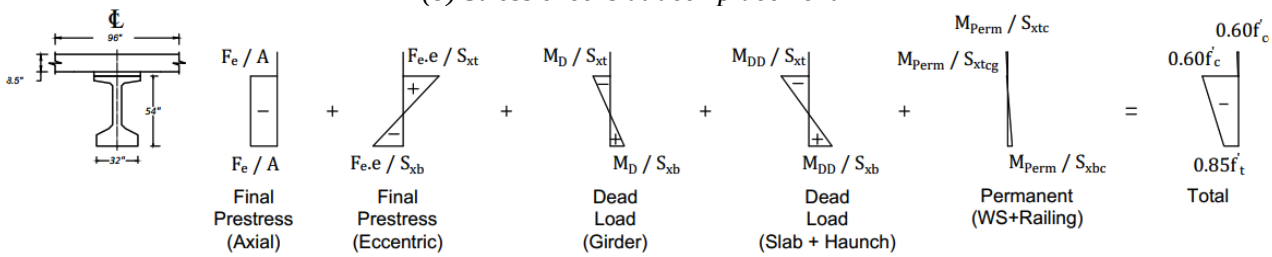

(c) Stress checks at service due to effective prestress and permanent (dead) loads

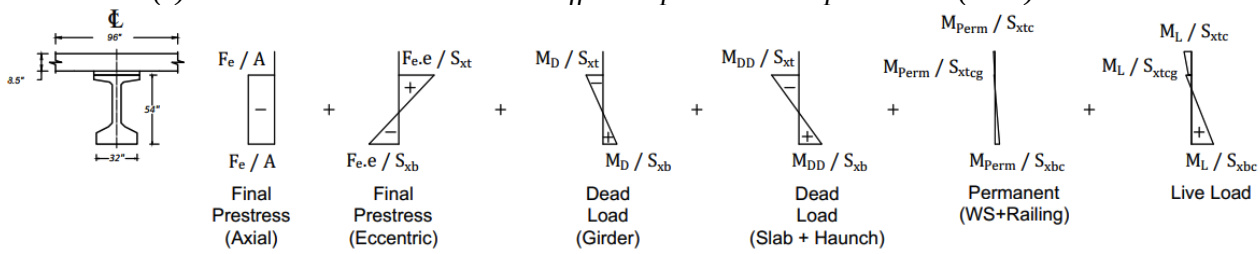

(d) Stress checks at service due to total and effective prestress

Figure 5.4. Stress Blocks for the Derived Inequalities.

Force in Prestressing

Force in prestressing strand at transfer, F_i = $NA_t(0.75f_{pu} - \Delta f_{pST})$ (5.61)

= (86) (0.217) (177.1) = 3305 kips

Force in prestressing strand after losses at deck placement, F_{ed} = $NA_t f_{ped}$ (5.62)

= (86) (0.217) (153.5) = 2865 kips

Force in prestressing strand after losses, F_e = $NA_t f_{pe}$ (5.63)

= (86) (0.217) (141.8) = 2647 kips

Figure 5.5 presents the feasible domain with the eccentricity on the y-axis and the inverse of the prestress force on the x-axis. Note that the top cross-sectional view represents the midspan section and the bottom cross section represents the girder end section. Unlike the girder specimen tested, no straight strands in the top flange were needed by design for this specimen. The transverse reinforcement R-bars are tied to the two non-stressed straight strands at the top of the girder cross-section that are present in the precast bed by default for the purpose of guiding and tying the transverse shear reinforcement bars.

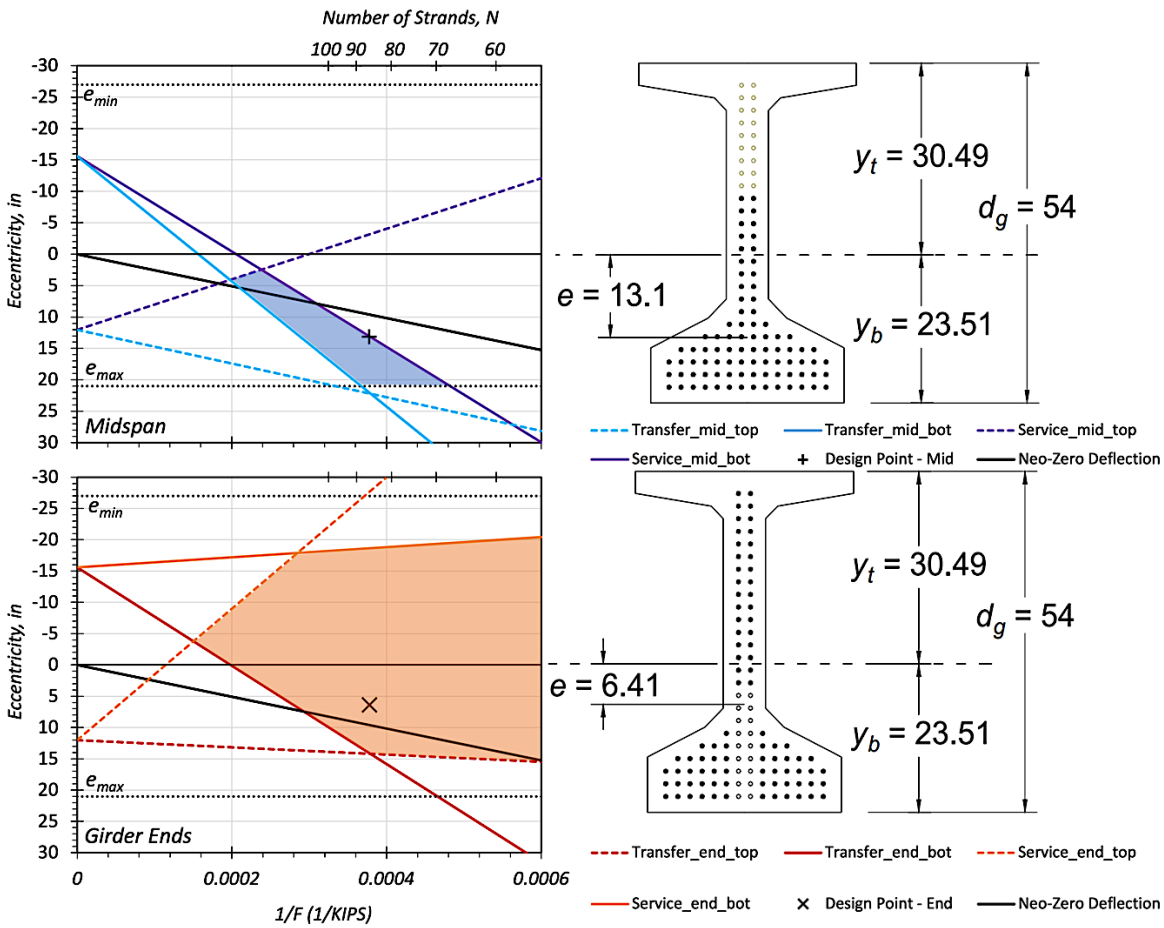

Figure 5.5. Feasible Domain for Flexure Design.

5.6.7.3 Stress Checks

The stresses will be evaluated at each of the critical stages within the bridge construction.

<u>Computation at Prestress Transfer</u>

Stress at bottom fiber at transfer length, f_{bottom}

$$= -\frac{F_i}{A_g} - \frac{F_i e_{end}}{S_b} + \frac{M_{Dt}}{S_b} \geq -0.65 f'_{ci} \tag{5.64}$$

$$= -\frac{3305}{817} - \frac{(3305)(6.41)}{12{,}749} + \frac{1160}{12{,}749} \geq -(0.65)(11.7)$$

$$= -4.04 - 1.66 + 0.09 = -5.61 \text{ ksi} \geq -7.61 \text{ ksi [Check OK]}$$

Stress at top fiber at transfer length, f_{top}

$$= -\frac{F_i}{A_g} + \frac{F_i e_{end}}{S_t} - \frac{M_{Dt}}{S_t} \leq 0.85 f'_{ti} \tag{5.65}$$

$$= -\frac{3305}{817} + \frac{(3305)(6.41)}{9831} - \frac{1160}{9831} \leq (0.85)(0.72)$$

$$= -4.04 + 2.15 - 0.12 = -2.01 \text{ ksi} \leq 0.61 \text{ ksi [Check OK]}$$

<u>Computation at Deck Placement</u>

Stress at top fiber at midspan, f_{top}

$$= -\frac{F_{ed}}{A_g} + \frac{F_{ed} e_{pg}}{S_t} - \frac{M_g + M_s + M_h}{S_t} \geq -0.45 f'_c \tag{5.66}$$

$$= -\frac{2865}{817} + \frac{(2865)(13.1)}{9831} - \frac{(27{,}457 + 25{,}709 + 2142)}{9831} \geq -(0.45)(18)$$

$$= -3.51 + 3.82 - 5.63 = -5.32 \text{ ksi} \geq -8.1 \text{ ksi [Check OK]}$$

Stress at bottom fiber at midspan, f_{bottom}

$$= -\frac{F_{ed}}{A_g} - \frac{F_{ed} e_{pg}}{S_b} + \frac{M_g + M_s + M_h}{S_b} \leq 0.85 f'_t \tag{5.67}$$

$$= -\frac{2865}{817} - \frac{(2865)(13.1)}{12{,}749} + \frac{(27{,}457 + 25{,}709 + 2142)}{12{,}749} \leq (0.85)(0.85)$$

$$= -3.51 - 2.94 + 4.34 = -2.11 \text{ ksi} \leq 0.72 \text{ ksi [Check OK]}$$

<u>Computation at Final</u>

Stress at top fiber at midspan (Permanent), $f_{top.perm}$

$$= -\frac{F_e}{A_g} + \frac{F_e e_{pg}}{S_t} - \frac{M_g + M_s + M_h}{S_t} - \frac{M_{ws} + M_r}{S_{tg}} \geq -0.45 f'_c \tag{5.68}$$

$$= -\frac{2647}{817} + \frac{(2647)(13.10)}{9831} - \frac{(27{,}457 + 25{,}709 + 2142)}{9831} - \frac{(5646 + 3851)}{40{,}838} \geq -(0.45)(18)$$

$$= -3.24 + 3.53 - 5.63 - 0.23 = -5.57 \text{ ksi} \geq -8.1 \text{ ksi [Check OK]}$$

Stress at top fiber at midspan, f_{top}

$$= -\frac{F_e}{A_g} + \frac{F_e e_{pg}}{S_t} - \frac{M_g + M_s + M_h}{S_t} - \frac{M_{ws} + M_r + M_L}{S_{tg}} \geq -0.6f_c' \quad (5.69)$$

$$= -\frac{2647}{817} + \frac{(2647)(13.10)}{9831} - \frac{(27{,}457 + 25{,}709 + 2142)}{9831} - \frac{(5646 + 3851 + 34{,}869)}{40{,}838} \geq -(0.60)(18)$$

$$= -3.24 + 3.53 - 5.63 - 1.09 = -6.43 \text{ ksi}$$

$$\geq -10.8 \text{ ksi [Check OK]}$$

Stress at bottom fiber at midspan, f_{bottom}

$$= -\frac{F_e}{A_g} - \frac{F_e e_{pg}}{S_b} + \frac{M_g + M_s + M_h}{S_b} + \frac{M_{ws} + M_r + M_L}{S_{bc}} \leq 0.85f_t' \quad (5.70)$$

$$= -\frac{2647}{817} - \frac{(2647)(13.10)}{12{,}749} + \frac{(27{,}457 + 25{,}709 + 2142)}{12{,}749} + \frac{(5646 + 3851 + 34{,}869)}{18{,}982} \leq (0.85)(0.85)$$

$$= -3.24 - 2.72 + 4.34 + 2.34 = 0.716 \text{ ksi}$$

$$\leq 0.72 \text{ ksi [Check OK]}$$

The section passes all the stress checks. Therefore, the selection of 86 strands with 13.10 in. eccentricity at midspan and 6.41 in. eccentricity at the girder ends (32 strands harped) may be used based on the service stress checks. Figure 5.6 presents the strand layout selected. Figure 5.7 presents the stress block diagrams of the critical sections at transfer and service.

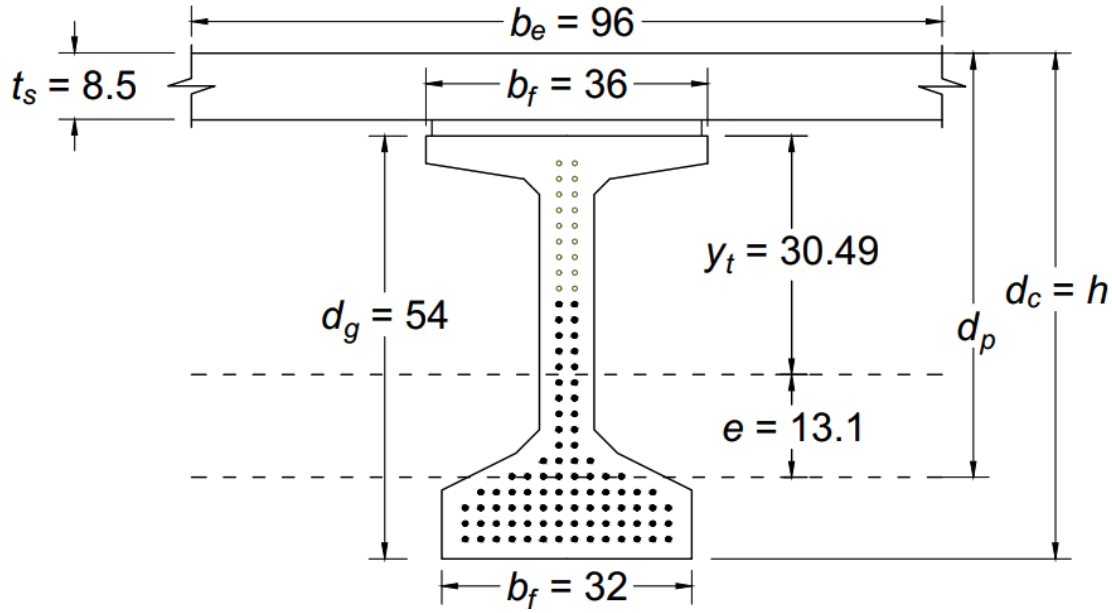

(a) Midspan

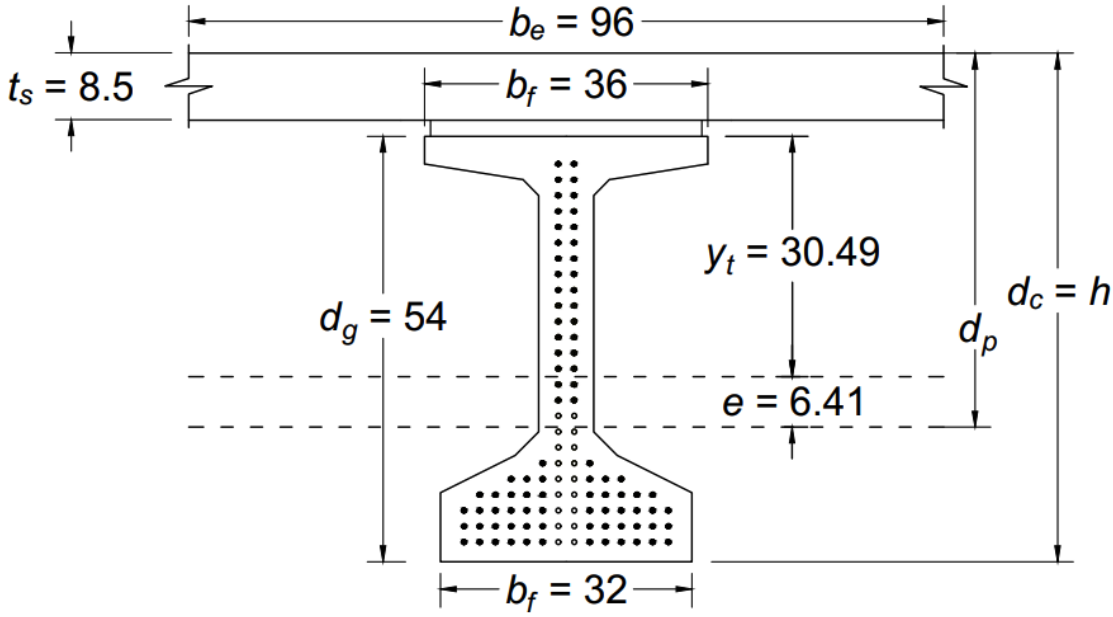

(b) End

Figure 5.6. Strand Layout.

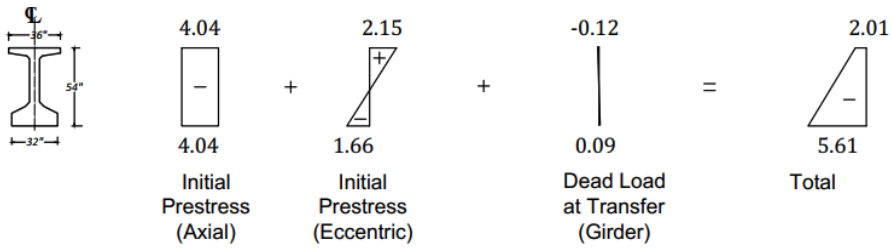

(a) Stress checks at transfer

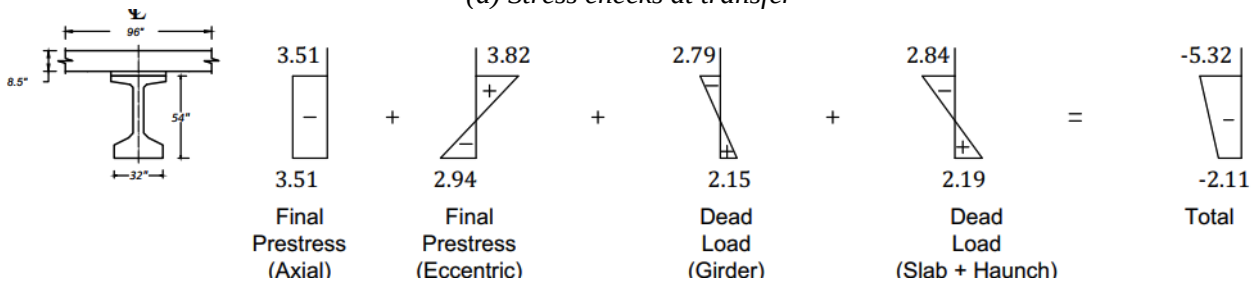

(b) Stress checks at deck placement

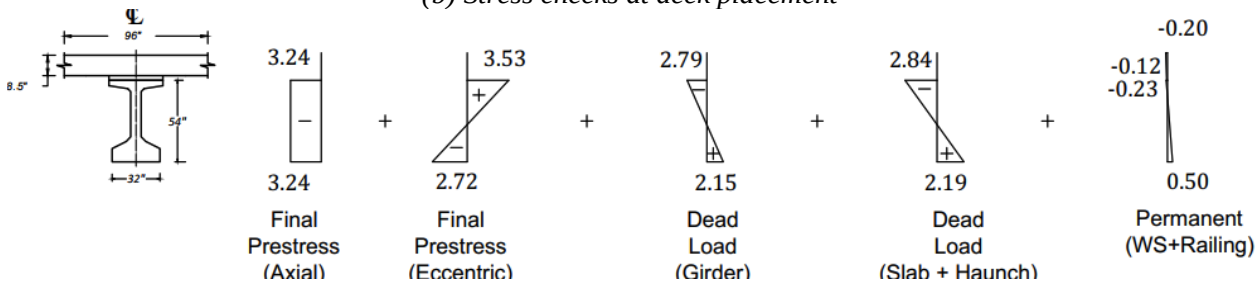

(c) Stress checks at service due to effective prestress and permanent (dead) loads

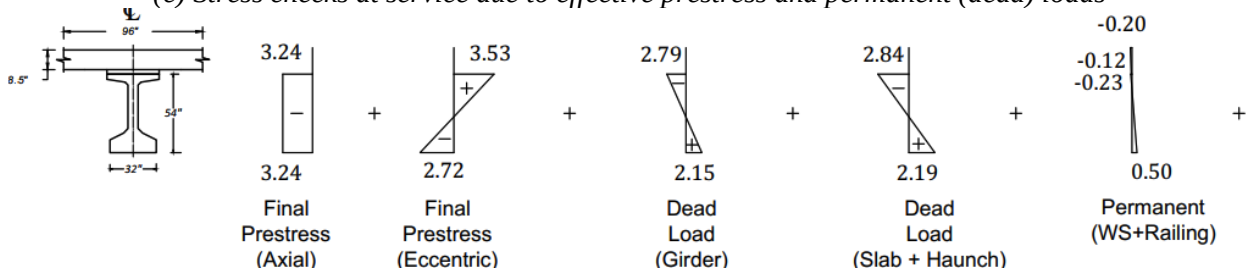

(d) Stress checks at service due to total and effective prestress

Figure 5.7. Stress Checks.

5.6.8 Camber Calculation

<u>Computation of Deflections</u>

Girder self-weight at transfer, Δ_{gtr} $= \dfrac{5w_g {L_g}^4}{384E_{gi}I_g}$

$$= \frac{(5)(0.908)(143.5^4)}{(384)(6742)\left(\dfrac{299{,}740}{144\ \text{in.}^2/\text{ft}^2}\right)} \times 12\ \text{in./ft}$$

$= 4.29$ in.

Girder self-weight at erection, Δ_{ger} $= \dfrac{5w_g L^4}{384E_{gi}I_g}$

$$= \frac{(5)(0.908)(142^4)}{(384)(6742)\left(\dfrac{299{,}740}{144\ \text{in.}^2/\text{ft}^2}\right)} \times 12\ \text{in./ft}$$

$= 4.11$ in.

Harp point (a) $= \dfrac{L_g}{2} - \max\left(\dfrac{L_g}{20}, 5\right) = \dfrac{143.5}{2} - \dfrac{143.5}{20} = 64.58$ ft

Prestressing strands, Δ_{PS} $= -\dfrac{F_i}{E_{gi}I_g}\left(\dfrac{e{L_g}^2}{8} - \dfrac{(e - e_{end})(a)^2}{6}\right)$

$$= -\frac{(3305)}{(6742)(299{,}740)}\left(\frac{(13.1)(143.5 \times 12\ \text{in./ft})^2}{8} - \frac{(13.1 - 6.41)(64.58 \times 12\ \text{in./ft})^2}{6}\right)$$

$=$ -6.85 in.

Deck and haunch, Δ_{sl} $= \dfrac{5(w_s + w_h)L^4}{384E_g I_{gc}}$

$$= \frac{(5)(0.85 + 0.071)(142^4)}{(384)(7423)\left(\dfrac{699{,}771}{144\ \text{in.}^2/\text{ft}^2}\right)} \times 12\ \text{in./ft}$$

$$= 1.62\ \text{in.}$$

Superimposed dead load, Δ_{SI} $= \dfrac{5(w_{ws} + w_{rl})L^4}{384E_g I_{gc}}$

$$= \frac{(5)(0.19 + 0.127)(142^4)}{(384)(7423)\left(\dfrac{699{,}771}{144\ \text{in.}^2/\text{ft}^2}\right)} \times 12\ \text{in./ft}$$

$$= 0.55\ \text{in.}$$

Prestress Loss, $\Delta_{PS_{loss}}(90\ days)$ $= \dfrac{A_{ps}\Delta f_{pLT}}{E_g I_g}\left(\dfrac{eL^2}{8} - \dfrac{(e - e_{end})(a)^2}{6}\right)$

$$= \frac{(18.66)(23.6)}{(7423)(299{,}740)}\left(\frac{(13.10)(142 \times 12\ \text{in./ft})^2}{8} - \frac{(6.69)(64.58 \times 12\ \text{in./ft})^2}{6}\right)$$

$$= 0.81\ \text{in.}$$

Prestress Loss, $\Delta_{PS_{loss}}(27{,}375\ days)$ $= \dfrac{A_{ps}\Delta f_{pLT}}{E_g I_g}\left(\dfrac{eL^2}{8} - \dfrac{(e - e_{end})(a)^2}{6}\right)$

$$= \frac{(18.66)(35.35)}{(7423)(299{,}740)}\left(\frac{(13.10)(142 \times 12\ \text{in./ft})^2}{8} - \frac{(6.69)(64.58 \times 12\ \text{in./ft})^2}{6}\right)$$

$$= 1.21\ \text{in.}$$

Creep coefficient is computed as per the experimental study conducted and reported in the Volume 1 report and in Section 3.4.2.2 of this report:

Creep coefficient at 90 days (deck placement) $\psi_{CR} = 0.53$

Creep coefficient at 27,375 days (final) $\psi_{CR} = 0.80$

Deflection at transfer, $\Delta_{at_transfer}$

$$= \left(\Delta_{gtr} + \Delta_{PS}\right)$$
$$= (4.29 - 6.85)$$
$$= -2.56 \text{ in.}$$

Deflection before deck placement, Δ_{before_deck}

$$= \left(\Delta_{g_{tr}} + \Delta_{PS}\right)(1 + \psi_{CR}) + \left(\Delta_{PS_loss}(1 + 0.7\psi_{CR})\right)$$
$$= (4.29 - 6.85)\ (1 + 0.53) + \left(0.81\left(1 + 0.7(0.53)\right)\right)$$
$$= -2.81 \text{ in.}$$

Deflection after casting deck, Δ_{after_deck}

$$= \left(\Delta_{g_{tr}} + \Delta_{PS}\right)(1 + \psi_{CR}) + \left(\Delta_{PS_loss}(1 + 0.7\psi_{CR})\right) + \Delta_{sl}$$
$$= (4.29 - 6.85)\ (1 + 0.53) + \left(0.81\left(1 + 0.7(0.53)\right)\right) + 1.62$$
$$= -1.19 \text{ in.}$$

Final deflection, Δ_{final}

$$= \left(\Delta_{g_{tr}} + \Delta_{PS}\right)(1 + \psi_{CR}) + \left(\Delta_{PS_loss}(1 + 0.7\psi_{CR})\right) + \Delta_{sl} + \Delta_{SI}$$
$$= (4.29 - 6.85)\ (1 + 0.80) + \left(1.21\left(1 + 0.7(0.80)\right)\right) + 1.62 + 0.55$$
$$= -0.55 \text{ in.}$$

5.6.9 Live Load Deflection Check

For the preliminary analysis and design purposes, this example considers the maximum allowable deflection limit to be span length *L* divided by 800 (AASHTO 2020).

<u>Maximum allowable deflection limit</u>

Maximum deflection limit, Δ_{limit}

$$= \frac{L}{800} \tag{5.71}$$
$$= \frac{142}{800} = 0.18 \text{ ft} = 2.13 \text{ in.}$$

Deflection due to uniformly distributed load, Δ_{UDL}

$$= mN_L \frac{5qL^4}{384E_gI_{br}} \tag{5.72}$$

$$= (0.85)(3)\left(\frac{(5)(0.64)(142^4)}{(384)(7423)\left(\frac{4{,}077{,}475}{144\text{ in.}^2/\text{ft}^2}\right)}\right) \times 12\text{ in./ft}$$

$$= 0.49\text{ in.}$$

Deflection due to HS20 truck, Δ_{HS20}

$$= 1.33mN_L \frac{\left(32L^3 + 40\left(\frac{L}{2} - 14\right)\left(3L^2 - 4\left(\frac{L}{2} - 14\right)^2\right)\right)}{48E_gI_{br}} \tag{5.73}$$

$$= (1.33)(0.85)(3)\left(\frac{\left(32(142)^3 + (40)\left(\frac{142}{2} - 14\right)\left(3 * 142^2 - 4\left(\frac{142}{2} - 14\right)^2\right)\right)}{(48)(7423)\left(\frac{4{,}077{,}475}{144\text{ in.}^2/\text{ft}^2}\right)}\right) \times 12\text{ in./ft}$$

$$= 0.81\text{ in.}$$

<u>Computation of Governing Live Load Deflection, Δ_{LL}</u>

Deflection due to live load, Δ_{LL}

$$= \max\left(\Delta_{HS20}, (\Delta_{UDL} + 0.25\Delta_{HS20})\right) \tag{5.74}$$

$$= 0.81\text{ in.} \leq 2.13\text{ in. [Check OK]}$$

5.6.10 Flexural Resistance at Strength Limit State

This section documents the ultimate strength check of the prestressed members based on the approach used in the AASHTO LRFD Specifications (AASHTO 2020). The load combination of Strength I is used for this check. The approach provided in the AASHTO draft specifications for UHPC (FHWA 2022) are also shown below for reference.

$$M_u = 1.25\left(M_g + M_s + M_h + M_r\right) + 1.50(M_{ws}) + 1.75(M_{LL}) \tag{5.75}$$

where:

M_u	=	Ultimate factored moment demand
M_g	=	Moment at midspan due to self-weight of the girder, kip-ft
M_s	=	Moment at midspan due to weight of the deck slab, kip-ft
M_h	=	Moment at midspan due to weight of the haunch, kip-ft
M_{ws}	=	Moment at midspan due to weight of the wearing surface, kip-ft
M_r	=	Moment at midspan due to weight of the railing, kip-ft
M_{LL}	=	Moment at midspan due to live loads, kip-ft

Moment Demand, M_u

$$= 1.25\left(M_g + M_s + M_h + M_r\right) + 1.50(M_{ws}) + 1.75(M_{LL}) \quad (5.76)$$

$$= 1.25(2288 + 2142 + 179 + 321) + 1.50(470.5) + 1.75(2906)$$

$$= 11{,}953 \text{ kip-ft}$$

The method of AASHTO LRFD Specifications (AASHTO 2020) from Article 5.6.3 using a rectangular stress distribution is shown below. This method is chosen for the composite CIP CC deck and UHPC girder in this example due to the large contribution of the deck to the internal compression force in bending. The nominal flexure capacity computed using the AASHTO LRFD Specifications (AASHTO 2020) assumes a rectangular distribution of stress in the compression zone and neglects the tensile strength of the concrete.

k = 0.28 [for low relaxation strands]

Distance between extreme compression fiber and centroid of strands, d_p

$$= y_t + e + t_s \quad (5.77)$$

$$= 30.5 + 13.1 + 8.5$$

$$= 52.1 \text{ in.}$$

Note: The haunch is conservatively being neglected when determining d_p.

Flexural resistance factor, ϕ

$$= 1.0 \quad (5.78)$$

(5.79)

Stress block parameter, α_1

$= 0.85$ for $f_{cd} \leq 10$

$= \max(0.85 - 0.02(f_{cd} - 10), 0.75)$ for $f_{cd} > 10$

$= 0.85$ $f_{cd} = 4 \leq 10$

Stress block parameter, α_2 (5.80)

$= \max(0.85 - 0.02(f_c - 10), 0.75)$

$= \max(0.85 - 0.02(18 - 10), 0.75)$

$= 0.75$

Stress block parameter for deck, β_1 (5.81)

$= \max(0.85 - 0.05(f_{cd} - 4), 0.65)$

$= \max(0.85 - 0.05(4 - 4), 0.65)$

$= 0.85$

Stress block parameter for UHPC girder, β_2 (5.82)

$= \max(0.85 - 0.05(f_c - 4), 0.65)$

$= \max(0.85 - 0.05(18 - 4), 0.65)$

$= 0.65$

Assuming $a < t_s$

Distance from the extreme compression fiber to the neutral axis, c (5.83)

$$= \frac{A_{ps}f_{pu} + A_s f_s + A_s' f_s'}{\alpha_1 f_c' \beta_1 b + kA_{ps}\left(\frac{f_{pu}}{d_p}\right)}$$

$$= \frac{(18.66)(270)}{(0.85)(4)(0.85)(96) + (0.28)(18.66)\left(\frac{270}{52.1}\right)}$$

$= 16.55$ in.

Depth of equivalent rectangular stress block, a (5.84)

$= \beta_1 c$

$= (0.85)(16.55)$

$= 14.06$ in.

$a = 14.06$ in. $\nless t_s = 8.5$ [Check not OK]

$a = t_s = 8.5$ in.

$$C = \alpha_1 f_{cd} a b_{eff} \tag{5.85}$$

$$C = (0.85)(4)(8.5)(96)$$

$$C = 2774 \text{ kips}$$

$$T = NA_t f_{pu}\left(1 - \frac{ka}{\beta_1 d_p}\right)$$

$$T = (86)(0.217)(270)\left(1 - \frac{(0.28)(8.5)}{(0.85)(52.1)}\right)$$

$$T = 4768 \text{ kips}$$

T>C, therefore, $a > t_s$

Since, $T > C$

a is incremented by 0.01

a is optimized such that $T = C$

Optimized value of a at $T = C$ is 13.67 in.

$t_s + t_h + h_{tf1}$

$$= 8.5 + 2 + 3.5$$

$$= 14 \text{ in.}$$

$t_s + t_h + h_{tf1} + h_{tf2}$

$$= 8.5 + 2 + 3.5 + 4$$

$$= 18 \text{ in.}$$

Since, $a > t_s$ and $a \leq t_s + t_h + h_{tf1}$

$$C_{tf1} = 2\alpha_2 f_c b_{tf1}(a - t_s - t_h) \tag{5.86}$$

$$C_{tf1} = 2(0.75)(18)(14.5)\big((12.25) - (8.5) - (2)\big)$$

$$C_{tf1} = 1240.22 \text{ kips}$$

$$y_{tf1} = \frac{(t_s + t_h + a)}{2}$$

$$y_{tf1} = \frac{8.5 + 2 + 13.67}{2}$$

$$y_{tf1} = 12.08 \text{ in.}$$

Compression in Slab, C_{slab}

$$= \alpha_1 f_{cd} t_s b_{eff} \tag{5.87}$$

$$= (0.85)(4)(8.5)(96)$$

$$= 2774 \text{ kips}$$

Compression in Slab, C_{haunch}

$$= \alpha_1 f_{cd} t_h b_{eff} \quad (5.88)$$
$$= (0.85)(4)(2)(34)$$
$$= 231 \text{ kips}$$

Compression in Web, C_{web}

$$= \alpha_2 f_c b_w (a - t_s) \quad (5.89)$$
$$= (0.75)(18)(7)(13.67 - 8.5 - 2)$$
$$= 299 \text{ kips}$$

Total compressive force, C

$$= C_{slab} + C_{haunch} + C_{tf1} + C_{web} \quad (5.90)$$
$$= 2774 + 231 + 1240 + 299$$
$$= 4545 \text{ kips}$$

Total tensile force, T

$$= NA_t f_{pu}\left(1 - \frac{ka}{\beta_{avg} d_p}\right) \quad (5.91)$$
$$= (86)(0.217)(270)\left(1 - \frac{(0.28)(13.67)}{(0.75)(52.1)}\right)$$
$$= 4545 \text{ kips}$$

$T - C$

$$= 4545 - 4545$$
$$= 0$$

Depth of compression CG form neutral axis, y_r

$$= \frac{C_{slab}\frac{t_s}{2} + C_{haunch}\left(t_s + \frac{t_h}{2}\right) + C_{tf1} y_{tf1} + C_{web}\frac{(a + t_s + t_h)}{2}}{C} \quad (5.92)$$
$$= \frac{(2774)\frac{8.5}{2} + (231)\left(8.5 + \frac{2}{2}\right) + (1240)(12.08) + (299)\frac{13.67 + 8.5 + 2}{2}}{(4545)}$$
$$= 7.2 \text{ in.}$$

Inner lever arm, z

$$= d_p - y_r \quad (5.93)$$
$$= 52.1 - 7.2$$
$$= 44.9 \text{ in.}$$

Nominal moment, M_n

$$= C_{slab}\left(d_p - \frac{t_s}{2}\right) + C_{haunch}\left(d_p - t_s - \frac{t_h}{2}\right) + C_{tf1}\left(d_p - y_{tf1}\right) + C_{tf2}\left(d_p - y_{tf2}\right) + C_{web}\left(d_p - \frac{(a + t_s)}{2}\right) \tag{5.94}$$

$$= (2774)\left(52.1 - \frac{8.5}{2}\right) + (231)\left(52.1 - 8.5 - \frac{2}{2}\right) + (1240)(52.1 - 12.08) + (299)\left(52.1 - \frac{13.67 + 8.5 + 2}{2}\right)$$

$$= 17{,}015 \text{ kip-ft}$$

Reduced nominal moment, M_r

$$= \phi M_n \tag{5.95}$$

$$= (1.0)(17{,}015)$$

$$= 17{,}015 \text{ kip-ft}$$

$M_r = 17{,}015$ kip-ft $> M_u = 11{,}953$ kip-ft

[Check OK]

The section passes the flexural resistance check for the strength limit state.

The method for computing the nominal moment capacity of a given section provided by the AASHTO draft specifications for UHPC (FHWA 2022) is applied below, similar to the Tx34 design example. The formulation for computing the moment capacity is explained in Section 3.7.3. The calculations for the approach provided in the AASHTO draft specifications for UHPC (FHWA 2022) are as follows.

Assuming $c < t_s$

Distance from the extreme compression fiber to the neutral axis, c

$$= \frac{A_{ps}f_{pu} + 0.5f'_t(2b_{tf1}h_{tf1} + b_{tf2}h_{tf2} - t_s b_w)}{\alpha_1 f'_c \beta_1 b + kA_{ps}\left(\frac{f_{pu}}{d_p}\right) - 0.5f'_t 3b_w} \quad (5.96)$$

$$= \frac{(18.66)(270) + 0.5(0.85)(2(14.5)(3.5) + (9.25)(4) - (8.5)(7))}{(0.85)(4)(0.85)(96) + (0.28)(18.66)\left(\frac{270}{52.1}\right) - 0.5(0.85)(3)(7)}$$

$$= 17.16 \text{ in.}$$

$c = 17.16 \nless t_s = 8.5$ [Check not OK]

$c = t_s = 8.5$ in.

$$C = \alpha_1 f_{cd}\beta_1 c b_{eff} \quad (5.97)$$

$$C = (0.85)(4)(0.85)(8.5)(96)$$

$$C = 2358 \text{ kips}$$

$$T = NA_t f_{pu}\left(1 - \frac{kc}{d_p}\right)$$

$$T = (86)(0.217)(270)\left(1 - \frac{(0.28)(8.5)}{(52.1)}\right)$$

$$T = 4808 \text{ kips}$$

T>C, therefore, $c > t_s$

Since, $T > C$

c is incremented by 0.01.

c is optimized such that $T = C$.

Optimized value of c at $T = C$ is 18.8 in.

$t_s + t_h + h_{tf1}$ $= 8.5 + 2 + 3.5$

$= 14$ in.

$t_s + t_h + h_{tf1} + h_{tf2}$ $= 8.5 + 2 + 3.5 + 4$

$= 18$ in.

Since, $c > t_s + t_h + h_{tf1} + h_{tf2}$

$$\varepsilon_{gt} = \frac{0.003(c - t_s)}{c} = 0.00164 \tag{5.98}$$

$$\varepsilon_{g1} = \frac{0.003(c - t_s - h_{tf1})}{c} = 0.00108$$

$$\varepsilon_{g2} = \frac{0.003(c - t_s - h_{tf1} - h_{tf2})}{c} = 0.00045$$

$$C_{tf1} = \frac{E_g(\varepsilon_{gt} + \varepsilon_{g1})}{2}(2h_{tf1}b_{tf1}) = 1027 \text{ kips}$$

$$C_{tf2} = \frac{E_g(\varepsilon_{g1} + \varepsilon_{g2})}{2}(h_{tf2}b_{tf2}) = 210 \text{ kips}$$

$$T_{bf1} = 0.5f'_t(2b_{bf1} * (3c + h_{bf1} - h)) = 6.8 \text{ kips}$$

$$T_{bf2} = 0.5f'_t(b_{bf2} * h_{bf2}) = 35 \text{ kips}$$

$$y_{tf1} = t_s + \frac{(h_{tf1})}{2} = 10.25 \text{ in.}$$

$$y_{tf2} = t_s + h_{tf1} + \frac{(h_{tf2})}{3} = 13.33 \text{ in.}$$

$$y_{bf1} = h - 0.5 * (3c + h_{bf1} - h) = 64.18 \text{ in.}$$

$$y_{bf2} = h - h_{bf1} - \frac{(h_{bf2})}{3} = 53.17 \text{ in.}$$

Compression in Slab, C_{slab}

$$= \alpha_1 f_{cd} t_s b_{eff} \tag{5.99}$$

$$= (0.85)(4)(8.5)(96)$$

$$= 2774 \text{ kips}$$

Compression in Slab, C_{haunch}

$$= \alpha_1 f_{cd} t_h b_{eff} \tag{5.100}$$

$$= (0.85)(4)(2)(34)$$

$$= 231 \text{ kips}$$

Compression in Web, C_{web}

$$= 0.5E_g \varepsilon_{gt} b_w (c - t_s) \tag{5.101}$$

$$= 440 \text{ kips}$$

Total compressive force, C

$$= C_{slab} + C_{haunch} + C_{tf1} + C_{tf2} + C_{web} \quad (5.102)$$

$$= 2774 + 231 + 1028 + 210 + 440$$

$$= 4683 \text{ kips}$$

Tension in Web, T_{web}

$$= 0.5f'_t b_w (c - t_s) 2c \quad (5.103)$$

$$= 112 \text{ kips}$$

Total tensile force, T

$$= NA_t f_{pu}\left(1 - \frac{kc}{d_p}\right) + T_{bf1} + T_{bf2} + T_{web} \quad (5.104)$$

$$= (86)(0.217)(270)\left(1 - \frac{(0.28)(18.8)}{(52.1)}\right) + 6.8 + 35 + 112$$

$$= 4683 \text{ kips}$$

$T - C$

$$= 4683 - 4683$$

$$= 0$$

Depth of compression CG from top, y_{rC}

$$= \frac{C_{slab}\frac{t_s}{2} + C_{haunch}\left(t_s + \frac{t_h}{2}\right) + C_{tf1}y_{tf1} + C_{tf2}y_{tf2} + C_{web}\frac{(c +}{}}{C} \quad (5.105)$$

$$= 7.1 \text{ in.}$$

Depth of tension CG from top, y_{rT}

$$= \frac{NA_t f_{pu}\left(1 - \frac{kc}{d_p}\right)d_p + T_{bf1}y_{bf1} + T_{bf2}y_{bf2} + T_{web}(d_p - \frac{(h +}{2}}{T} \quad (5.106)$$

$$= 51.7 \text{ in.}$$

Inner lever arm, z

$$= y_{rT} - y_{rC} \quad (5.107)$$

$$= 51.7 - 7.1$$

$$= 44.6 \text{ in.}$$

Nominal moment, M_n

$$= C_{slab}\left(d_p - \frac{t_s}{2}\right) + C_{haunch}\left(d_p - t_s - \frac{t_h}{2}\right) + C_{tf1}(d_p - y_{tf1}) + C_{tf2}(d_p - y_{tf2}) + C_{web}\left(d_p - \frac{(c + 2t_s)}{3}\right) - T_{bf1}(d_p - y_{bf1}) + T_{bf2}(d_p - y_{bf2}) - T_{web}(d_p - 1.83c) \tag{5.108}$$

$$= 17{,}462 \text{ kip-ft}$$

Reduced nominal moment, M_r

$$= \phi M_n \tag{5.109}$$

$$= (0.9)(17{,}462)$$

$$= 15{,}715 \text{ kip-ft}$$

$M_r = 15{,}715$ kip-ft $> M_u = 11{,}953$ kip-ft

[Check OK]

The section passes the flexural resistance check for the strength limit state.

Table 5.13 compares the nominal moment capacity, neutral axis depth, and the lever arm calculated by the two approaches, AASHTO LRFD Specifications (AASHTO 2020) and the proposed UHPC draft specifications. Note that for this example the simplified approach based on the AASHTO LRFD Specifications provides a value close to that of the proposed UHPC draft specifications but is slightly more conservative.

Table 5.13. Comparison of Nominal Moment Capacity.

Description	**AASHTO LRFD**	**FHWA (2022)**	**Ratio**
Nominal Moment M_n, k-ft	17,015	17,462	0.97
Neutral Axis c, in.	18.22	18.8	0.97
Lever Arm z, in.	44.92	44.62	1.00

5.7 SHEAR RESISTANCE AT STRENGTH LIMIT STATE

Shear design of the UHPC bridge considers the additional strength due to the presence of steel fibers. The recommendations from El-Helou and Graybeal (2022) were used for computing the design shear strength.

5.7.1 Critical Section for Shear

The critical section for the maximum design V_u is computed as per the AASHTO LRFD Specifications (AASHTO 2020) Article 5.7.3.2 and is taken at a distance d_v from the inside face of the support.

5.7.2 Nominal Shear Resistance

Factored Shear Demand, V_u

$$= 1.25(\mathrm{V_g} + \mathrm{V_h} + \mathrm{V_s} + \mathrm{V_r}) + 1.50(\mathrm{V_{ws}}) + 1.75(\mathrm{V_{LL}})$$
$$= (1.25)(60.2 + 4.7 + 56.4 + 8.4) + (1.50)(12.4) + (1.75)(104.9)$$
$$= 364.3 \text{ kips} \quad (5.110)$$

Ultimate shear resistance of UHPC, V_{Rd}

$$= V_{Rd,UHPC} + V_{Rd,S} + V_{Rd,P} \quad (5.111)$$

Based on the AASHTO draft specifications for UHPC (FHWA 2022):

Shear failure angle, θ $=27.3^{o}$

d_v is computed as per Section 5.5.4.

Effective shear depth (d_v)

$$= \max(\text{inner lever arm (z)}, \max(0.9d_p, 0.72\text{h})) \quad (5.112)$$
$$= \max(44.9, \max(0.9\,(52.1), 0.72\,(64.5))$$
$$= \max(44.9, \max(46.9, 46.4)$$
$$= \max(44.9, 46.9)$$
$$= 46.9 \text{ in.}$$

Note: Computation of z and d_p are shown in Section 5.6.10 under flexure resistance at strength limit state.

UHPC contribution term, $V_{Rd,UHPC}$

$$= f'_t b_w d_v cot(\theta)$$
$$= (0.85)(7)(46.9)\cot(27.3) \quad (5.113)$$
$$= 540.5 \text{ kips}$$

Transverse steel contribution, $V_{Rd,S}$ $= \dfrac{A_v f_y d_v \cot(\theta)}{s}$

where:

A_v = Area of transverse steel = (2)(0.20) = 0.40 in^2

f_y = Yield strength of transverse steel = 60 ksi

s = Spacing between transverse steel = 24 in.

$= 0.25 d_v \cot(\theta) \leq 24$ in. = $0.25(46.9)\cot(27.3) = 22.7$ in.

Use #4 R bars at 24 in. spacing for minimum transverse reinforcement.

$$V_{Rd,S} = \frac{(0.40)(60)(46.9)\cot(27.3)}{22.7}$$

$$= 96.0 \text{ kips}$$

Harped strands contribution, $V_{Rd,P}$ $= N_H A_p f_{pe} \sin(\alpha)$ (5.114)

where:

N_H = Number of strands harped = 32

α = Angle of harped strands

$$= \tan^{-1}\left({(d_{s_top} - d_s)}/{a}\right)$$

$$= \tan^{-1}\left({(50.5 - 30.5)}/{(64.58 \times 12)}\right)$$

$$= 1.48^{o}$$

where:

d_{s_top} = The distance from the bottom of girder to the centerline of the uppermost harped strand at the girder end, in.

d_s = The distance from the bottom of girder to the centerline of the uppermost harped strand at the location where harping begins near the girder midspan, in.

$$V_{Rd,P} = (32)(0.217)(141.8)\sin(1.48) \quad (5.115)$$

$$= 25.41 \text{ kips}$$

With no transverse reinforcement

$\therefore\ V_{Rd} = V_{Rd,UHPC} + V_{Rd,P}$ (5.116)

$= 540.5 + 25.31$

$= 565.8$ kips

Factored shear resistance $= \phi_v V_{Rd}$

$= 0.9 \times 565.8$

$= 509.3$ kips

Because $V_u = 364.3$ kips $\geq$ $(0.5)(509.3)$kips $= 254.6$ kips.

$V_u \geq 0.5\ V_{Rd}$

therefore, minimum shear reinforcement is required per AASHTO (2020). Note that the AASHTO draft specifications for UHPC (FHWA 2022) does not require minimum shear reinforcement in this case. However, based on the results of this research project it is recommended that minimum shear reinforcement be used.

With minimum transverse reinforcement

$\therefore\ V_{Rd} = V_{Rd,UHPC} + V_{Rd,S} + V_{Rd,P}$ (5.117)

$= 540.5 + 96.0 + 25.31$

$= 662.0$ kips

Factored shear resistance $= \phi_v V_{Rd}$

$= 0.9 \times 662.0$

$= 595.7$ kips > $V_u = 364.3$ kips [Check OK]

5.8 SPLITTING RESISTANCE

Splitting resistance of the end anchorage zone is checked based on the AASHTO draft specifications for UHPC (FHWA 2022). The splitting resistance of pretensioned anchorage zones is computed as follows:

$P_r = 0.04P_i = 0.04 \times 3305$ (5.118)

$= 132.2$ kips

To account for the resistance, a steel stress of f_s of 20 ksi is assumed and the reinforcement zone is limited to a distance of $h/4$ from the end of the girder. To consider the effects of steel fibers two options are explored.

Option 1: The resistance to splitting forces contributed by the steel fibers of UHPC are assumed as per the AASHTO draft specifications for UHPC (FHWA 2022) and the formula is listed below.

$$f_s A_s + 0.25\gamma_u f'_t h b_v \geq 0.04 P_i \tag{5.119}$$

Rewriting the above expression, the area of transverse steel located within a distance of h/4 from the girder ends, is determined as:

$$\begin{aligned} A_s &\geq \frac{(0.04P_i - 0.25\gamma_u f'_t h b_v)}{f_s} \\ &\geq \frac{(132.2 - 0.25 \times 0.85 \times 0.72 \times 54 \times 7)}{20} \\ &= 3.72 \text{ in.}^2 \end{aligned}$$

Using #6 R-bars (two legs), the number of bars, $N_{stirrups} = A_s/A_v$

$$N_{stirrups} = 3.72/(0.44 \times 2) = 4.22 \sim 5$$

$$\text{Spacing, } s = \frac{\frac{h}{4} - cover}{N_{stirrups} - 1} = \frac{54/4 - 2.5}{(5-1)} = 2.75 \sim 3 \text{ in.}$$

Option 2: The alternate mechanics-based method explained in Section 3.10.3 of this report is demonstrated. The resistance to splitting forces contributed by the steel fibers of UHPC are assumed based on the orientation of fibers. The fiber orientation is assumed to be in three directions. Therefore, 1/3 is considered as a reasonable reduction factor to account for the orientation of fibers in the vertical direction. The equivalent area of transverse reinforcement provided by the steel fibers is determined as follows.

$$f_s A_s \geq 0.04 P_i \tag{5.120}$$

$$\begin{aligned} A_{s,req.} &\geq 0.04 P_i / f_s \\ &\geq 0.04 \times 3305/20 \\ &\geq 6.61 \text{ in.}^2 \end{aligned}$$

Contribution of fiber:

Volume of steel fibers, ρ_{fiber} $= 1.5\% = 0.015$

Tensile strength of steel fibers, f_{fiber} $= 406$ ksi

Yield strength of stirrups, $f_{stirrup}$ $= 60$ ksi

To determine the equivalent area of transverse reinforcement:

$$\frac{\rho_{fiber} f_{fiber}}{3} = \frac{A_{v_eq} f_{stirrup}}{b_v \, {}^{h}/_{4}}$$

$$A_{v_eq} = \frac{\rho_{fiber} f_{fiber} b_v \, {}^{h}/_{4}}{3 f_{stirrup}}$$

$$A_{v_eq} = \frac{0.015 \times 406 \times 7 \times {}^{54}/_{4}}{3 \times 60}$$

$$= 2.95 \text{ in.}^2$$

Total area of stirrups may be calculated as follows:

$$A_{s,req.} = A_s + A_{v_eq}$$

$$A_s = A_{s,req.} - A_{v_eq}$$

$$A_s = 6.61 - 2.95$$

$$= 3.66 \text{ in.}^2$$

Using #6 R-bars, the number of bars, $N_{stirrups} = A_s / A_v$

$$N_{stirrups} = 3.66/(0.44 \times 2) = 4.16 \sim 5$$

Spacing, s $= \dfrac{\frac{h}{4} - cover}{N_{stirrups} - 1} = \dfrac{54/4 - 2.5}{(5 - 1)} = 2.75 \sim 3$ in.

5.9 INTERFACE SHEAR DESIGN

As discussed in Section 3.9.1, the interface shear design approach below follows Section 5.7.4.3 of the AASHTO LRFD Specifications (AASHTO (2020) where the interface consists of

placement of CC on clean, laitance free concrete without intentional roughening. These recommendations are consistent with those of FHWA (2022) for CC on clean, laitance free UHPC. The interface shear resistance is determined as follows

The factored shear force at the critical section (at a distance d_v from the inside face of the support) is considered:

Factored vertical shear	$V_1 = V_u = 365.5$ kips
Distance between the centroid of the tension steel and the mid-thickness of the slab	$d_{v1} = \frac{t_s}{2} + Y_t + e = 47.84$ in.
Factored horizontal shear per unit length of girder (AASHTO LRFD 5.7.4.5):	$V_{h1} = \frac{V_u}{d_{v1}} = 7.64$ kips/in.
Area of interface per unit length	$A_{cv} = b_{vi} \times 1 = 36$ in.^{2}/in.

Note: b_{vi} = top flange width, b_f = 36 in. in this case.

Provide at least the minimum interface shear reinforcement as per the recommendations of the AASHTO draft specifications for UHPC (FHWA 2022).

Try providing #5 bars at a 6 in. center-to-center spacing at the interface.

$$A_{vf} = \frac{2 \text{ legs} \times 2 \text{ UC bars} \times 0.31}{6} = 0.206 \text{ in.}^2/\text{in.}$$

According to AASHTO LRFD 5.7.4.2, the minimum shear interface reinforcement is given as follows:

$$A_{vf} \geq \frac{0.05 A_{cv}}{f_y} = 0.027 \text{ in.}^2/\text{in.}$$

The values for concrete placed against a clean concrete surface, free of laitance, but not intentionally roughened provided in AASHTO LRFD Art. 5.7.4.4 are used as recommended by FHWA (2022).

Cohesion factor,	$c = 0.075$ ksi
Friction factor,	$\mu = 0.6$

Fraction of concrete strength available to resist interface shear, $K_1 = 0.2$

Limiting interface shear resistance, $K_2 = 0.8$ ksi

Compressive force, $P_c = 0$ kips

According to AASHTO LRFD Eq. 5.7.4.3-3:

$$V_{ni} = cA_{cv} + \mu\left(A_{vf}f_y + P_c\right)$$

$$= 0.075 \times 36 + 0.6\left(\frac{0.31 \times 2 \text{ legs} \times 2 \text{ UC bars}}{6 \text{ in. spacing}} \times 60 + 0\right)$$

$$= 10.12 \text{ kip/in.}$$

The nominal shear resistance shall not exceed either of the following:

$V_{ni} \leq K_1 f'_c A_{cv} = 0.2 \times 4 \times 36 = 28.8$ kip/in. [Check OK]

$V_{ni} \leq K_2 A_{cv} = 0.8 \times 36 = 28.8$ kip/in. [Check OK]

$\phi_v V_{ni} = 0.9 \times 10.12 = 9.1$ kip/in.

The factored horizontal shear per unit length of girder is calculated at different sections along the span length of the girder. The spacing between the UC bars is changed to ensure that the factored horizontal shear force per unit length (V_{h1}) does not exceed the reduced nominal shear resistance ($\phi_v V_{ni}$). Based on the interface shear demand computed as per AASHTO LRFD Art. 5.7.4.5 along the span length, the spacing is adjusted and the following layout is suggested.

Provide additional interface shear reinforcement in the form of bundled UC bars, with the following arrangement:

- two (bundled) #5 UC bars at a center-to-center spacing of 6 in. up to 9 ft from each girder end, with end cover of 2.5 in.
- followed by two (bundled) #5 UC bars at a center-to-center spacing of 9 in. up to 21 ft from each girder end

- followed by two (bundled) #5 UC bars at a center-to -center spacing of 12 in. up to 40 ft from each girder end
- followed by two (bundled) #5 UC bars at a center-to-center spacing of 24 in. from each girder end

5.10 END BLOCK REINFORCEMENT

End block reinforcement to be provided as per TxDOT standard detailing for I-girders (TxDOT 2017).

5.11 DESIGN SUMMARY

The following Table 5.14 summarizes the key aspects of the design example.

Table 5.14. Summary of Design Details.

Design Details	Value
Bridge Geometry:	
Bridge Width, W	46 ft
Back-wall to back-wall distance, L_{br}	144 ft
Number of girders	6
UHPC:	
Compressive strength at release, f'_{ci}	11.7 ksi
28-day compressive strength at service, f'_c	18 ksi
Elastic tensile strength at release, f'_{ti}	0.72 ksi
Elastic tensile strength at service, f'_t	0.85 ksi
Post cracking tensile strength, f'_{tu}	0.85 ksi
MOE at release, E_{gi}	6742 ksi
MOE at release, E_g	7423 ksi
Conventional Concrete:	
28-day compressive strength at service, f'_{cd}	4.0 ksi
MOE at release, E_d	3987 ksi
Prestressing Strand Details:	
Ultimate strength of steel strands, f_{pu}	270 ksi
Yield strength of steel strands, f_{py}	243 ksi
MOE of strands, E_p	28,500 ksi
Diameter of strands, d_b	0.6 in.
Girder Section:	
Length of girder, L_g	143.5 ft
Depth of girder, h_g	54 in.

Table 5.14. (Continued).

Composite Section:	
Total Height, H	64.5 in.
Effective width of the section, B_e	96 in.
Distance of neutral axis from top of girder, y_{tc}	27.6 in.
Distance of neutral axis from bottom of girder, y_{bc}	36.9 in.
Area of girder, A_{gc}	1292 in^2
Moment of inertial about x-axis, I_{cg}	699,771 in^4
Dead Load Moment Demand:	
Girder, M_g	2288 kip-ft
Deck Slab, M_s	2142 kip-ft
Haunch, M_h	179 kip-ft
Wearing surface, M_{ws}	471 kip-ft
Barrier T551, M_r	321 kip-ft
Self-weight of girder at transfer length, M_{Dt}	96.7 kip-ft
Live Load Moment Demand:	
Factored Live Load Moment, M_{LL}	2906 kip-ft
Dead Load Shear Demand:	
Girder, V_g	60.2 kips
Deck slab, V_s	56.4 kips
Haunch, V_h	4.7 kips
Wearing surface, V_{ws}	12.4 kips
Barrier T551, V_r	8.4 kips
Factored Shear Demand, V_u	364.3 kips
Live Load Shear Demand:	
Factored Live Load Shear, V_{LL}	104.9 kips

Table 5.14. (Continued).

Prestressing Losses:	
Initial, f_{pi}	177.1 ksi
Final, f_{pe}	141.8 ksi
Flexure Design:	
Number of strands, N	86
Force in prestressing strand immediately, F_i	3305 kips
Force in prestressing strand after losses, F	2647 kips
All stress checks pass in flexure.	
Camber and Deflection:	
Camber with deck, Δ_{final}	0.55 in.
Design passes the deflection check, Δ_{LL}	0.81 in. < 2.13 in.
Flexural resistance at strength limit state:	
Moment demand, M_u	11,953 kip-ft
Reduced nominal moment, ϕM_n	17,015 kip-ft
$\phi M_n > M_u$ → section has sufficient flexural resistance for strength limit state	
Shear Design:	
Shear demand, V_u	364.3 kips
Reduced nominal shear, ϕV_n	595.7 kips
Nominal shear reinforcement is recommended.	
Splitting resistance reinforcement	Provide #6 R bars at 3 in. spacing c/c up to $h/4$ (13.5 in.) distance from the ends (a total of 5-#6 R bars)
Interface Shear Resistance	Provide 2 (bundled) #5 UC bars at c/c spacing of 6 in. up to 9 ft from the end with end cover of 2.5 in., followed by 2 (bundled) #5 UC bars with c/c spacing of 9 in. up to 21 ft, followed by 2 (bundled) #5 UC bars at c/c spacing of 12 in. up to 40 ft, followed by 2 (bundled) #5 UC bars at c/c spacing of 24 in.
End block reinforcement to be provided as per TxDOT (2017)	

REFERENCES

AASHTO (2018). "AASHTO LRFD Bridge Design Specifications, Ninth Edition." American Association of State Highway and Transportation Officials, Washington DC.

AASHTO (2020). "AASHTO LRFD Bridge Design Specifications, Ninth Edition." American Association of State Highway and Transportation Officials, Washington DC.

AASHTO T 358 (2017). "Standard Method of Test for Surface Resistivity Indication of Concrete's Ability to Resist Chloride Ion Penetration." American Association of State Highway and Transportation Officials, Washington, DC.

AASHTO T 397 Draft (2022). "Standard Method of Test for Uniaxial Tensile Response of Ultra-High Performance Concrete." American Association of State Highway and Transportation Officials, Washington, DC.

ACI 544.4R-18 (2018). "Guide to Design with Fiber-Reinforced Concrete." American Concrete Institute, Farmington Hills, MI.

AFGC (2013). "Ultra High Performance Fibre-Reinforced Concretes (Bétons Fibrés à Ultra-Hautes Performances)." AFGC-SETRA, Bagneux, France.

ASTM 512 (2015). "Standard Test Method for Creep of Concrete in Compression." ASTM International, West Conshohocken, PA.

ASTM C33 (2018). "Standard Specification for Concrete Aggregates." ASTM International, West Conshohocken, PA.

ASTM C39 (2020). "Standard Test Method for Compressive Strength of Cylindrical Concrete Specimens." ASTM International, West Conshohocken, PA.

ASTM C138 (2015). "Standard Test Method for Density (Unit Weight), Yield, and Air Content (Gravimetric) of Concrete." ASTM International, West Conshohocken, PA.

ASTM C144 (2018). "Standard Specification for Aggregate for Masonry Mortar." ASTM International, West Conshohocken, PA.

ASTM C157 (2017). "Standard Test Method for Length Change of Hardened Hydraulic-Cement Mortar and Concrete." ASTM International, West Conshohocken, PA.

ASTM C191 (2018). "Standard Test Methods for Time of Setting of Hydraulic Cement by Vicat Needle." ASTM International, West Conshohocken, PA.

ASTM C469 (2014). "Standard Test Method for Static Modulus of Elasticity and Poisson's Ratio of Concrete in Compression." ASTM International, West Conshohocken, PA.

ASTM C512 (2015). "Standard Test Method for Creep of Concrete in Compression." ASTM International, West Conshohocken, PA.

ASTM C666 (2015). "Standard Test Method for Resistance of Concrete to Rapid Freezing and Thawing." ASTM International, West Conshohocken, PA.

ASTM C672 (2012). "Standard Test Method for Scaling Resistance of Concrete Surfaces Exposed to Deicing Chemicals." ASTM International, West Conshohocken, PA.

ASTM C944 (2012). "Standard Test Method for Abrasion Resistance of Concrete or Mortar Surfaces by the Rotating-Cutter Method." ASTM International, West Conshohocken, PA.

ASTM C1064 (2017). "Standard Test Method For Temperature of Freshly Mixed Hydraulic-Cement Concrete." ASTM International, West Conshohocken, PA.

ASTM C1202 (2017). "Standard Test Method for Electrical Indication of Concrete's Ability to Resist Chloride Ion Penetration." ASTM International, West Conshohocken, PA.

ASTM C1437 (2015). "Standard Test Method for Flow of Hydraulic Cement Mortar." ASTM International, West Conshohocken, PA.

ASTM C1609 (2019). "Standard Test Method for Flexural Performance of Fiber-Reinforced Concrete (Using Beam With Third-Point Loading)." ASTM International, West Conshohocken, PA.

ASTM C1760 (2021). "Standard Test Method for Bulk Electrical Conductivity of Hardened Concrete." ASTM International, West Conshohocken, PA.

ASTM C1856 (2017). "Standard Practice for Fabricating and Testing Specimens of Ultra-High-Performance Concrete." ASTM International, West Conshohocken, PA.

Barcelo, L., Boivin, S., Acker, P., Toupin, J., and Clavaud, B. (2001). "Early Age Shrinkage of Concrete: Back to Physical Mechanisms." *Concrete Science and Engineering*, 3(10), 85-91.

Bentz, D. P., and Aitcin, P.-C. (2008). "The Hidden Meaning of Water-Cement Ratio." *Concrete International*, 30(5), 51-54.

Berkshire Engineering Supplier (2022). "Fibre Dosing Systems." <https://www.berk-eng.com/concrete/fibre-dosing-systems>.

Crane, C. K. (2010). "Shear and Shear Friction of Ultra-High Performance Concrete Bridge Girders." Georgia Institute of Technology.

de Larrard, F., and Sedran, T. (1994). "Optimization of Ultra-High-Performance Concrete by the Use of a Packing Model." *Cement and Concrete Research*, 24(6), 997-1009.

eConstruct (2020). "Implementation of Ultra-High-Performance Concrete in Long-Span Precast Pretensioned Elements for Concrete Buildings and Bridges." Wiss, Janney, Elstner Associates, University of Nebraska-Lincoln, The NCSU Constructed Facilities Laboratory, Precast/Prestressed Concrete Institute, Chicago, IL.

El-Helou, R. G., and Graybeal, B. A. (2022). "Flexural Behavior and Design of Ultrahigh-Performance Concrete Beams." *ASCE Journal of Structural Engineering*, 148(4), 04022013.

El-Helou, R. G., and Graybeal, B. A. (2022). "Shear Behavior of Ultrahigh-Performance Concrete Pretensioned Bridge Girders." *ASCE Journal of Structural Engineering*, 148(4), 04022017.

El-Helou, R. G., and Graybeal, B. A. (2023). "Shear Design of Strain–Hardening Fiber-Reinforced Concrete Beams." *ASCE Journal of Structural Engineering*.

El-Tawil, S., Tai, Y.-S., Meng, B., Hansen, W., and Liu, Z. (2018). "Commercial Production of Non-Proprietary Ultra High Performance Concrete." Michigan Department of Transportation, Lansing, MI.

FHWA (2022). "Proposed AASHTO LRFD Guide Specifications for Structural Design with UHPC." *Draft Under Review*, American Association of State Highway and Transportation Officials, Washington, DC.

Gelardi, G., and Flatt, R. (2016). "Working Mechanisms of Water Reducers and Superplasticizers." *Science and Technology of Concrete Admixtures*, Elsevier, 257-278.

Granju, J., and Grandet, J. (1989). "Relation Between the Hydration State and the Compressive Strength of Hardened Portland Cement Pastes." *Cement and Concrete Research*, 19(4), 579-585.

Graybeal, B. (2019). "Design and Construction of Field-Cast UHPC Connections." Federal Highway Administration, McLean, VA.

Haber, Z. B., De la Varga, I., Graybeal, B. A., Nakashoji, B., and El-Helou, R. (2018). "Properties and Behavior of UHPC-class Materials." Federal Highway Administration, McLean, VA.

Hermann, A., Langaro, E., SILVA, S. L. D., and Klein, N. S. (2016). "Particle Packing of Cement and Silica Fume in Pastes Using an Analytical Model." *Revista IBRACON de Estruturas e Materiais*, 9(1), 48-65.

Li, L. G., and Kwan, A. K. H. (2014). "Packing Density of Concrete Mix Under Dry and Wet Conditions." *Powder Technology*, 253, 514-521.

Model Code (2010). "Model Code 2010, fib-CEB FIP, bulletin 65." *International Federation for Structural Concrete (fib)*, Volume 1.

Mohebbi, A., and Graybeal, B. (2022). "Prestress Loss Model for Ultra-High Performance Concrete." *Engineering Structures*, 252, 113645.

Mukhopadhyay, A., Liu, K.-W., and Jalal, M. (2018). "Further Validation of ASR Testing and Approach for Formulating ASR-Resistant Concrete Mix: Technical Report." TxDOT, Austin, TX.

Nkinamubanzi, P.-C., Mantellato, S., and Flatt, R. (2016). "Superplasticizers in Practice." *Science and Technology of Concrete Admixtures*, Elsevier, 353-377.

NPCA (2013). "White Paper Ultra High Performance Concrete." National Precast Concrete Association, CARMEL, IN.

Ozyildirim, C. (2011). "Evaluation of Ultra-High-Performance Fiber-Reinforced Concrete." Virginia Department of Transportation, Richmond, VA.

Park, J., Ryu, K., Kang, S.-T., Koh, G.-T., and Kihong Ahn (2010). "Development of Ultra High Performance Concrete for Hybrid Cable Stayed Bridges." Korea Institute of Civil Engineering and Building Technology, Seoul, South Korea.

Richard, P., and Cheyrezy, M. (1995). "Composition of Reactive Powder Concretes." *Cement and Concrete Research*, 25(7), 1501-1511.

Richardson, I. (2004). "Tobermorite/Jennite-and Tobermorite/Calcium Hydroxide-Based Models for the Structure of CSH: Applicability to Hardened Pastes of Tricalcium Silicate, β-Dicalcium Silicate, Portland Cement, and Blends of Portland Cement with Blast-Furnace Slag, Metakaolin, or Silica Fume." *Cement and Concrete Research*, 34(9), 1733-1777.

Russell, H. G., Graybeal, B. A., and Russell, H. G. (2013). "Ultra-high performance concrete: A state-of-the-art report for the bridge community." United States. Federal Highway Administration.

Tadros, M. (2021). "Application of PCI Ultra-High-Performance Concrete to Bridge Super Structures." AASHTO CBS T-10 Committee Meeting, Presenter-Maher Tadros, Technical Committee for Concrete Design T-10, Web Meeting.

Taly, N. (2014). *Highway Bridge Superstructure Engineering: LRFD Approaches to Design and Analysis*, CRC Press.

Tattersall, G. H., and Banfill, P. F. (1983). *The Rheology of Fresh Concrete*, Pitman Advanced Pub. Program, Boston, MA.

Tue, N. V., Ma, J., and Orgass, M. (2008). "Influence of Addition Method of Superplasticizer on the Properties of Fresh UHPC." *Proc., The 2nd International Symposium on Ultra-High Performance Concrete*, Kassel University Press, 93-100.

TxDOT (2014). "Traffic Rail-Type T551." TxDOT Bridge Division Standard, Austin, Texas.

TxDOT (2015). "TxDOT Elastomeric Bearing and Girder End Details Prestressed Concrete I-Girders." *IGEB*, Texas Department of Transportation, Austin, Tx.

TxDOT (2017). "Prestressed Concrete I-Girder Details." TxDOT, Austin, TX.

TxDOT (2017). "TxDOT Standard Drawings." TxDOT, Austin, TX.

TxDOT (2018). "TxDOT Bridge Design Manual - LRFD." Texas Department of Transportation, Austin, TX.

TxDOT (2019). "TxDOT Bridge Standards." Texas Department of Transportation, Austin, TX.

TxDOT (2023). "Bridge Design Manual - LRFD." TxDOT, Austin, TX.

Wille, K., and Boisvert-Cotulio, C. (2015). "Material Efficiency in the Design of Ultra-High Performance Concrete." *Construction and Building Materials*, 86, 33-43.

Wille, K., Tue, N. V., and Parra-Montesinos, G. J. (2014b). "Fiber Distribution and Orientation in UHP-FRC Beams and Their Effect on Backward Analysis." *Materials and Structures*, 47(11), 1825-1838.

Yahia, A., Mantellato, S., and Flatt, R. (2016). "Concrete Rheology: A Basis for Understanding Chemical Admixtures." *Science and Technology of Concrete Admixtures*, Elsevier, 97-127.

Yoo, D. Y., and Yoon, Y. S. (2016). "A Review on Structural Behavior, Design, and Application of Ultra-High-Performance Fiber-Reinforced Concrete." *International Journal of Concrete Structures and Materials*, 10(2), 125-142.

Zdeb, T. (2013). "Ultra-High Performance Concrete Properties and Technology." *Bulletin of the Polish Academy of Sciences: Technical Sciences*, 61(1), 183-193.

APPENDIX A.
DRAWINGS FOR DESIGN EXAMPLES

This section presents the detailing of the example discussed.

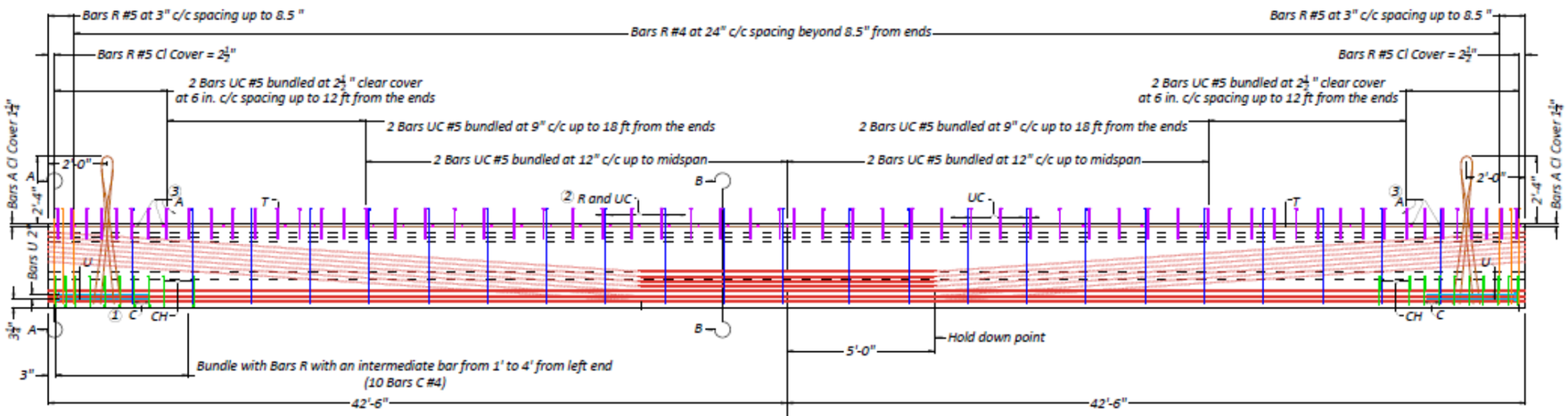

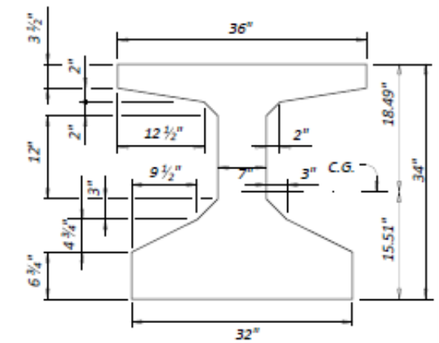

Cross-section Geometry

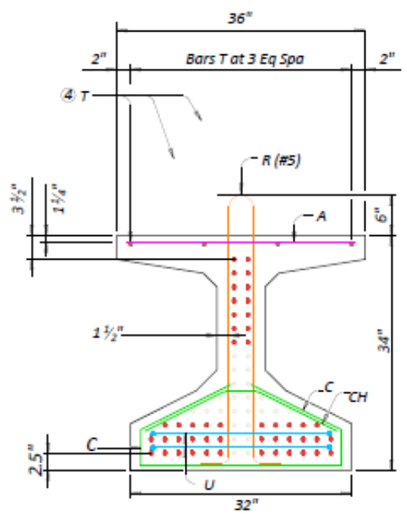

SECTION A-A

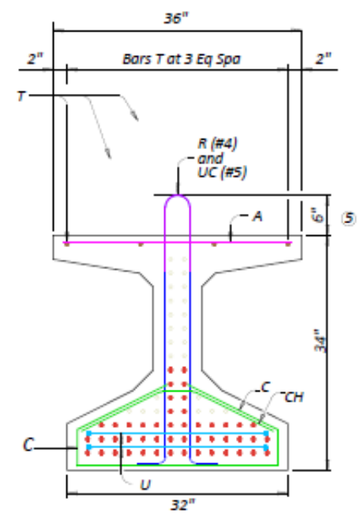

SECTION B-B

① Bundled with Bars R with intermediates in between bars R from 1' to 4' on left end only.

② The average of the top and bottom spacing of Bars R cannot exceed the required spacing.

③ Bars A as per standard TxDOT detailing

④ Bars T as per standard TxDOT detailing

⑤ Projection of Bars UC above the top flange of girder is between 5"-6".

General Notes:

1. R bar (#5) are provided for splitting resistance and R bars (#4) are provided for minimum transverse shear resistance.
2. U-composite bars (Bars UC) are provided for interface shear between the girder and the deck slab.
3. 1½" clear cover unless noted otherwise.
4. Cover dimensions are clear dimensions, unless noted otherwise.
5. Reinforcing bar dimensions shown are out-to-out of bar.
6. 0.6 in. diameter, low relaxation prestressing strands, 14 strands are draped: 34 at bottom and 14 at top at ends; 48 at bottom and 0 at top at midspan.
7. Total girder length of this sheet is 85'-0".

Texas A&M Transportation Institute Texas A&M University		
Utilization of UHPC Bridge Superstructures in Texas		
Tx34 Elevation and Cross-sections		
TxDOT Project No.	Drawing No.	Date
0-6982	S6982 – 1	02/03/2023

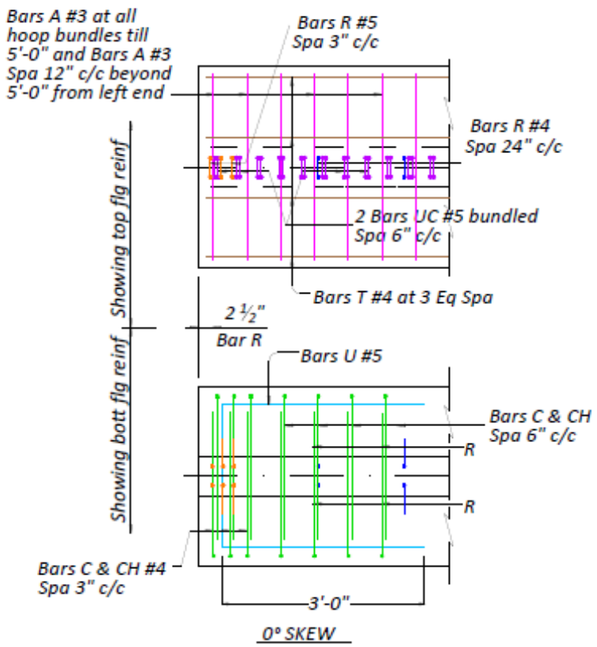

① No portion of bar less than 10 ft.

② Out-to-out dimension

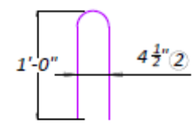

BARS UC34 (#5)

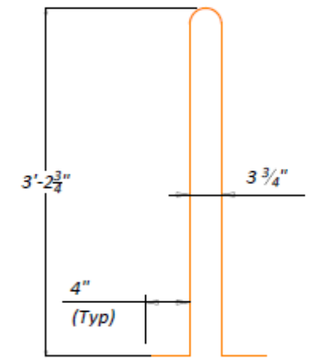

BARS R34 (#5)

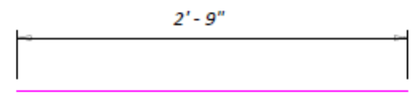

BARS A34 (#3)

To control top flange cracking that may occur during form removal, additional top flange reinforcing may be placed as shown in girder ends at the Fabricator's option.

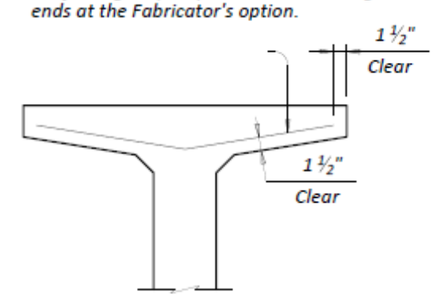

OPTIONAL TOP FLANGE REINFORCING DETAIL

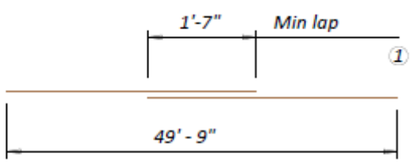

BARS T34 (#4)

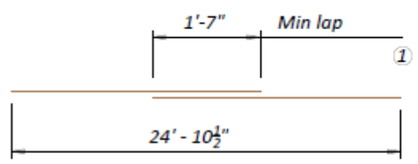

BARS T34 (#4)

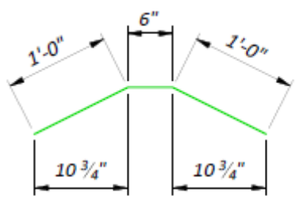

BARS CH34 (#4)

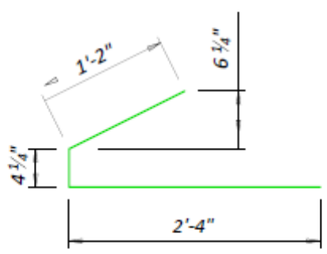

BARS C34 (#4)

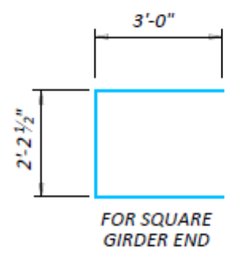

BARS U34 (#5)

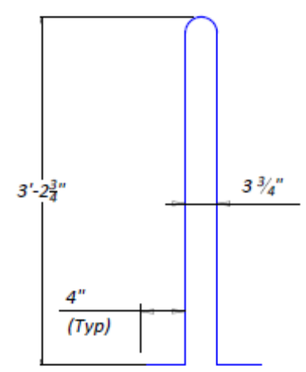

BARS R34 (#4)

Texas A&M Transportation Institute Texas A&M University		
Utilization of UHPC Bridge Superstructures in Texas		
Tx34 Bar Bending and Flange Details		
TxDOT Project No.	Drawing No.	Date
0-6982	S6982 – 2	02/03/2023

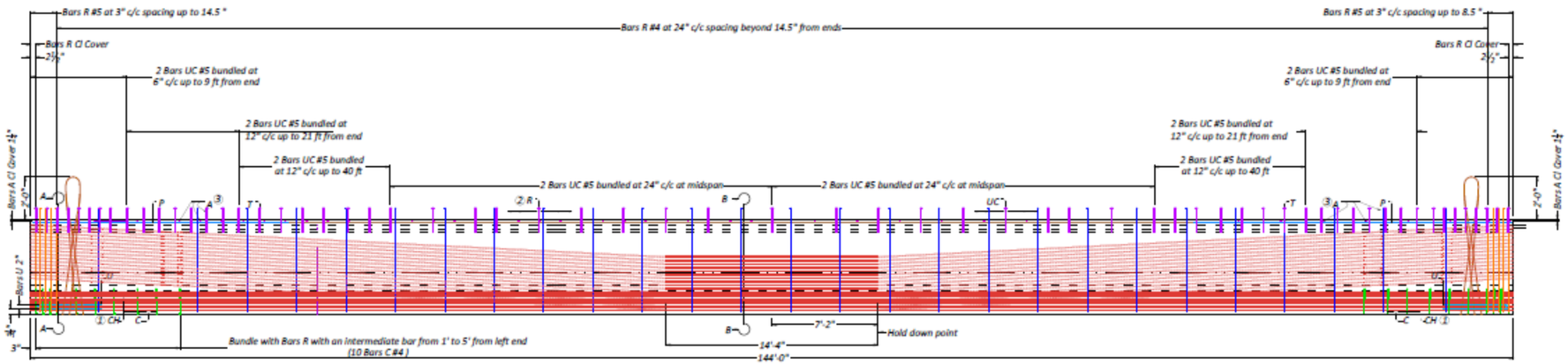

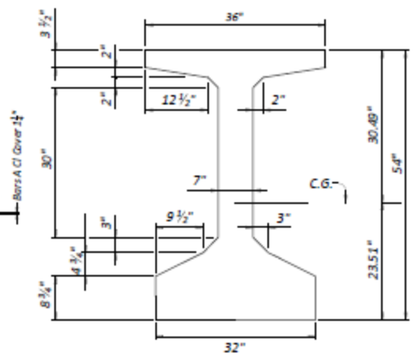

Cross-section Geometry

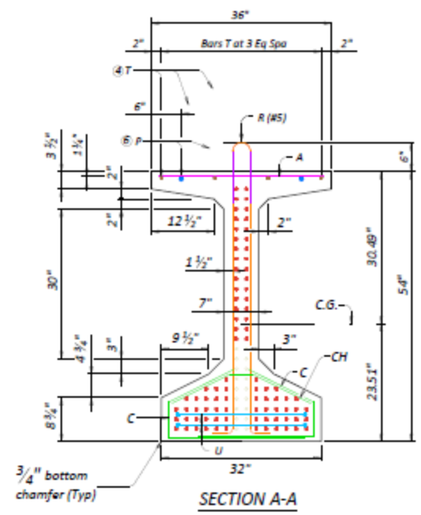

SECTION A-A

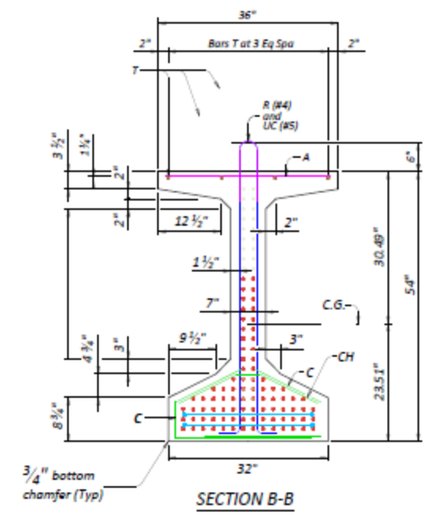

SECTION B-B

① Bundled with Bars R with intermediates in between bars R from 1' to 5' on left end only.

② The average of the top and bottom spacing of Bars R cannot exceed the required spacing.

③ Bars A as per standard TxDOT detailing

④ Bars T as per standard TxDOT detailing

⑤ Projection of U composite bars above the top flange of girder is between 5-6".

⑥ Bars P as per standard TxDOT detailing

General Notes:

1. R bar (#5) are provided for splitting resistance and R bars (#4) are provided for minimum transverse shear resistance.
2. U-composite bars (Bars UC) are provided for interface shear between the girder and the deck slab.
3. 1½" clear cover unless noted otherwise.
4. Cover dimensions are clear dimensions, unless noted otherwise.
5. Reinforcing bar dimensions shown are out-to-out of bar.
6. 0.6 in. diameter, low relaxation prestressing strands, 32 strands are draped: 54 at bottom and 32 at top at ends; 86 at bottom and 0 at top at midspan.
7. Total girder length of this sheet is 144'-0".

Texas A&M Transportation Institute Texas A&M University		
Utilization of UHPC Bridge Superstructures in Texas		
Tx54 Elevation and Cross-sections		
TxDOT Project No.	Drawing No.	Date
0-6982	S6982 – 1	02/03/2023

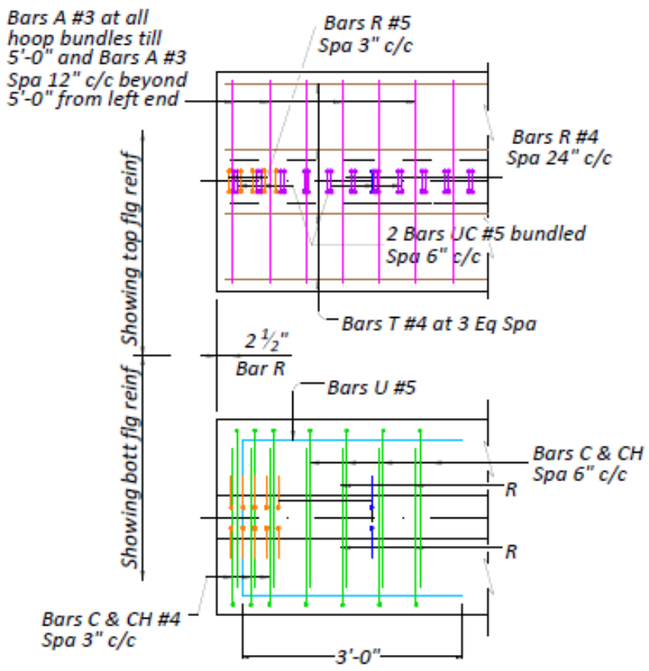

0° SKEW

① No portion of bar less than 10 ft.

② Out-to-out dimension

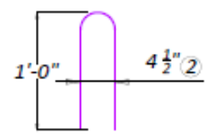

BARS UC54 (#5)

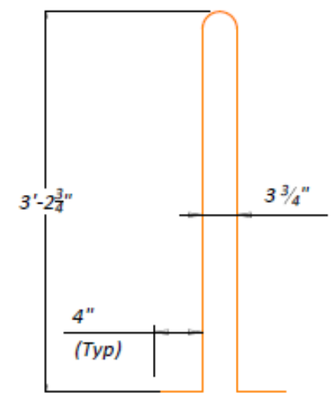

BARS R54 (#5)

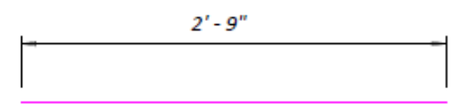

BARS A54 (#3)

To control top flange cracking that may occur during form removal, additional top flange reinforcing may be placed as shown in girder ends at the Fabricator's option.

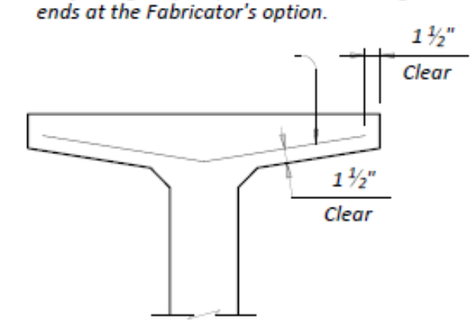

OPTIONAL TOP FLANGE REINFORCING DETAIL

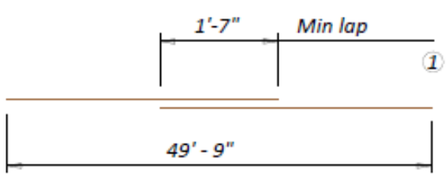

BARS T54 (#4)

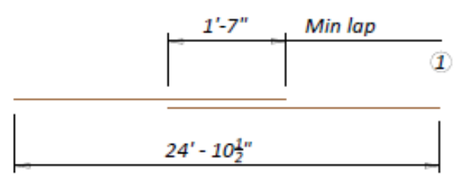

BARS T54 (#4)

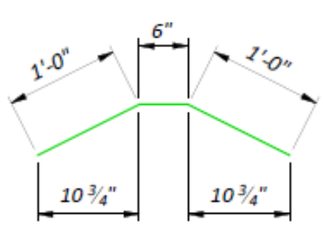

BARS CH54 (#4)

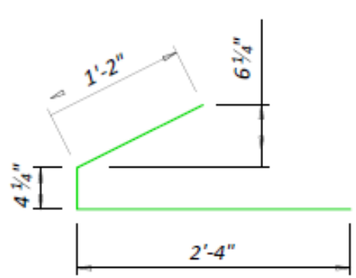

BARS C54 (#4)

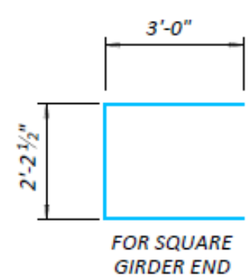

BARS U54 (#5)

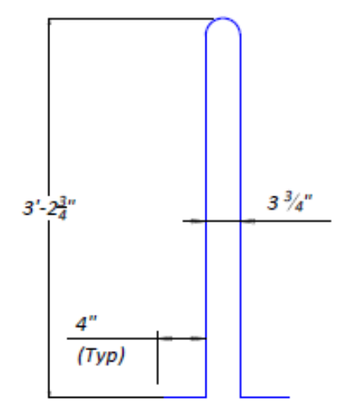

BARS R54 (#4)

Texas A&M Transportation Institute Texas A&M University		
Utilization of UHPC Bridge Superstructures in Texas		
Tx54 Bar Bending and Flange Details		
TxDOT Project No.	Drawing No.	Date
0-6982	S6982 – 2	02/03/2023